Endosomolytic Biomaterial Vaccines for Cancer Therapy

Albert Yen

A dissertation

submitted in partial fulfillment of the

requirements for the degree of

Doctor of Philosophy

University of Washington

2021

Reading Committee:

Suzie H. Pun, Chair

Patrick S. Stayton

Wayne R. Gombotz

Program Authorized to Offer Degree:

Bioengineering

University of Washington

Abstract

Endosomolytic Biomaterial Vaccines for Cancer Therapy

Albert Yen

Chair of the Supervisory Committee:

Suzie H. Pun

Department of Bioengineering

Stimuli-responsive biomaterials are useful for a variety of therapeutic applications because they function in concert with naturally occurring biological processes. This dissertation is focused on applications of a pH-responsive biomaterial known as the "Virus-Inspired Polymer for Endosomal Release," or VIPER. VIPER is a cationic polymer-peptide conjugate designed for intracellular delivery of nucleic acids. It self-assembles into nanoparticles at neutral pH and disassembles at acidic pH to expose melittin, a membrane-lytic peptide. Using this pH-responsive lytic mechanism, VIPER disrupts endosome membranes after cellular uptake into acidic endosomal compartments, delivering its cargo to the cytosol in a virus-like fashion. We aim to use VIPER as a platform technology for delivery of cancer vaccines. Because the bioactivities of tumor antigens and vaccine adjuvants may be augmented by VIPER's membrane-lytic properties, VIPER-mediated delivery of vaccine components to immune cell populations may potentiate anticancer immune responses.

DEDICATION

To my family, friends, and colleagues, and to Dr. Dong-Keun Lee, one of my first mentors in science. May you rest in peace, D.K.

ACKNOWLEDGEMENTS

Graduate school is a chapter in the dissertation we call *Life*. I would like to acknowledge some of the people who helped me author this chapter.

First and foremost, **Prof. Suzie Pun**, my PhD adviser. Thank you for your mentorship and for giving me the freedom to forge my own path forward. I could not have asked for a better adviser or a better lab in which to complete my dissertation.

Drs. David Peeler, **Shixian Lv**, and **Yilong Cheng**, my primary collaborators. Thank you for synthesizing the biomaterials reported in this dissertation and for many other essential contributions. This dissertation is only possible because of your expertise and camaraderie.

Drs. Chayanon Ngambenjawong, **Gary Liu**, **Bob Lamm**, and **Brynn Olden**, esteemed alumni of the Pun Lab. Thank you for being role models to me and newer generations of graduate students.

Meilyn Sylvestre and **Emmeline Cheng**, my officemates throughout most of graduate school. Thank you for your friendship and for always believing in my abilities as a scientist. I will miss our office conversation and everyday lab shenanigans.

Ian Cardle, an excellent scientist, and an even better colleague. Thank you for your friendship and positive attitude. I will miss our dinners on the Ave (usually with Emmeline—sorry for third wheeling).

Lucy Yang, a true Renaissance woman. You have come a long way since we first met during recruitment week, and I am sure you will continue to thrive.

Alex Prossnitz, a mutual fan of tennis. I fondly remember watching the 2017 Australian Open Men's Singles final with you (even though you cheered for Roger instead of Rafa).

Clinton Heinze, with whom I endured many fruitless animal studies. Your work ethic is commendable, and I hope your current research efforts are more fruitful.

Audrey Olshefsky, often found in King Lab instead of Pun Lab. But your cheerful disposition when in Pun Lab is always appreciated.

Pacino Wang, who starts the day after most end it. Do you ever sleep? In all seriousness, keep up the great work. I will miss seeing you around in lab at the strangest of hours.

Trey Pichon, who inherited the hemostatic polymers research mantle from Dr. Bob Lamm. Your scientific acumen and global health mindset will take you far.

Kefan Song and **Ben Nguyen**, who inherit the cancer vaccine research mantle from me. Thank you for being such willing learners. I am excited to hear about the science you do!

Dr. Drew Sellers and **Nataly Kacherovsky**, the Pun Lab stalwarts. Thank you for being guiding figures to all graduate students in the lab.

Drs. Dean Ho, **Dong-Keun Lee**, and **Kangyi Zhang**, my mentors while at the UCLA School of Dentistry. Thank you for giving me my start in science. Nanodiamonds are forever!

Drs. Andrea Valladao and **Jennifer McCullar**, my supervisors at CoMotion. Thank you for the opportunity to intern at CoMotion. This internship was the foundation for my pursuit of a career away from the bench.

Tianwei Shen, whose resilience I admire. No matter how rocky the circumstance, you manage to find your footing. Thank you for your friendship.

Dr. Daniel Corbett, my roommate for much of graduate school. Thank you for your friendship and good humor. I will miss our spontaneous apartment chats about anything and everything, and I wish you nothing but success in post-PhD life.

Frank Chen, a fellow California transplant in Washington, and an old college friend. Your "Dr. Yen" caricature is still on my desk. I live up to it now! Thank you for supporting me during my PhD journey.

Angela Lam, who I have known and trusted since the earliest days of college. Things have changed a lot since those innocent Tinychat days, but I am fortunate to still call you a friend. Thank you for supporting me through this formative stage of life.

Matt Au, **Lucy Bi**, **Dr. Felix Chen**, **Lena Quang**, **Stacey Yu**, **Alex Oka**, **Raymond Liu**, **Bradian Muliadi**, **Tony Phe**, **Angelica Jue**, **Andrew Kao**, **Evelyn Chin**, **Jay Chak**, **Vivian Wu**, and many other UCLA alumni who I befriended during (and in some cases, after) college. Thank you for making the effort to maintain our friendship. Although we are all in different places now, it has been wonderful to see you all grow and evolve.

Salina Thai, my girlfriend, and my best friend. Thank you for advising me when I felt lost, for comforting me when I struggled, and for loving me all the same (and for feeding me, for giving me haircuts during a pandemic…the list goes on). I can only hope to support you the way you have supported me.

Last, but certainly not least, **my family**—especially **my mother**—for their unconditional love and for molding me into the person I am today.

EXECUTIVE SUMMARY

This dissertation is formatted as a collection of articles. Opening and concluding remarks are provided in *Chapter 1* and *Chapter 6*, respectively. *Chapter 2* and *Chapter 3* are adapted with permission from published works.[1,2] *Chapter 4* and *Chapter 5* build upon the research described in *Chapter 3*, and they contain data that may be included in future publications.

In *Chapter 1*, we provide an overview of how biomaterials synergize with cancer therapies. We also introduce the "Virus-Inspired Polymer for Endosomal Release" (VIPER), a pH-responsive biomaterial that may be utilized as a cancer nanovaccine.

In *Chapter 2*, we describe development efforts for a VIPER-based mRNA nanovaccine.[1]

In *Chapter 3*, we report a VIPER polyplex nanovaccine loaded with both lytic and antigenic peptides.[2] We show that this polyplex nanovaccine primes antigen-specific immune responses by inducing local cell death.

In *Chapter 4* and *Chapter 5*, we highlight a mannosylated VIPER nanovaccine that modulates immune responses in unexpected ways.

In *Chapter 6*, we propose future research directions for the VIPER nanovaccine platform.

[1] **Yen, A.**; Cheng, Y.; Sylvestre, M.; Gustafson, H. H.; Puri, S.; Pun, S. H. Serum Nuclease Susceptibility of mRNA Cargo in Condensed Polyplexes. *Mol. Pharm.* **2018**, *15* (6), 2268–2276.

[2] Peeler, D. J.*; **Yen, A.***; Luera, N.; Stayton, P. S.; Pun, S. H. Lytic Polyplex Vaccines Enhance Antigen-Specific Cytotoxic T Cell Response through Induction of Local Cell Death. *Adv. Ther.* **2021**, 2100005.

*Equally contributing authors.

TABLE OF CONTENTS

LIST OF FIGURES AND TABLES

CHAPTER 1

CHAPTER 2

CHAPTER 3

CHAPTER 4

CHAPTER 5

CHAPTER 1

Biomaterial Strategies for Cancer Therapy

Synopsis. Although cancer afflicts many people around the world each year, we are becoming increasingly proficient at treating it. According to a 2020 report by the American Cancer Society, the overall cancer mortality rate declined by 29% in the United States from 1991–2017.[1] This chapter describes biomaterial-based strategies for improving cancer therapies.

1.1 An Age-Old Disease

Cancer was first documented in 3,000 B.C. by a scribe in Ancient Egypt.[2] He wrote, rather ominously:

"There is no treatment."[2]

The scribe's pessimism was warranted. For much of history, the only available cancer treatments were surgery and cauterization.[3]

At the turn of the 20th century, treatment regimens for cancer began to evolve.[3] Ionizing radiation was widely implemented as a cancer therapy within a few decades after the discovery of X-rays in 1896.[3] Shortly after the end of World War II, the first chemotherapeutic compounds were derived from mustard gas, the infamous chemical warfare agent.[3] Today, we have an astounding variety of cancer therapies available to us, ranging from small molecules to antibodies to genetically engineered cell therapies.[3,4]

1.2 Biomaterials Synergize with Existing Cancer Therapies

Most cancers are treated with a combination of surgery, radiotherapy, and chemotherapy.[4] Each of these treatment modalities has its disadvantages. Surgical resection and radiotherapy are only applicable for patients with accessible, solid tumors.[4] Chemotherapy is useful for patients presenting with disseminated tumors, but it often causes adverse side effects due to off-target drug toxicity.[5]

Biomaterials—defined by the National Institute of Biomedical Imaging and Bioengineering as materials "used in medical applications to support, enhance, or replace damaged tissue or a biological function"[6]—synergize well with existing cancer therapies and can mitigate some of their shortcomings.[5] Many researchers are using biomaterials to reduce the side

effects of chemotherapy drugs without sacrificing their potency.[5] This is usually accomplished by encapsulating drug molecules within a biomaterial or by conjugating drug molecules to the biomaterial.[5] By encapsulating the drug or forming a drug conjugate, the physicochemical properties of the drug may be altered in a therapeutically beneficial manner. For instance, loading a small molecule drug into lipid nanoparticles can increase the drug's stability and circulation half-life, reducing the dose required for therapeutic efficacy.[5,7]

Biomaterials can also be synthesized with stimuli-responsive properties, enabling fine control over how, where, and when a drug is released.[8] Some stimuli-responsive biomaterials respond to external stimuli administered by the user (e.g., focused ultrasound), while others react to physiological stimuli (e.g., enzyme activity).[8] For cancer drug delivery applications, biomaterials are often programmed to retain drug when circulating in healthy tissues, releasing their payloads after exposure to tumor-specific stimuli.[9–11] This concentrates drug at the tumor site, enhancing tumor killing without increasing systemic drug toxicity.[9–11]

While much biomaterials-related cancer research is focused on improving the efficiency of chemotherapeutic drug delivery, biomaterials can also augment the effectiveness of other cancer treatment modalities. For example, tumor-targeted gold nanoparticles may boost the intensity of locally administered ionizing radiation.[12] pH-sensitive "nanoprobes" that fluoresce in the acidic tumor microenvironment may help surgeons pinpoint and resect otherwise invisible tumors.[13] Given the array of raw materials, synthesis schemes, and biologically relevant stimuli available to researchers, biomaterials with unique designs and functions are constantly reported in the literature.

1.3 Potentiating Anticancer Immunity with Biomaterials

Immunotherapy—a form of therapy that leverages the body's immune system to eliminate tumors—is quickly emerging as a frontline treatment modality for cancer.[14] Several types of cancer

immunotherapy have been tested in the clinic, including immune checkpoint inhibitors (e.g., anti-PD-1 antibody therapies), cancer-targeted cell therapies (e.g., CAR T cell therapies), and cancer vaccines.[14–16]

Cancer immunotherapy only works because tumor cells may be recognized as foreign entities by the immune system, similar to how infectious pathogens are recognized and cleared from the body.[14,16,17] In general, an immune response against a pathogen is mounted upon recognition of an antigen, a biomolecule signature unique to the pathogen.[17,18] Antigen-presenting cells (APCs) take up antigen, process them, and present processed antigens to naïve T cells.[14,19] Upon recognition of an antigen presented by APCs, naïve T cells adopt functional effector phenotypes. $CD8^+$ "cytotoxic" T cells seek out and destroy cells that express the antigen (e.g., a lung cell infected by the pathogen), and $CD4^+$ "helper" T cells secrete cytokines that potentiate the activity of other immune cells.[14,19]

Like pathogens, tumor cells may express antigens recognized by the immune system.[14,17,18] However, tumor antigens are often poorly immunogenic—in other words, they do not activate sufficiently strong immune responses for tumor clearance.[14,20,21] Since tumor cells are dysregulated or mutated versions of healthy somatic cells, their antigens are frequently identical or similar to self-antigens, biomolecule signatures of healthy cells that the immune system does not recognize.[21,22] Furthermore, tumor cells normally do not express "danger signals" like pathogen-associated molecular patterns (PAMPs), which must be detected by an APC during antigen processing for the APC to prime effector T cell responses.[17,23]

The minimal immunogenicity of many tumor antigens has limited the efficacy of cancer vaccines developed to date.[21,24] Like most traditional vaccines for infectious diseases, cancer vaccines often consist of disease-specific antigens co-formulated with vaccine adjuvants, substances designed to enhance immune responses.[24,25] However, since many cancers occur spontaneously and are characterized by unpredictable antigen profiles, cancer vaccines are typically administered after a tumor is already established, whereas vaccines against infectious

diseases may be administered prophylactically.[22,24,26–29] This established disease burden, when coupled with low tumor antigen immunogenicity, renders many cancer vaccines ineffective.[21,24]

Biomaterials may improve the therapeutic efficacy of cancer vaccines. For instance, prior research has shown that encapsulation of antigens within nanoparticles can increase antigen trafficking to lymph nodes—small organs rich in immune cells—after subcutaneous or intradermal injection.[20,25,30–32] In addition, both antigens and vaccine adjuvants can be conjugated to a single biomaterial, maximizing antigen-specific immune responses by delivering both vaccine components into the same APC.[33–35] Incorporation of stimuli-responsive delivery mechanisms into a biomaterial vaccine allows for sustained release of vaccine components and/or controlled delivery into specific intracellular compartments after APC uptake.[25,36–39] Further research is needed to fully elucidate the physicochemical parameters—including size, shape, and surface charge—that determine biomaterial vaccine efficacy.[20,25,40]

1.4 Virus-Inspired Polymer for Endosomal Release

Our group recently reported a stimuli-responsive biomaterial known as the "Virus-Inspired Polymer for Endosomal Release," or VIPER.[41] This biomaterial was originally designed as a nonviral vector for nucleic acid delivery.[41–43] It is a copolymer of two blocks: a cationic hydrophilic block and an acid-responsive hydrophobic block (**Figure 1.1**).[41] The first block, consisting of water-soluble oligo(ethylene glycol) monomethyl ether methacrylate (OEGMA) monomers and positively charged 2-(dimethylamino)ethyl methacrylate (DMAEMA) monomers, interfaces electrostatically with nucleic acids and cell membranes, facilitating both nucleic acid complexation and cellular uptake. Under acidic conditions (pH < 6.5), hydrophobic 2-diisopropylaminoethyl methacrylate (DIPAMA) monomers in VIPER's second block transition into a hydrophilic state. Therefore, VIPER assembles into nanoparticulate micelles at neutral pH and disassembles back into free polymer at acidic pH.

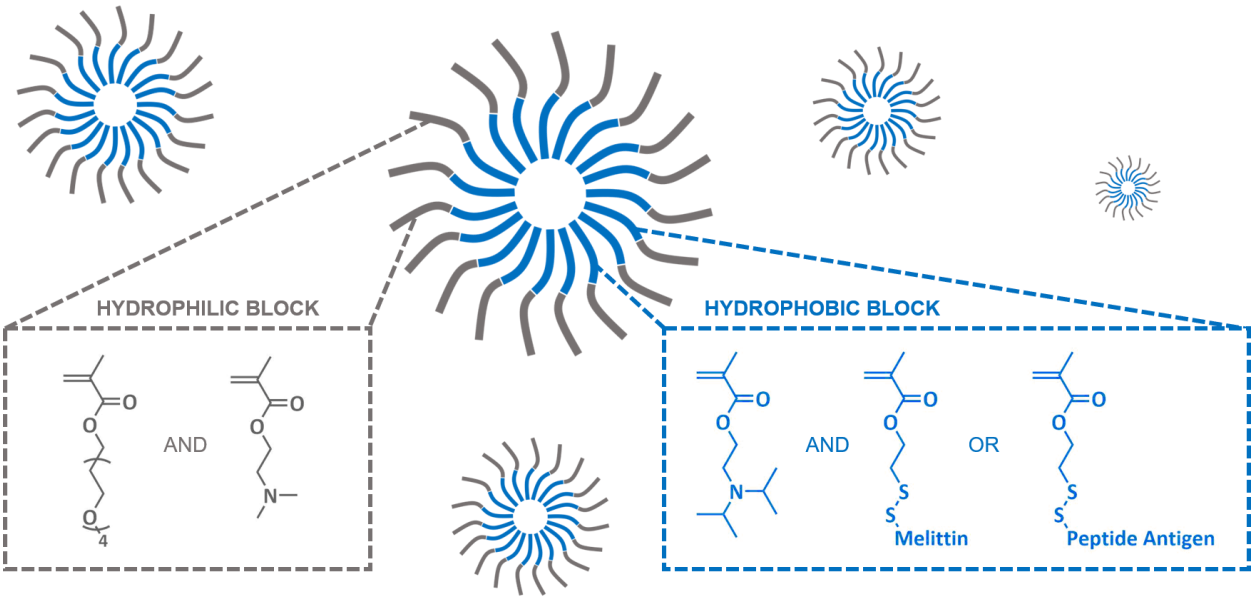

Figure 1.1 **Composition and function of VIPER.**[41] The cationic first block of VIPER (left) complexes nucleic acids and mediates their cellular uptake. The hydrophobic block (right) acts as a pH-responsive switch that assembles soluble polymer into micelles (at neutral pH) and disassembles micelles back into soluble polymer (at acidic pH). This second block is also functionalized with disulfide side groups for covalent conjugation of bioactive peptides. We have conjugated both melittin, a membrane-lytic peptide, and peptide antigen to the VIPER backbone.[41,44,45]

VIPER's (conditionally) hydrophobic second block is also interspersed with pyridyl disulfide ethyl methacrylate (PDSEMA) monomers for conjugation of cysteine-bearing peptides via a reversible disulfide bond (**Figure 1.1**).[41] Since VIPER micelle disassembly occurs under acidic conditions, PDSEMA-conjugated peptides are encapsulated within the micelle core under neutral pH conditions found in the extracellular space. Once the micelle is internalized into cells, the acidic pH of intracellular endosomal compartments drives micelle disassembly, exposing the attached peptides. The first generation of VIPER was conjugated to melittin, a cytolytic peptide that disrupts lipid membranes.[41,46] By shielding melittin within the VIPER micelle core until entry into acidic endosomal compartments, melittin's membrane-lytic effects are directed to endosomal membranes, enabling cytosolic delivery of complexed nucleic acids while minimizing melittin-associated cytotoxicity.[41] In principle, a multitude of thiolated biomolecules can be conjugated to

the VIPER backbone, and VIPER may be used to localize their bioactivities to the endosome and/or cytosol (**Figure 1.1**).[45,47]

This dissertation is focused on the application of VIPER as a cancer vaccine carrier. The modular nature of VIPER allows for conjugation and/or complexation of different peptide antigens and vaccine adjuvants.[45,47] We hypothesize that the membrane-disruptive properties of VIPER will enhance the bioactivity of co-formulated vaccine cargo. The subsequent chapters of this dissertation highlight our research efforts and describe next-generation VIPER variants for intracellular cancer vaccine delivery.

1.5 References

(1) Siegel, R. L.; Miller, K. D.; Jemal, A. Cancer Statistics, 2020. *CA. Cancer J. Clin.* **2020**, *70* (1), 7–30.

(2) American Cancer Society. Early History of Cancer. https://www.cancer.org/cancer/cancer-basics/history-of-cancer/what-is-cancer.html.

(3) Falzone, L.; Salomone, S.; Libra, M. Evolution of Cancer Pharmacological Treatments at the Turn of the Third Millennium. *Front. Pharmacol.* **2018**, *9*.

(4) Gale, R. P. Combination Cancer Therapy. https://www.merckmanuals.com/home/cancer/prevention-and-treatment-of-cancer/combination-cancer-therapy.

(5) Coburn, J. M.; Kaplan, D. L. Engineering Biomaterial-Drug Conjugates for Local and Sustained Chemotherapeutic Delivery. *Bioconjug. Chem.* **2015**, *26* (7), 1212–1223.

(6) National Institute of Biomedical Imaging and Bioengineering. Biomaterials. https://www.nibib.nih.gov/science-education/science-topics/biomaterials.

(7) Fenton, O. S.; Olafson, K. N.; Pillai, P. S.; Mitchell, M. J.; Langer, R. Advances in Biomaterials for Drug Delivery. *Adv. Mater.* **2018**, *30* (29), 1705328.

(8) Badeau, B. A.; DeForest, C. A. Programming Stimuli-Responsive Behavior into Biomaterials. *Annu. Rev. Biomed. Eng.* **2019**, *21* (1), 241–265.

(9) Huang, W.-C.; Chen, S.-H.; Chiang, W.-H.; Huang, C.-W.; Lo, C.-L.; Chern, C.-S.; Chiu, H.-C. Tumor Microenvironment-Responsive Nanoparticle Delivery of Chemotherapy for Enhanced Selective Cellular Uptake and Transportation within Tumor. *Biomacromolecules* **2016**, *17* (12), 3883–3892.

(10) Li, H.-J.; Du, J.-Z.; Du, X.-J.; Xu, C.-F.; Sun, C.-Y.; Wang, H.-X.; Cao, Z.-T.; Yang, X.-Z.; Zhu, Y.-H.; Nie, S.; et al. Stimuli-Responsive Clustered Nanoparticles for Improved Tumor Penetration and Therapeutic Efficacy. *Proc. Natl. Acad. Sci.* **2016**, *113* (15), 4164–4169.

(11) Chen, J.; Ding, J.; Wang, Y.; Cheng, J.; Ji, S.; Zhuang, X.; Chen, X. Sequentially Responsive Shell-Stacked Nanoparticles for Deep Penetration into Solid Tumors. *Adv. Mater.* **2017**, *29* (32), 1701170.

(12) Ngwa, W.; Boateng, F.; Kumar, R.; Irvine, D. J.; Formenti, S.; Ngoma, T.; Herskind, C.; Veldwijk, M. R.; Hildenbrand, G. L.; Hausmann, M.; et al. Smart Radiation Therapy Biomaterials. *Int. J. Radiat. Oncol.* **2017**, *97* (3), 624–637.

(13) Zhao, T.; Huang, G.; Li, Y.; Yang, S.; Ramezani, S.; Lin, Z.; Wang, Y.; Ma, X.; Zeng, Z.; Luo, M.; et al. A Transistor-like pH Nanoprobe for Tumour Detection and Image-Guided Surgery. *Nat. Biomed. Eng.* **2017**, *1*, 0006.

(14) Chen, D. S.; Mellman, I. Oncology Meets Immunology: The Cancer-Immunity Cycle. *Immunity* **2013**, *39* (1), 1–10.

(15) Topalian, S. L.; Taube, J. M.; Pardoll, D. M. Neoadjuvant Checkpoint Blockade for Cancer Immunotherapy. *Science* **2020**, *367* (6477), eaax0182.

(16) Knutson, K. L.; Schiffman, K.; Cheever, M. A.; Disis, M. L. Immunization of Cancer Patients with a HER-2/Neu, HLA-A2 Peptide, P369–377, Results in Short-Lived Peptide-Specific Immunity. *Clin. Cancer Res.* **2002**, *8* (5), 1014–1018.

(17) Galluzzi, L.; Buqué, A.; Kepp, O.; Zitvogel, L.; Kroemer, G. Immunogenic Cell Death in Cancer and Infectious Disease. *Nat. Rev. Immunol.* **2017**, *17* (2), 97–111.

(18) Black, M.; Trent, A.; Tirrell, M.; Olive, C. Advances in the Design and Delivery of Peptide Subunit Vaccines with a Focus on Toll-like Receptor Agonists. *Expert Rev. Vaccines* **2010**, *9* (2), 157–173.

(19) Chaplin, D. D. Overview of the Immune Response. *J. Allergy Clin. Immunol.* **2010**, *125* (2), S3–S23.

(20) Ke, X.; Howard, G. P.; Tang, H.; Cheng, B.; Saung, M. T.; Santos, J. L.; Mao, H. Q. Physical and Chemical Profiles of Nanoparticles for Lymphatic Targeting. *Adv. Drug Deliv. Rev.*

2019, *151–152*, 72–93.
(21) Bezu, L.; Kepp, O.; Cerrato, G.; Pol, J.; Fucikova, J.; Spisek, R.; Zitvogel, L.; Kroemer, G.; Galluzzi, L. Trial Watch: Peptide-Based Vaccines in Anticancer Therapy. *OncoImmunology* **2018**, *7* (12), e1511506.
(22) Finn, O. J. Human Tumor Antigens Yesterday, Today, and Tomorrow. *Cancer Immunol. Res.* **2017**, *5* (5), 347–354.
(23) Seya, T.; Shime, H.; Ebihara, T.; Oshiumi, H.; Matsumoto, M. Pattern Recognition Receptors of Innate Immunity and Their Application to Tumor Immunotherapy. *Cancer Sci.* **2010**, *101* (2), 313–320.
(24) Hollingsworth, R. E.; Jansen, K. Turning the Corner on Therapeutic Cancer Vaccines. *npj Vaccines* **2019**, *4*, 7.
(25) Irvine, D. J.; Hanson, M. C.; Rakhra, K.; Tokatlian, T. Synthetic Nanoparticles for Vaccines and Immunotherapy. *Chem. Rev.* **2015**, *115* (19), 11109–11146.
(26) Tomasetti, C.; Li, L.; Vogelstein, B. Stem Cell Divisions, Somatic Mutations, Cancer Etiology, and Cancer Prevention. *Science* **2017**, *355* (6331), 1330–1334.
(27) Barrow, C. Tumor Antigen Expression in Melanoma Varies According to Antigen and Stage. *Clin. Cancer Res.* **2006**, *12* (3), 764–771.
(28) Wang, S.; He, Z.; Wang, X.; Li, H.; Liu, X.-S. Antigen Presentation and Tumor Immunogenicity in Cancer Immunotherapy Response Prediction. *eLife* **2019**, *8*.
(29) Ehx, G.; Perreault, C. Discovery and Characterization of Actionable Tumor Antigens. *Genome Med.* **2019**, *11*, 29.
(30) Zhu, G.; Lynn, G. M.; Jacobson, O.; Chen, K.; Liu, Y.; Zhang, H.; Ma, Y.; Zhang, F.; Tian, R.; Ni, Q.; et al. Albumin/Vaccine Nanocomplexes That Assemble In Vivo for Combination Cancer Immunotherapy. *Nat. Commun.* **2017**, *8*, 1954.
(31) Lynn, G. M.; Sedlik, C.; Baharom, F.; Zhu, Y.; Ramirez-Valdez, R. A.; Coble, V. L.; Tobin, K.; Nichols, S. R.; Itzkowitz, Y.; Zaidi, N.; et al. Peptide–TLR-7/8a Conjugate Vaccines Chemically Programmed for Nanoparticle Self-Assembly Enhance CD8 T-Cell Immunity to Tumor Antigens. *Nat. Biotechnol.* **2020**, *38* (3), 320–332.
(32) Reddy, S. T.; Rehor, A.; Schmoekel, H. G.; Hubbell, J. A.; Swartz, M. A. In Vivo Targeting of Dendritic Cells in Lymph Nodes with Poly(Propylene Sulfide) Nanoparticles. *J. Control. Release* **2006**, *112* (1), 26–34.
(33) Wilson, D. S.; Hirosue, S.; Raczy, M. M.; Bonilla-Ramirez, L.; Jeanbart, L.; Wang, R.; Kwissa, M.; Franetich, J.-F.; Broggi, M. A. S.; Diaceri, G.; et al. Antigens Reversibly Conjugated to a Polymeric Glyco-Adjuvant Induce Protective Humoral and Cellular Immunity. *Nat. Mater.* **2019**, *18* (2), 175–185.
(34) Scott, E. A.; Stano, A.; Gillard, M.; Maio-Liu, A. C.; Swartz, M. A.; Hubbell, J. A. Dendritic Cell Activation and T Cell Priming with Adjuvant- and Antigen-Loaded Oxidation-Sensitive Polymersomes. *Biomaterials* **2012**, *33* (26), 6211–6219.
(35) Miao, L.; Li, L.; Huang, Y.; Delcassian, D.; Chahal, J.; Han, J.; Shi, Y.; Sadtler, K.; Gao, W.; Lin, J.; et al. Delivery of mRNA Vaccines with Heterocyclic Lipids Increases Anti-Tumor Efficacy by STING-Mediated Immune Cell Activation. *Nat. Biotechnol.* **2019**, *37* (10), 1174–1185.
(36) Keller, S.; Wilson, J. T.; Patilea, G. I.; Kern, H. B.; Convertine, A. J.; Stayton, P. S. Neutral Polymer Micelle Carriers with pH-Responsive, Endosome-Releasing Activity Modulate Antigen Trafficking to Enhance $CD8^+$ T Cell Responses. *J. Control. Release* **2014**, *191*, 24–33.
(37) Wilson, J. T.; Keller, S.; Manganiello, M. J.; Cheng, C.; Lee, C. C.; Opara, C.; Convertine, A.; Stayton, P. S. pH-Responsive Nanoparticle Vaccines for Dual-Delivery of Antigens and Immunostimulatory Oligonucleotides. *ACS Nano* **2013**, *7* (5), 3912–3925.
(38) Qiu, F.; Becker, K. W.; Knight, F. C.; Baljon, J. J.; Sevimli, S.; Shae, D.; Gilchuk, P.; Joyce, S.; Wilson, J. T. Poly(Propylacrylic Acid)-Peptide Nanoplexes as a Platform for Enhancing

the Immunogenicity of Neoantigen Cancer Vaccines. *Biomaterials* **2018**, *182*, 82–91.
(39) Li, A. W.; Sobral, M. C.; Badrinath, S.; Choi, Y.; Graveline, A.; Stafford, A. G.; Weaver, J. C.; Dellacherie, M. O.; Shih, T.-Y.; Ali, O. A.; et al. A Facile Approach to Enhance Antigen Response for Personalized Cancer Vaccination. *Nat. Mater.* **2018**, *17* (6), 528–534.
(40) Irvine, D. J.; Swartz, M. A.; Szeto, G. L. Engineering Synthetic Vaccines Using Cues from Natural Immunity. *Nat. Mater.* **2013**, *12* (11), 978–990.
(41) Cheng, Y.; Yumul, R. C.; Pun, S. H. Virus-Inspired Polymer for Efficient In Vitro and In Vivo Gene Delivery. *Angew. Chemie Int. Ed.* **2016**, *55* (39), 12013–12017.
(42) Feldmann, D. P.; Cheng, Y.; Kandil, R.; Xie, Y.; Mohammadi, M.; Harz, H.; Sharma, A.; Peeler, D. J.; Moszczynska, A.; Leonhardt, H.; et al. In Vitro and In Vivo Delivery of siRNA via VIPER Polymer System to Lung Cells. *J. Control. Release* **2018**, *276*, 50–58.
(43) Yen, A.; Cheng, Y.; Sylvestre, M.; Gustafson, H. H.; Puri, S.; Pun, S. H. Serum Nuclease Susceptibility of mRNA Cargo in Condensed Polyplexes. *Mol. Pharm.* **2018**, *15* (6), 2268–2276.
(44) Sylvestre, M.; Lv, S.; Yang, L. F.; Luera, N.; Peeler, D. J.; Chen, B.-M.; Roffler, S. R.; Pun, S. H. Replacement of L-Amino Acid Peptides with D-Amino Acid Peptides Mitigates Anti-PEG Antibody Generation against Polymer-Peptide Conjugates in Mice. *J. Control. Release* **2021**, *331*, 142–153.
(45) Peeler, D. J.; Yen, A.; Luera, N.; Stayton, P. S.; Pun, S. H. Lytic Polyplex Vaccines Enhance Antigen-Specific Cytotoxic T Cell Response through Induction of Local Cell Death. *Adv. Ther.* **2021**, 2100005.
(46) Huang, C.; Jin, H.; Qian, Y.; Qi, S.; Luo, H.; Luo, Q.; Zhang, Z. Hybrid Melittin Cytolytic Peptide-Driven Ultrasmall Lipid Nanoparticles Block Melanoma Growth In Vivo. *ACS Nano* **2013**, *7* (7), 5791–5800.
(47) Peeler, D. J.; Thai, S. N.; Cheng, Y.; Horner, P. J.; Sellers, D. L.; Pun, S. H. pH-Sensitive Polymer Micelles Provide Selective and Potentiated Lytic Capacity to Venom Peptides for Effective Intracellular Delivery. *Biomaterials* **2019**, *192*, 235–244.

CHAPTER 2

Serum Nuclease Susceptibility of mRNA Cargo in Condensed Polyplexes[†]

Albert Yen, Yilong Cheng, Meilyn Sylvestre, Heather H. Gustafson,
Sanyogitta Puri, and Suzie H. Pun

Synopsis. As the biomolecular "blueprint" for cellular protein synthesis, messenger RNA (mRNA) has many promising clinical applications. However, the instability of mRNA and its susceptibility to degradation by ribonucleases (RNases) necessitate the use of specialized formulations for delivery. Polycations are an emerging class of synthetic materials capable of packaging nucleic acids and may serve as stable, RNase-resistant carriers for mRNA administration. Here, we investigate whether the "Virus-Inspired Polymer for Endosomal Release" (VIPER) and the "sunflower" polycation—two cationic polymers previously synthesized by our group—could be used for delivery of mRNA. Both polycations efficiently deliver plasmid DNA (pDNA) to cultured cells. Although initial transfection studies were conducted with reporter gene mRNAs, our ultimate goal was to use VIPER and sunflower polycation for mRNA vaccine delivery. However, despite condensing and packaging mRNA with high efficiency, VIPER and sunflower polycation only transfect mRNA under serum-free conditions, whereas pDNA transfection was achieved even in the presence of serum. RNase resistance studies confirm that nuclease degradation of mRNA cargo remains a significant barrier to mRNA delivery using these polycations. These results emphasize that protection of administered mRNA drugs from endogenous nuclease activity may require more than just electrostatic complexation with polycation.

[†]Adapted with permission from: **Yen, A.**; Cheng, Y.; Sylvestre, M.; Gustafson, H. H.; Puri, S.; Pun, S. H. Serum Nuclease Susceptibility of mRNA Cargo in Condensed Polyplexes. *Mol. Pharm.* **2018**, *15* (6), 2268–2276.

2.1 Introduction

Messenger RNA (mRNA) therapies are emerging as an attractive alternative to plasmid DNA (pDNA) therapies. mRNA initially garnered less interest as a drug than pDNA because it is highly susceptible to degradation by ribonucleases (RNases) and difficult to produce on a clinically relevant scale.[1] However, recent advances in nucleoside chemistry have led to the improved stability, increased protein production yield, and reduced immunogenicity of mRNA synthesized by in vitro transcription.[2–5] Consequently, there has been a resurgence of interest in mRNA therapeutics.[6,7]

While both mRNA and pDNA are "blueprints" for therapeutic protein production, mRNA offers several benefits over pDNA. First, mRNA-induced effects are transient and do not carry risk of chromosomal integration and mutagenesis.[8] Second, mRNA is translated in the cytoplasm, allowing for efficient therapeutic protein expression in nondividing cell populations by circumventing nuclear translocation.[9–11] In contrast, pDNA must be delivered into the nucleus for transcription to occur, a major challenge for certain viral vectors and all synthetic carriers.[12,13] Finally, self-amplifying mRNA, which encode RNA replication machinery alongside therapeutic proteins, are potentially more effective than pDNA for vaccine applications because of their increased protein yield.[14,15] Despite the promise of mRNA therapies, administration of mRNA is complicated by several biological barriers. First, the negative charge of mRNA limits cytoplasmic translocation.[16,17] Furthermore, RNases present in serum rapidly degrade naked mRNA.[16] Therefore, mRNA administration requires carriers that can facilitate cytoplasmic entry of mRNA cargo while protecting this cargo from RNase activity, without compromising mRNA translation and subsequent protein expression.[11,16]

Due to their relatively high transduction efficiency, viruses are one of the most commonly used carriers for therapeutic genes.[16] But the prohibitive cost, immunogenicity, and mutagenic potential of viral vectors have motivated the development of alternative platforms for gene

delivery.[18] Lipid-based formulations for gene delivery have been described extensively in the literature, and a number of pharmaceutical companies are currently conducting gene therapy clinical trials with lipid nanoparticle technology.[19] However, the overall efficacy of lipid-based gene delivery is limited by rapid clearance kinetics, suboptimal serum stability, and immunogenicity of formulation components.[16,19]

Cationic polymers, or polycations, are another promising nonviral formulation for the delivery of genes.[18] Electrostatic interactions between the positively charged side chains of polycations and the negatively charged sugar phosphate backbones of nucleic acids mediate the formation of nucleic acid–polycation complexes, or polyplexes.[18] After cellular uptake, polyplexes typically escape the endolysosomal network via endosomal buffering mechanisms.[18] pDNA cargo is subsequently translocated to the nucleus for transcription, or mRNA cargo is translated in the cytoplasm.[16,18]

Numerous monomers and polymerization techniques are available for syntheses of polycations with diverse structures and functions. Our group has synthesized many polycations for nucleic acid delivery both in vitro and in vivo.[20–22] Two of these polycations are (i) the "Virus-Inspired Polymer for Endosomal Release" (VIPER) and (ii) the "sunflower" polycation.[21,22] VIPER is a block copolymer functionalized with melittin, a lytic peptide that ruptures the endosomal membrane, allowing polyplex cargo to rapidly escape into the cytoplasm.[21] Sunflower polycation is a cyclic polymer with cationic "petals" grafted from a circular backbone (**Figure 2.1**).[22] Both polycations possess unique properties that make them suitable for delivery of pDNA.[21,22]

Here, we utilize VIPER and sunflower polycation for mRNA delivery in comparison to branched polyethylenimine (bPEI), a commercially available "gold standard" polycation used for transfection.[18] We specifically investigate the mechanisms by which mRNA polyplex transfection differs from pDNA polyplex transfection. The results of this work demonstrate that proper protection of nucleic acid cargo from nuclease activity is more critical for mRNA polyplexes than pDNA polyplexes. Neither VIPER nor sunflower polycation protect mRNA cargo during

transfection in serum-containing media; nuclease resistance assays confirm that mRNA remains susceptible to nuclease digestion even when packaged by VIPER or sunflower polycation. Synthetic modifications to our polycation delivery systems must be implemented to achieve mRNA transfection in RNase-rich conditions.

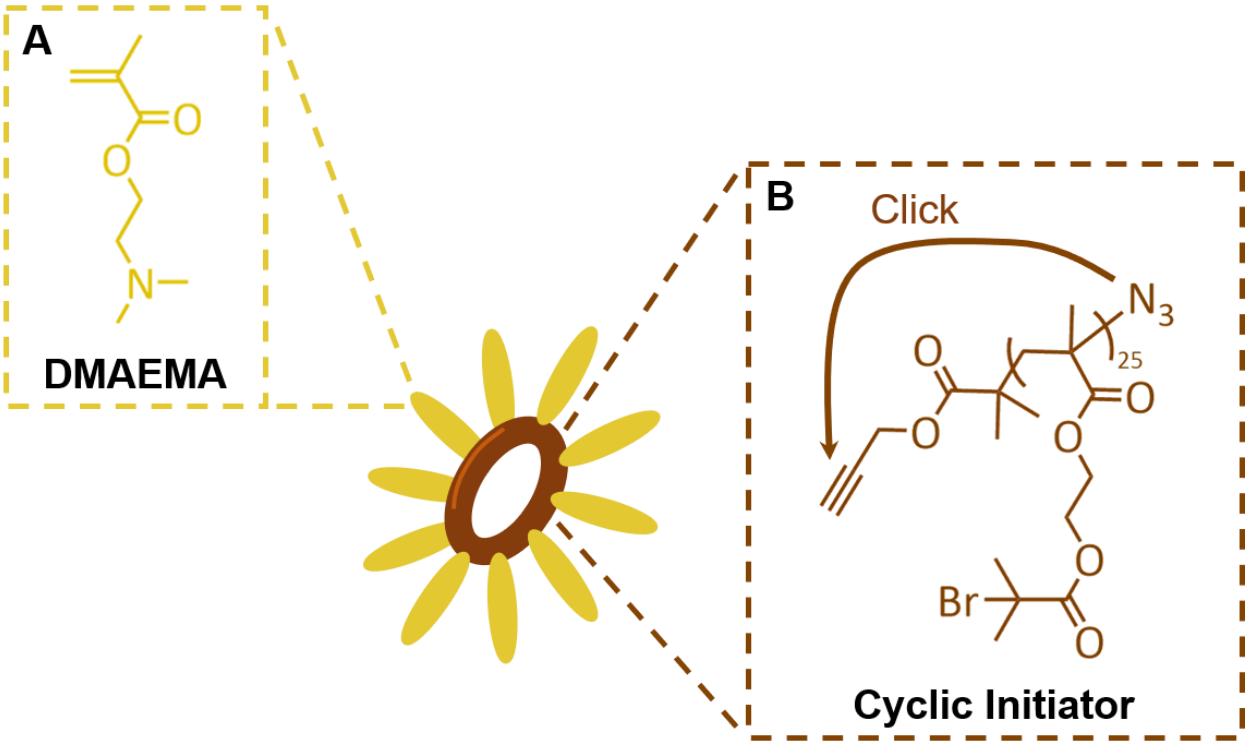

Figure 2.1 **Structure of the sunflower polycation.[22] (A)** Cationic, petal-like polymer chains decorate a **(B)** cyclic polymer backbone. See *Section 2.2.3* for a brief description of the synthesis scheme.

2.2 Experimental Section

2.2.1 Materials

Firefly luciferase mRNA (5meC, Ψ, L-6107), enhanced green fluorescent protein mRNA (5meC, Ψ, L- 6101), and cyanine 5 enhanced green fluorescent protein mRNA (5meC, Ψ, L-6402) were purchased from TriLink BioTechnologies. Branched polyethylenimine (bPEI), average M_w ~25,000, was purchased from Sigma-Aldrich.

2.2.2 VIPER synthesis

VIPER was synthesized using reversible addition–fragmentation chain-transfer polymerization (RAFT) as previously described.[21] Briefly, the hydrophilic block was copolymerized from oligo(ethylene glycol) monomethyl ether methacrylate (OEGMA) and 2-(dimethylamino)ethyl methacrylate (DMAEMA). p(OEGMA-DMAEMA) was then used as a macro chain transfer agent to polymerize the hydrophobic block, which consisted of 2-diisopropylaminoethyl methacrylate (DIPAMA) and pyridyl disulfide ethyl methacrylate (PDSEMA). The lytic peptide melittin was conjugated to PDSEMA via disulfide exchange, and the final product p($OEGMA_{11}$-$DMAEMA_{56}$)-*b*-p($DIPAMA_{26}$-(PDSE-melittin)$_1$) was obtained.

2.2.3 Sunflower polycation synthesis

Sunflower polycation was synthesized using atom transfer radical polymerization (ATRP) as previously described.[22] Briefly, the cyclic 2-hydroxylethyl methacrylate (HEMA) backbone was synthesized using ATRP and an interchain click macrocyclization (**Figure 2.1**). DMAEMA side chains were subsequently polymerized from the p(HEMA) backbone using a grafting-from approach, and the final product *c*-p$(HEMA)_{25}$-*g*-(p$(DMAEMA)_{22})_{25}$ was obtained.

2.2.4 Polyplex formulation

Polycations and nucleic acids were suspended in molecular biology grade water for in vitro studies and 5% (w/v) glucose for in vivo studies. Polyplexes were then formulated by adding aqueous polycation to an equivalent volume of 0.1 mg/mL nucleic acid at the desired nitrogen to phosphate (N/P) ratio.

2.2.5 ζ-potentials and hydrodynamic diameters of polyplexes

Polyplexes were formulated at N/P = 5. Twenty microliters of polyplex were diluted to a final volume of 800 μL in 10 mM NaCl, and diluted polyplex was loaded into a DTS1070 Zetasizer cell

(Malvern Instruments). A Zetasizer Nano ZS (Malvern Instruments) was used to measure the ζ-potentials and hydrodynamic diameters of polyplexes.

2.2.6 Transmission electron microscopy

Polyplexes were formulated at N/P = 5. Ten microliters of polyplex solution were applied onto 400 mesh Formvar/copper grids (Ted Pella). After 30 min, grids were whisked dry by filter paper, and polyplex samples were stained with 4% (w/v) aqueous uranyl acetate. After uranyl acetate staining, grids were again whisked dry by filter paper and allowed to dry overnight. Polyplex images were taken at 20,000× magnification with a JEOL JEM 1400 electron microscope (Fred Hutchinson Cancer Research Center).

2.2.7 Gel condensation assay

Polyplexes were formulated at N/P = 5 and loaded onto a denaturing 1% (w/v) agarose gel composed of 1× MOPS buffer (Thermo Fisher Scientific) and 37% (w/v) formaldehyde (Sigma-Aldrich). Gels were electrophoresed at 110 V for 45 min and subsequently stained with SYBR™ Gold (Thermo Fisher Scientific). Gels were then imaged with a Gel Doc EZ Gel Documentation System (Bio-Rad).

2.2.8 Fluorophore packaging assay

Polyplexes were formulated at N/P = 5. A working solution of RiboGreen™ nucleic acid dye (Thermo Fisher Scientific) was prepared by diluting RiboGreen™ stock solution 200-fold in 1× TE buffer. One hundred microliters of polyplex (diluted in 1× TE buffer to a final nucleic acid concentration of 2 μg/mL) was added to 100 μL of RiboGreen™ working solution and incubated at room temperature for 5 min. The fluorescence intensity of polyplex cargo was measured via fluorescence spectroscopy at excitation/emission wavelengths of 480/520 nm.

2.2.9 Luciferase reporter gene transfection

HeLa cells (ATCC) were seeded in 12-well plates at 4×10^4 cells/well. Cells were incubated overnight in complete media formulated by adding 10% fetal bovine serum (FBS; Gibco) to Minimal Essential Media (MEM; Gibco). After overnight incubation, parallel transfections were performed in complete media and serum-free OptiMEM (Gibco). For complete media transfections, cells were transfected with 2 μg/well of either pCMV-Luc2 plasmid (Luc pDNA) or luciferase mRNA (Luc mRNA). VIPER, sunflower polycation, and bPEI were used as transfection reagents with all polyplexes formulated at N/P = 5. Cells were incubated with transfection reagent for 4 h at 37 °C. For serum-free OptiMEM transfections, cells were transfected with 1 μg/well of either Luc pDNA or Luc mRNA. VIPER, sunflower polycation, and bPEI were used as transfection reagents, with polyplexes formulated at N/P = 3, 5, and 5, respectively. Cells were incubated with transfection reagent for 1 h at 37 °C. After transfection, cells were washed with phosphate-buffered saline (PBS) and incubated for 24 h. Luciferase reporter gene expression was subsequently quantified with a Luciferase Assay System (Promega) according to manufacturer protocol, and total protein content per well was quantified by a Micro BCA™ assay (Thermo Fisher Scientific). Luciferase expression was then reported in relative light units (RLU) and normalized to total protein content on a per well basis.

2.2.10 GFP reporter gene transfection

HeLa cells were seeded in 12-well plates at 4×10^4 cells/well and incubated overnight in complete media formulated by adding 10% FBS to MEM. After overnight incubation, parallel transfections were performed in complete media and serum-free OptiMEM. For complete media transfections, cells were transfected with 2 μg/well of either pmaxGFP plasmid (GFP pDNA) or enhanced green fluorescent protein mRNA (GFP mRNA). VIPER, sunflower polycation, and bPEI were used as transfection reagents, with all polyplexes formulated at N/P = 5. Cells were incubated with transfection reagent for 4 h at 37 °C. For serum-free OptiMEM transfections, cells were

transfected with 1 μg/well of either GFP pDNA or GFP mRNA. VIPER, sunflower polycation, and bPEI were used as transfection reagents, with polyplexes formulated at N/P = 3, 5, and 5, respectively. Cells were incubated with transfection reagent for 1 h at 37 °C. After transfection, cells were washed with PBS and incubated for 24 h. Cells were then stained with Zombie NIR™ (BioLegend), and the percentage of viable cells expressing GFP was quantified by flow cytometry.

2.2.11 Cellular association of mRNA polyplexes

In a first experiment, HeLa cells were seeded in 24-well plates at 4×10^4 cells/well and incubated overnight in complete media formulated by adding 10% FBS to MEM. VIPER, sunflower, and bPEI polyplexes were formulated at N/ P = 3, 5, and 5, respectively, with cargo consisting of GFP mRNA labeled with cyanine 5 (Cy5). HeLa cells were then incubated with these polyplex formulations in serum-free OptiMEM at an equivalent mRNA dose of 0.5 μg/well. After 30 min of incubation at 37 °C, transfection media containing polyplexes was collected from each well, and the Cy5 fluorescence intensity remaining in the media was quantified by fluorescence spectroscopy at excitation/emission wavelengths of 649/666 nm. To determine the percentage of polyplexes bound to cells, the measured Cy5 fluorescence intensities of transfection media samples were divided by the Cy5 fluorescence intensities of those obtained from wells containing no cells. In a second experiment, HeLa cells were seeded in 12-well plates at 8×10^4 cells/well and incubated overnight in complete media formulated by adding 10% FBS to MEM. After overnight incubation, parallel transfections were performed in complete media and serum-free OptiMEM. For both complete media and serum-free OptiMEM transfections, 1 μg/well of Cy5-labeled GFP mRNA was administered. VIPER, sunflower polycation, and bPEI were used as transfection reagents, with VIPER, sunflower, and bPEI polyplexes formulated at N/P = 3, 5, and 5, respectively. After 30 min of incubation with polyplexes at 37 °C, cells were immediately harvested for staining with Zombie Violet™ (BioLegend). The percentage of viable Cy5-positive cells, along with Cy5 median fluorescence intensity, was quantified by flow cytometry.

2.2.12 Nuclease resistance assay

Polyplexes were formulated at N/P = 5 and incubated at 37 °C in the presence of 15 μg/mL ribonuclease (RNase) A (Thermo Fisher Scientific) or 10% FBS for 1 h. The formulation pH was then increased to 10.2 for VIPER and sunflower polyplexes and to 12.8 for bPEI polyplexes to reverse binding of mRNA to polycation. mRNA fragments greater than 200 nucleotides in length were recovered using a RNeasy Mini Kit (Qiagen). During the recovery process, RNA spin columns were rinsed with a denaturing buffer, inactivating RNases in the polyplex samples. Recovered mRNA was stained with RiboGreen™ nucleic acid dye, and fluorescence spectroscopy was used to measure the fluorescence intensity of recovered mRNA at excitation/emission wavelengths of 480/520 nm. A RiboGreen™ standard curve was prepared according to the manufacturer protocol, and the quantity of recovered mRNA was determined using this standard curve. The quantities of recovered RNase- and FBS-treated mRNA were normalized to that of untreated mRNA.

2.2.13 Intratumoral mRNA delivery

All animal procedures were conducted under protocols approved by the Institutional Animal Care and Use Committee at the University of Washington. Intratumoral transfection efficiency in mice was measured as previously described.[21] Female BALB/c mice (Charles River Laboratories), 4–5 weeks old, were subcutaneously inoculated in the right hind flank with 10^6 CT26 mouse colon carcinoma cells (ATCC). Tumor volumes were calculated every two days after inoculation using the equation $V = (L \times W^2)/2$, with tumor dimensions obtained via caliper measurements. After 11 days, when tumor volumes reached ~150 mm^3, tumors were transfected with 10 μg of Luc mRNA using VIPER and bPEI as transfection reagents, with polyplexes formulated at N/P = 10 in 50 μL of 5% (w/v) glucose. Tumors were harvested 10 h after mRNA transfection and immersed in Reporter Lysis Buffer (Promega) with added cOmplete™ protease inhibitor (Roche). After three freeze-thaw cycles in liquid nitrogen, tumors were mechanically homogenized. Homogenized

tumor samples were then centrifuged at 2.1×10^4 rcf for 15 min at 4 °C. Luciferase content in recovered supernatant was quantified with a Luciferase Assay System according to manufacturer protocol. Total protein content per tumor was quantified by a Micro BCA™ assay. Luciferase expression was then reported in RLU and normalized to total protein content on a per tumor basis.

2.2.14 Statistical analyses

Significance between two group means was calculated using a two-tailed Student's t-test. Significance across multiple group means was calculated using an one-way ANOVA with post-hoc Tukey HSD test. All statistical analyses were performed in Microsoft Excel or GraphPad Prism. All flow cytometry data were analyzed in FlowJo software.

2.3 Results and Discussion

2.3.1 Reporter gene mRNA packaging by VIPER and sunflower polycation

VIPER (p(OEGMA$_{11}$-DMAEMA$_{56}$)-*b*-p(DIPAMA$_{26}$-(PDSE-melittin)$_1$)) and sunflower (*c*-p(HEMA)$_{25}$-*g*-(p(DMAEMA)$_{22}$)$_{25}$) polycations have been shown to efficiently package pDNA of varying size.[21,22] We first investigated whether VIPER and sunflower polycation could also package mRNA. To assess the mRNA packaging efficiency of these two polycations, we selected a 996-nucleotide enhanced green fluorescent protein mRNA (GFP mRNA) and a 1,921-nucleotide firefly luciferase mRNA (Luc mRNA). Polyplexes were formulated by adding polycation solution directly to an equal volume of mRNA solution (**Figure 2.2A**). Corresponding pDNA polyplexes were formulated with pCMV-Luc2 (Luc pDNA) and pmaxGFP (GFP pDNA) plasmids. Successful packaging of both GFP mRNA and Luc mRNA by VIPER and sunflower polycation at N/P = 5 was demonstrated by a gel condensation assay (**Supplemental Figure 2.1**). A fluorophore packaging assay further showed mRNA packaging by these polycations, where fluorescent signal

associated with free mRNA was quenched upon the addition of polycation (**Supplemental Figure 2.2**). The ζ-potentials and hydrodynamic diameters of VIPER and sunflower mRNA polyplexes were comparable to those of their pDNA counterparts and were also similar to those reported for bPEI mRNA polyplexes (**Supplemental Figure 2.3**).[23] Transmission electron microscopy (TEM) images confirmed formation of amorphous but distinct mRNA polyplexes with diameters of approximately 50–200 nm (**Figure 2.2B**).

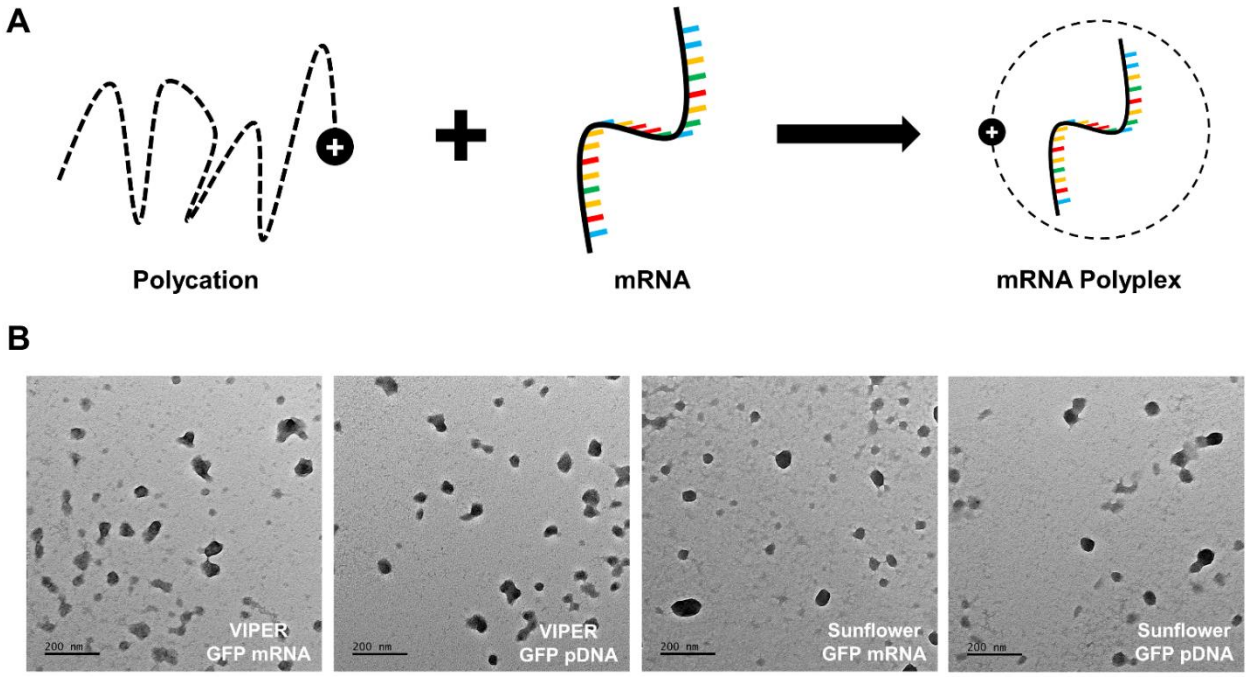

Figure 2.2 **VIPER and sunflower polycation readily form polyplexes with mRNAs of varying length. (A)** Polyplexes were formulated by adding polycations directly to either GFP mRNA (996 nucleotides) or Luc mRNA (1,921 nucleotides). **(B)** As shown by transmission electron microscopy, VIPER and sunflower polycation formed polyplexes of approximately 50–200 nm in diameter when formulated with GFP mRNA or Luc mRNA. The diameters of VIPER and sunflower pDNA polyplexes were comparable to those of corresponding mRNA polyplexes (20,000× magnification; scale bar = 200 nm).

2.3.2 Reporter gene mRNA transfection in cultured cells

We previously showed that VIPER and sunflower polycation could deliver pDNA with high efficiency.[21,22] To determine whether VIPER and sunflower polycation could also deliver mRNA

with high efficiency, we used Luc mRNA and GFP mRNA as transgene reporters in cell transfection studies. First, HeLa cells were transfected with Luc mRNA using VIPER, sunflower polycation, and bPEI as transfection reagents, and cellular bioluminescence was quantified 24 h after transfection. Transfections were performed in complete media, which was formulated by adding 10% fetal bovine serum (FBS) to minimal essential media (MEM). Because serum proteins may block transfection by adsorbing to polyplexes and disrupting nucleic acid–polycation interactions, we also performed parallel transfections in serum-free OptiMEM to ascertain whether removing serum could improve mRNA transfection efficiency.[18,20] For complete media transfections, we transfected 2 μg/well of nucleic acid using a N/P = 5 for all polyplexes. For serum-free OptiMEM transfections, we transfected only 1 μg/well of nucleic acid at optimized N/P ratios for VIPER, sunflower, and bPEI polyplexes to minimize polymer toxicity, which is normally mitigated by serum proteins in complete media (**Supplemental Table 2.1**). Transfection of Luc mRNA in serum-free OptiMEM gave rise to significant levels of bioluminescence (**Figure 2.3A**). However, no bioluminescence was observed in HeLa cells 24 h after transfection in complete media with either VIPER or sunflower polycation, whereas minimal bioluminescence was observed in cells transfected with bPEI (**Figure 2.3A**). In contrast, significant luciferase expression was observed in cells transfected with Luc pDNA, regardless of media condition or polycation used for transfection (**Figure 2.3B**).

Transfections of HeLa cells with GFP mRNA and GFP pDNA were then performed under conditions identical to those used for Luc mRNA and Luc pDNA transfections. The percentage of HeLa cells transfected with GFP mRNA was quantified by flow cytometry and compared to the percentage of HeLa cells transfected with GFP pDNA. Despite administering only half the amount of mRNA used for complete media transfections, we observed significant transfection of GFP mRNA (over 60% of cells transfected) in serum-free OptiMEM (**Figure 2.3C**). Conversely, VIPER and sunflower polycation were unable to efficiently transfect HeLa cells with GFP mRNA in complete media (**Figure 2.3C**). VIPER and sunflower polycation could transfect HeLa cells

with GFP pDNA in complete media, although GFP pDNA transfection by sunflower polycation was attenuated to some degree (**Figure 2.3D**). Minimal transfection of both GFP mRNA and GFP pDNA (less than 5% of cells transfected) was observed in both complete media and serum-free OptiMEM when bPEI was used as the transfection reagent, with no significant difference in transfection efficiency between the two media conditions (**Figure 2.3C,D**).

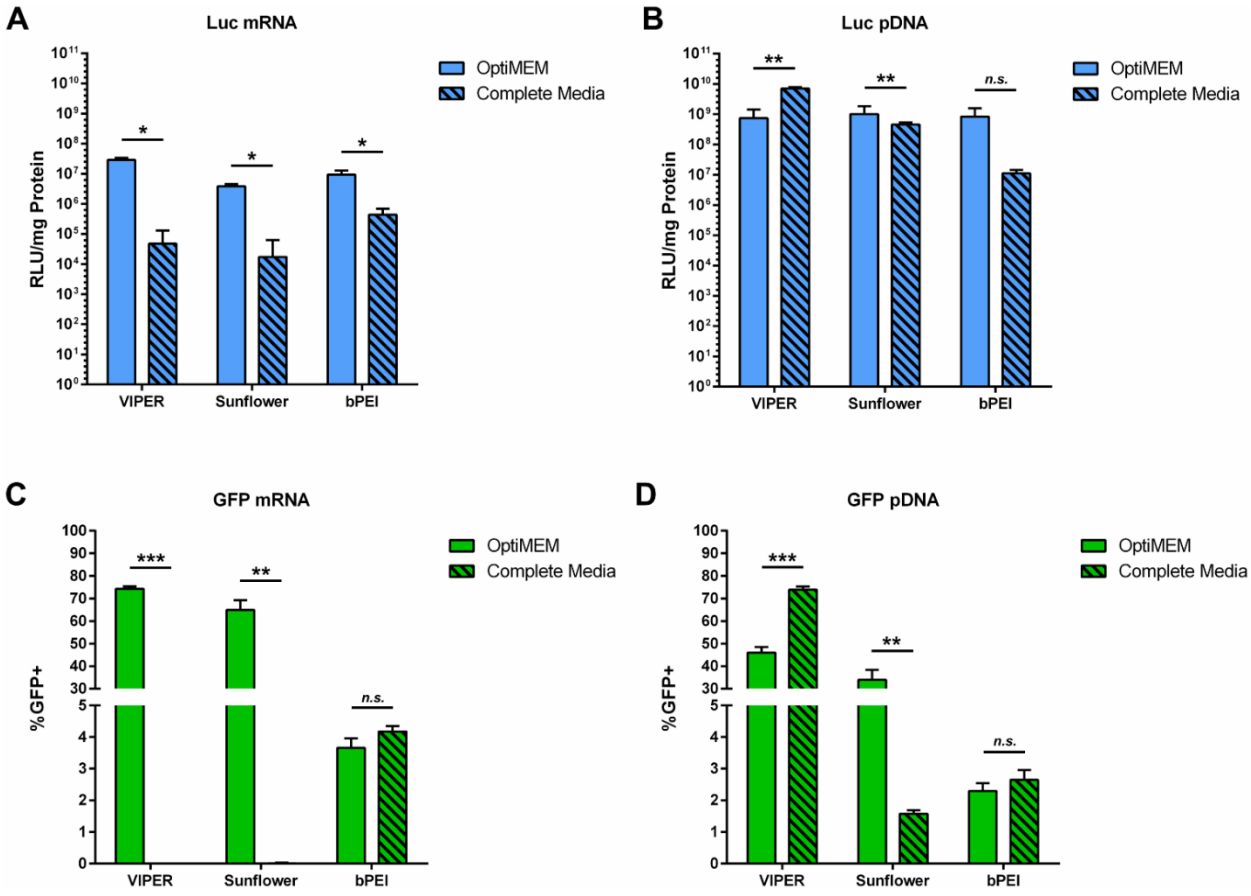

Figure 2.3 **The presence of serum prevents transfection by mRNA polyplexes. (A)** Luc mRNA transfection efficiency was poor in complete media regardless of polycation used. Significantly greater mRNA transfection levels were observed in serum-free OptiMEM. **(B)** For all polycations, significant transfection of Luc pDNA was observed in both complete media and serum-free OptiMEM. **(C)** Significant GFP mRNA transfection was achieved in serum-free OptiMEM using VIPER and sunflower polycation, but no transfection was observed in serum-containing complete media using these same polycations. Some expression of GFP was observed in complete media with bPEI mRNA polyplexes. **(D)** All polycations transfected GFP pDNA in complete media. Data are expressed as mean + SD, $n = 3$ (*p-value ≤ 0.05; **p-value ≤ 0.01; ***p-value ≤ 0.001; *n.s.* = no significance; Student's t-test). Bioluminescence is expressed in relative light units (RLU).

2.3.3 Cellular association of mRNA polyplexes

Because VIPER and sunflower polycation could efficiently transfect HeLa cells with mRNA under serum-free conditions, we identified serum proteins as a potential barrier to mRNA transfection by these polycations. We first confirmed binding of polyplexes to cells by incubating HeLa cells in serum-free OptiMEM with VIPER, sunflower, and bPEI polyplexes packaging a GFP mRNA labeled with cyanine 5 (Cy5). After a 30 min incubation period, the decrease in Cy5 fluorescence intensity of the transfection media was used to quantify the percentage of polyplexes bound to cells. We then investigated whether serum proteins were blocking cellular association of mRNA polyplexes by transfecting HeLa cells with Cy5-labeled GFP mRNA using VIPER, sunflower polycation, and bPEI as transfection reagents. Cells were harvested 30 min after the addition of transfection reagent, and Cy5-positive cells were analyzed by flow cytometry to measure the cellular association of mRNA polyplexes.

We showed that approximately 13% of VIPER mRNA polyplexes, 12% of sunflower mRNA polyplexes, and 16% of bPEI mRNA polyplexes were bound to HeLa cells after 30 min of incubation in serum-free OptiMEM (**Supplemental Figure 2.4**). More importantly, VIPER, sunflower, and bPEI polyplexes formulated with Cy5-labeled GFP mRNA were bound to or endocytosed by 100% of cells exposed to transfection reagent, as virtually all cells were positive for Cy5 fluorescence (**Figure 2.4A**). However, cells transfected with VIPER and sunflower polyplexes in complete media exhibited markedly lower Cy5 median fluorescence intensity (Cy5MFI) relative to those transfected in serum-free OptiMEM (**Figure 2.4B**). For bPEI transfections, a low Cy5MFI was observed under both serum-containing and serum-free conditions, where Cy5MFI under serum-containing conditions was marginally higher than that measured under serum-free conditions (**Figure 2.4B**). We suspected that the reduction in Cy5MFI associated with VIPER- and sunflower polycation–mediated transfections was due to the abundance of serum ribonucleases (RNases) in complete media. While virtually all cells

associated with mRNA polyplexes to some degree, the amount of cell-associated mRNA may have been significantly reduced by these serum RNases.

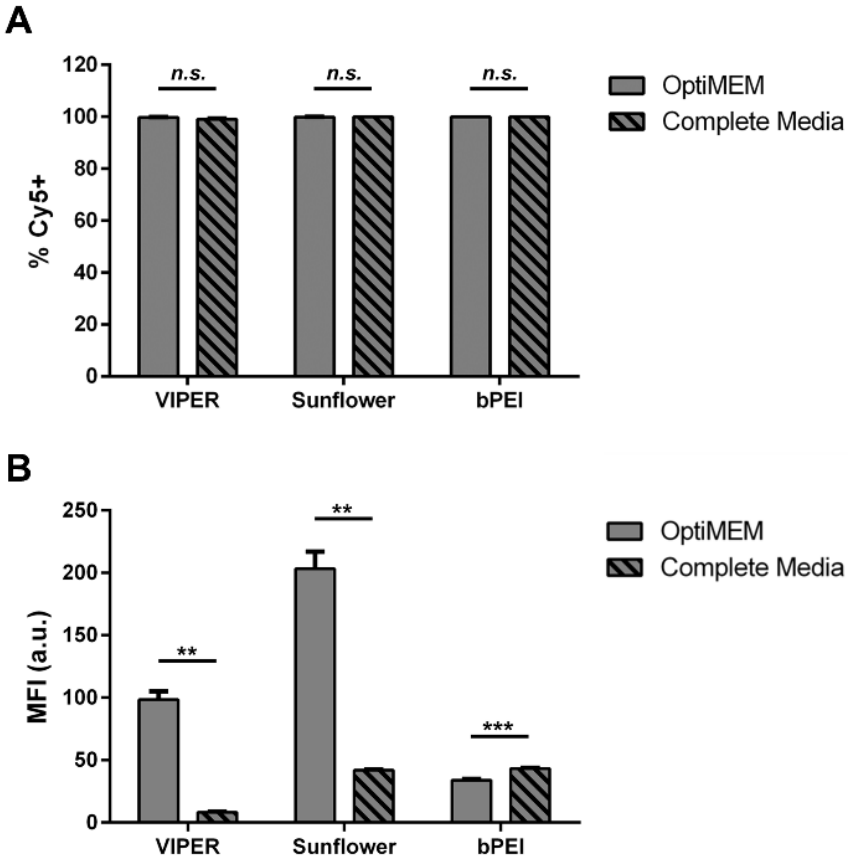

Figure 2.4 **The presence of serum does not restrict cellular association of mRNA polyplexes, but the amount of cell-associated mRNA is significantly reduced.** Cy5-labeled mRNA polyplexes were formulated by adding VIPER or sunflower polycation to Cy5-labeled GFP mRNA. **(A)** Although GFP mRNA transfection of HeLa cells by VIPER and sunflower polycation was eliminated when performed in serum-containing media, Cy5-labeled mRNA polyplexes underwent some degree of cellular association under both serum-rich and serum-free conditions. **(B)** The Cy5 median fluorescence intensity (Cy5MFI) of transfected HeLa cells was noticeably reduced by the presence of serum, indicating that significantly less mRNA was associated with transfected cells under serum-containing conditions than under serum-free conditions. Data are expressed as mean + SD, $n = 3$ (*p-value ≤ 0.05; **p-value ≤ 0.01; ***p-value ≤ 0.001; *n.s.* = no significance; Student's t-test).

2.3.4 Nuclease resistance of mRNA polyplexes

Serum RNases may have degraded mRNA polyplex cargo without completely blocking cellular association of polyplexes, resulting in reduced gene expression despite successful mRNA delivery

to the cell. To test our hypothesis that RNases degraded mRNA polyplex cargo, we conducted a nuclease resistance assay to determine whether VIPER and sunflower polycation could protect mRNA cargo from serum RNase activity.

VIPER, sunflower, and bPEI Luc mRNA polyplexes were formulated at N/P = 5 and incubated in 15 μg/mL of RNase A or 10% FBS for 1 h at 37 °C (**Figure 2.5A**). After 1 h of incubation, we reversed mRNA-polycation binding interactions by increasing VIPER and sunflower polyplex formulation pH to 10.2 and bPEI polyplex formulation pH to 12.8, neutralizing the positive charge of amine-functionalized side chains present on our polycations and releasing mRNA polyplex cargo into solution. mRNA fragments greater than 200 nucleotides in length were subsequently recovered with a RNA spin column, whereas shorter mRNA fragments were eluted from the column and discarded (recall that Luc mRNA is 1,921 nucleotides in length). The quantity of recovered mRNA was determined using a fluorescent nucleic acid stain. Note that we rinsed the RNA spin columns with a denaturing buffer (provided in the RNA recovery kit), inactivating RNases during the recovery process. Overall, we recovered significantly less mRNA from RNase-treated and FBS-treated polyplexes than from untreated polyplexes, indicating that VIPER, sunflower, and bPEI mRNA polyplex cargo were cleaved into short mRNA fragments (less than or equal to 200 nucleotides in length) when polyplexes were incubated in the presence of RNases (**Figure 2.5B**). In conclusion, VIPER, sunflower polycation, and bPEI do not completely shield mRNA cargo from RNase degradation.

While the results of our nuclease resistance assay show the amount of mRNA recovered from our polyplexes is significantly reduced after exposure to RNase, we did observe slight expression of GFP mRNA when using bPEI as the transfection reagent for both complete media and serum-free OptiMEM transfections (**Figure 2.3C,D**). This suggests that the mRNA recovered after RNase treatment of bPEI polyplexes—albeit small in quantity—may be fully intact. bPEI has been shown to bind nucleic acid cargo with very high affinity.[10,24] It forms a very tight complex with pDNA and may interact so strongly with mRNA that ribosomes cannot access the

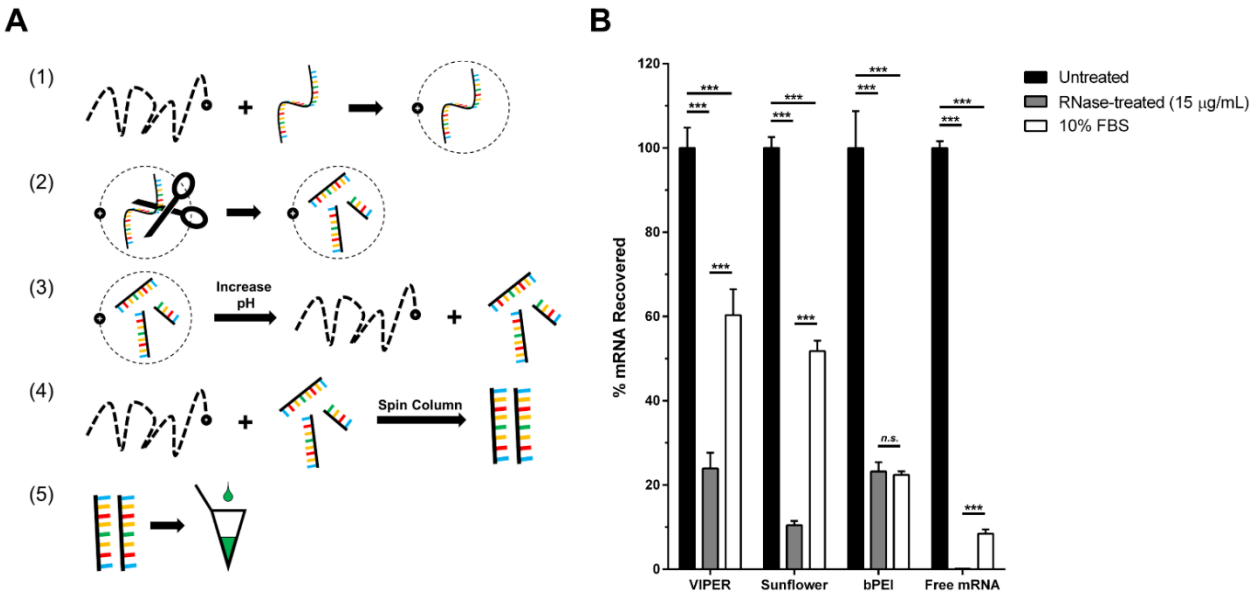

Figure 2.5 **VIPER, sunflower polycation, and bPEI do not fully protect mRNA cargo from RNase activity. (A)** Luc mRNA polyplexes were formulated by (1) adding VIPER, sunflower polycation, or bPEI to Luc mRNA at N/P = 5. (2) Polyplexes were incubated for 1 h at 37 °C in the presence of RNase. (3) Binding of mRNA to polycations was reversed by raising polyplex formulation pH (pH = 10.2 for VIPER and sunflower polycation, and 12.8 for bPEI), neutralizing the positive charge of amine-functionalized side chains. (4) mRNA cargo was recovered by a spin column–based RNA recovery kit, which contains denaturing buffers to inactivate RNases during the recovery process. (5) The amount of recovered mRNA was quantified by a fluorescent nucleic acid stain. **(B)** A significantly smaller percentage of Luc mRNA was recovered from RNase- or FBS-treated polyplexes than from untreated polyplexes. Data are expressed as mean + SD, $n = 3$ (*p-value ≤ 0.05; **p-value ≤ 0.01; ***p-value ≤ 0.001; *n.s.* = no significance; one-way ANOVA with post-hoc Tukey HSD test).

transcript to initiate translation.[10,24] We experienced firsthand the high packaging efficiency of bPEI when we conducted our nuclease resistance assay. A formulation pH of 10.2, which was sufficient for recovery of mRNA from VIPER and sunflower polyplexes, resulted in no mRNA recovery from bPEI polyplexes. Only after increasing formulation pH to 12.8 did we recover enough mRNA for quantification by fluorescence spectroscopy. Furthermore, we observed slight transfection of GFP mRNA when using bPEI as the reagent for both complete media and serum-free OptiMEM transfections (**Figure 2.3C**). Because bPEI packages mRNA tightly, full mRNA strands within a bPEI polyplex may have been partially shielded from both serum RNases and ribosomes, giving rise to a minimal expression profile. A similar hypothesis was presented by

Lallana et al.[25], who showed that the transfection efficiency of chitosan mRNA nanoparticles increases as a function of chitosan avidity towards mRNA, a trend partially attributed to improved protection of mRNA cargo from nuclease activity.

2.3.5 Intratumoral mRNA delivery with VIPER

The poor RNase protection offered by VIPER and sunflower polycation ruled out the possibility of employing these polycations for intravenous mRNA delivery.[16] However, localized mRNA delivery into tissues with low serum content may have still been possible, as VIPER and sunflower polycation both transfected cells with high efficiency in the absence of serum RNase (**Figure 2.3**). The tumor microenvironment is often characterized by a lack of blood vessels.[26] Therefore, we expected the tumor microenvironment to contain relatively little serum and be more conducive to mRNA delivery by our polycations. To test this hypothesis, we attempted intratumoral Luc mRNA transfections in BALB/c mice bearing syngeneic CT26 flank tumors. Flank tumors were transfected with 10 μg of Luc mRNA using either VIPER or bPEI as transfection reagents (N/P = 10), and intratumoral luciferase expression was quantified 10 h post-transfection. An initial study showed that VIPER transfection induced significantly greater intratumoral luciferase expression than bPEI transfection (**Figure 2.6**). Interestingly, we observed no significant difference in luciferase expression between VIPER-treated tumors and free Luc mRNA–treated tumors (**Figure 2.6**). The high level of luciferase expression associated with injection of free Luc mRNA was not surprising, as previous studies have shown that endocytosis of free mRNA can occur through scavenger receptor–mediated pathways.[27] We sought to improve the intratumoral transfection efficiency of VIPER relative to that of free mRNA by conducting further studies to optimize N/P ratio and mRNA dose.

Unfortunately, no luciferase expression was observed in all subsequent intratumoral transfection studies using this CT26 flank tumor model, regardless of whether polyplex or free Luc mRNA was injected into the tumor (data not shown). Serum-free transfections of cultured

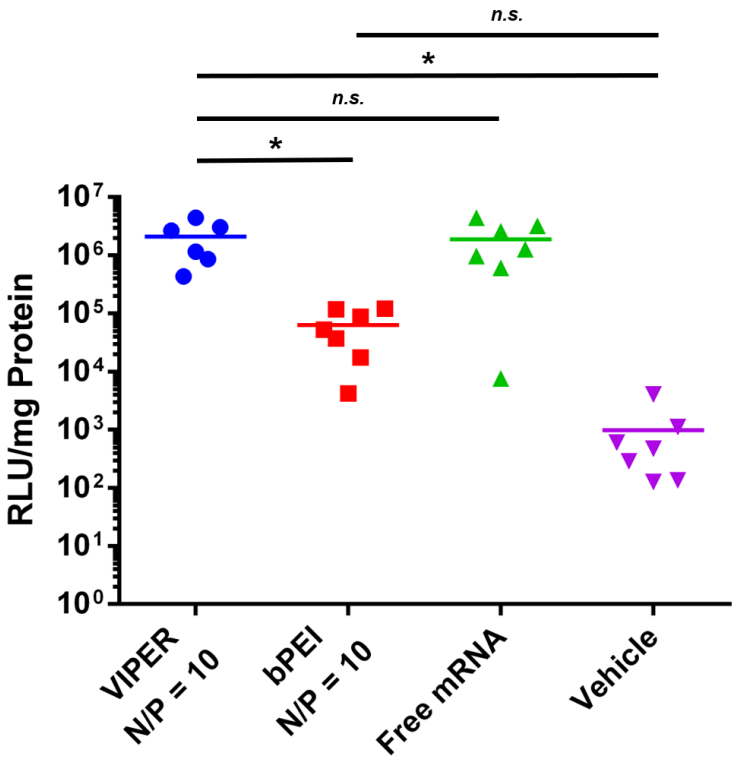

Figure 2.6 **Intratumoral mRNA transfection with VIPER induces local gene expression.** Luciferase expression in CT26 flank tumors was measured 10 h after Luc mRNA transfection. VIPER-treated tumors expressed significantly more luciferase than bPEI-treated and vehicle-treated tumors but not free mRNA–treated tumors. Data are expressed as mean with individual biological replicates shown, n = 6 for VIPER and n = 7 for all other treatments (*p-value ≤ 0.05; *n.s.* = no significance; one-way ANOVA with post-hoc Tukey HSD test).

CT26 cells with VIPER–Luc mRNA polyplexes resulted in measurable cellular luciferase expression, confirming that neither polycation nor mRNA stocks were compromised by RNase contamination (data not shown). Because the RNase content of transplanted CT26 tumors was not quantified prior to transfection, we could not definitively conclude that tumor RNase activity impeded intratumoral mRNA transfection by our polycations. Nonetheless, the data from our in vitro transfection studies and nuclease resistance assay strongly suggest that tumor RNases did contribute to the irreproducibility of our intratumoral VIPER transfection data. Other physiological barriers may have also reduced intratumoral transfection efficiency. For example,

extracellular matrix in the tumor may destabilize mRNA-polycation interactions and expose mRNA polyplex cargo to RNases.[28]

To fully realize mRNA delivery with our polycations in vivo, modifications to our current polyplex formulations must be implemented to improve physiological stability and protect mRNA cargo against serum RNase activity. Other polycations reported for mRNA delivery also require serum-free conditions for in vitro transfection.[23,29,30] One potential polyplex modification is the incorporation of a lipid bilayer around the polyplex, forming a lipid-encapsulated polyplex, or lipopolyplex.[11,31–35] This lipid coating, which usually consists of charged lipids mixed with helper lipids, serves numerous functions.[36] First, the lipid coating can decrease cytotoxicity associated with naked polyplex, as the lipids may neutralize positive charge associated with the polycationic lipopolyplex core.[37] Furthermore, the lipid coating acts as a physical barrier against nucleases, protecting nucleic acid cargo from nuclease degradation.[11,33]

Indeed, lipid nanoparticles are currently utilized as nuclease-resistant delivery vehicles for mRNA vaccines against SARS-CoV-2, the virus behind the COVID-19 pandemic.[38] Hybrid lipopolyplex formulations have been shown to transfect cells more efficiently than formulations comprising solely lipids or polycations, combining the cargo-protective effects of lipid encapsulation with endosomal escape mechanisms conferred by polycations.[18,36] We anticipate that lipopolyplexes based on VIPER and sunflower polycation will exhibit greater RNase resistance and transfection efficiency than the polyplexes we have used to date.

2.4 Conclusions

In this work, we investigated mechanistic differences between VIPER- and sunflower polycation–mediated delivery of pDNA and mRNA, with the goal of confirming whether these polycations are applicable for delivery of mRNA therapies. An effective mRNA therapy must (i) produce sufficient therapeutic protein after administration to generate a beneficial effect (e.g., sufficient production

of tumor suppressor protein after intratumoral delivery) or (ii) transfect a significant percentage of the target cell population (e.g., widespread transfection of tissue-resident antigen-presenting cells after injection of mRNA vaccines). In vitro transfections of Luc mRNA and GFP mRNA, respectively, were used to assess whether VIPER and sunflower mRNA polyplexes could satisfy these two criteria while protecting mRNA cargo from serum RNase activity. Luciferase expression levels correlated to the total amount of translated mRNA in a transfected cell population, whereas GFP expression levels correlated to the total percentage of cells transfected.

Although both VIPER and sunflower polycation could readily package mRNA, their ability to deliver mRNA was limited by RNases. We showed that RNases degraded the cargo of VIPER and sunflower mRNA polyplexes, preventing mRNA translation after endocytosis (**Figure 2.7**). Therefore, delivery of intact mRNA in vitro by VIPER and sunflower polycation was only achieved under serum-free conditions (**Figure 2.7**). In contrast, VIPER and sunflower polycation delivered pDNA to cells in vitro under serum-rich conditions without a total loss of gene expression. The poor degree of RNase protection offered by VIPER and sunflower polycation rules out the possibility of employing these polycations for in vivo mRNA delivery. However, ex vivo mRNA delivery may still be possible, as VIPER and sunflower polycation transfected cells with high efficiency in serum-free media. Overall, the results of this work highlight polycation design parameters required for efficient delivery of mRNA. These parameters may include (i) rapid induction of endosomolysis, (ii) chemical moieties that bind mRNA without blocking translation, and (iii) mechanisms to protect mRNA cargo from RNase activity.[10,29,39–42]

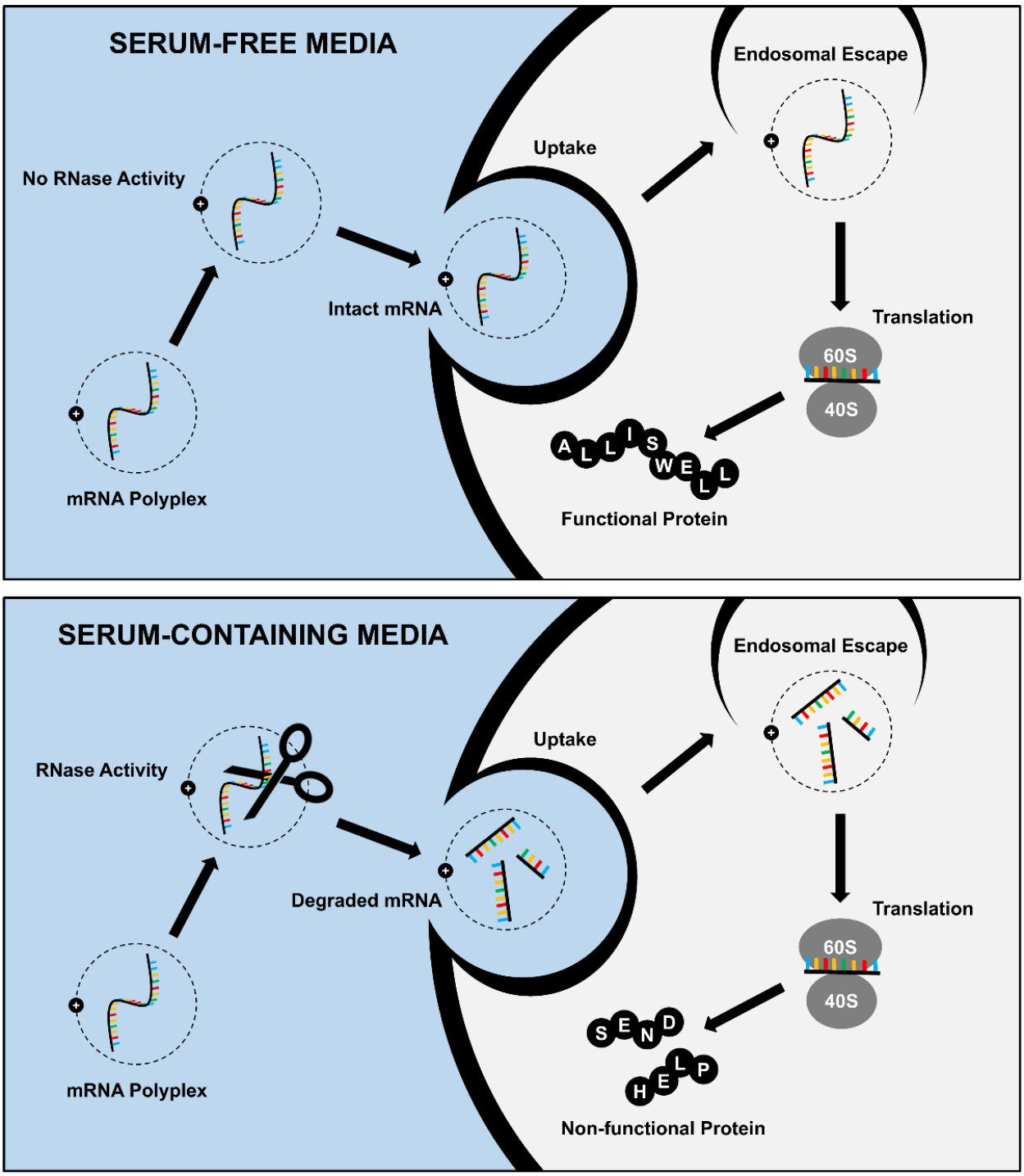

Figure 2.7 **RNases hinder mRNA transfection by VIPER and sunflower polycation in serum-containing media.** In serum-free media (top), there are no serum RNases present. mRNA polyplex uptake occurs unobstructed. After endosomal escape of the polyplex, mRNA is translated into functional protein. In serum-containing media (bottom), serum RNases degrade mRNA polyplex cargo before cellular uptake. After endosomal escape of the polyplex, any remaining mRNA fragments (if translated) give rise to non-functional protein.

2.5 Acknowledgements

This work was supported by NIH grants 1R01CA177272 and R01NS064404. Albert Yen was supported by a National Science Foundation Graduate Research Fellowship under grant DGE-1256082. We are grateful to Prof. Paul Yager (University of Washington) for allowing the use of his lab's gel imager. We are grateful to Prof. Shaoyi Jiang (Cornell University) for allowing the use of his lab's Zetasizer. Finally, we thank Bobbie Schneider and Steve MacFarlane (Cellular Imaging Core Facility, Fred Hutchinson Cancer Research Center) for providing assistance with transmission electron microscopy studies.

2.6 Supporting Information

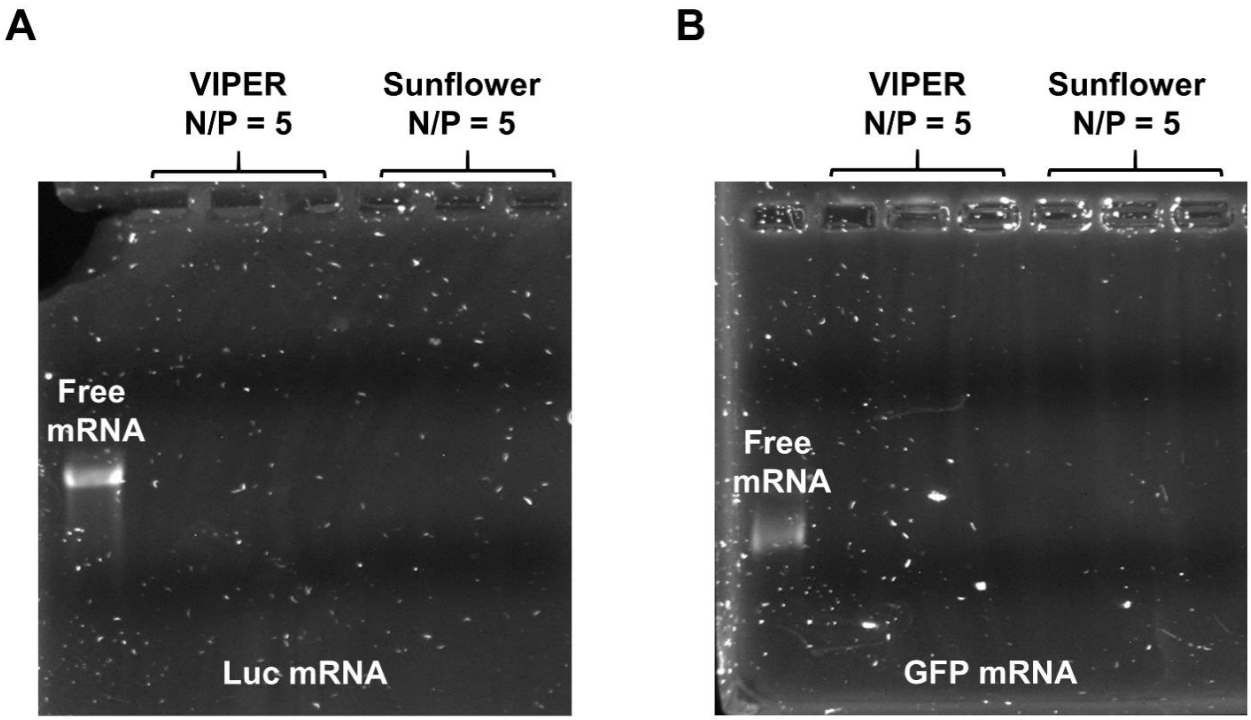

Supplemental Figure 2.1 **Gel condensation assays show that VIPER and sunflower polycation package both Luc mRNA and GFP mRNA. (A)** As evidenced by the lack of free Luc mRNA in the polyplex lanes, Luc mRNA was readily packaged by VIPER and sunflower polycation at N/P = 5. **(B)** Similar packaging efficiency was observed with GFP mRNA polyplexes.

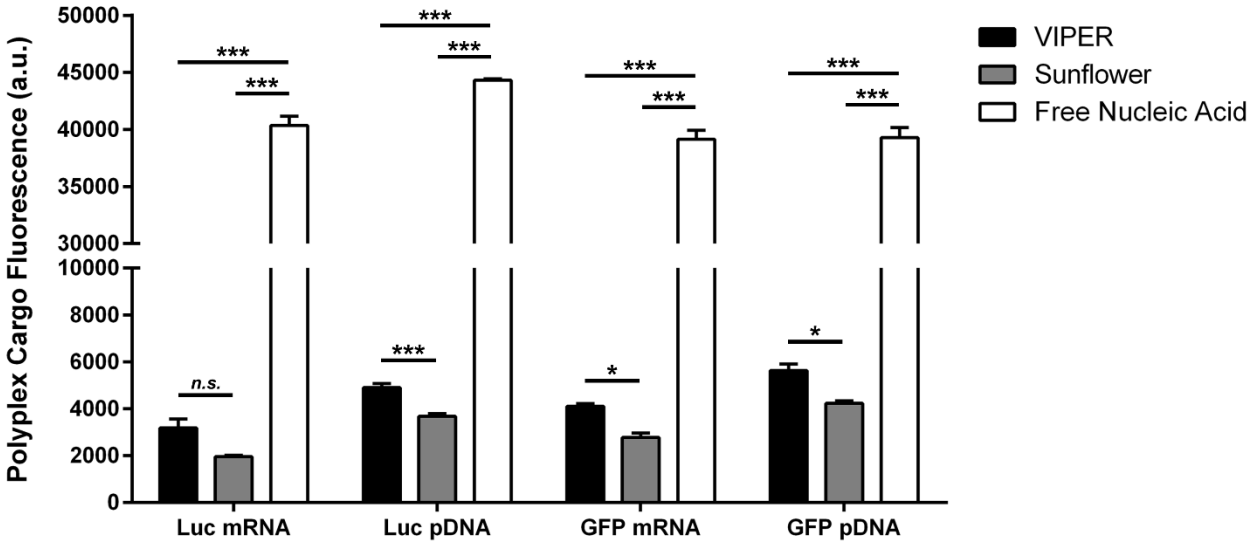

Supplemental Figure 2.2 **Fluorophore labeling of mRNA polyplex cargo confirms packaging of mRNA by VIPER and sunflower polycation.** Luc mRNA and pDNA polyplexes were formulated with VIPER and sunflower polycation at N/P = 5, and polyplexes were subsequently stained with RiboGreen™ nucleic acid dye. Luc mRNA cargo fluorescence of both VIPER and sunflower polyplexes was significantly decreased relative to that of free Luc mRNA, indicating successful packaging of free mRNA by polycations. Similarly, GFP mRNA cargo fluorescence of both VIPER and sunflower polyplexes was also significantly decreased relative to that of free GFP mRNA. Data are expressed as mean + SD, $n = 3$ (*p-value ≤ 0.05; **p-value ≤ 0.01; ***p-value ≤ 0.001; *n.s.* = no significance; one-way ANOVA with post-hoc Tukey HSD test).

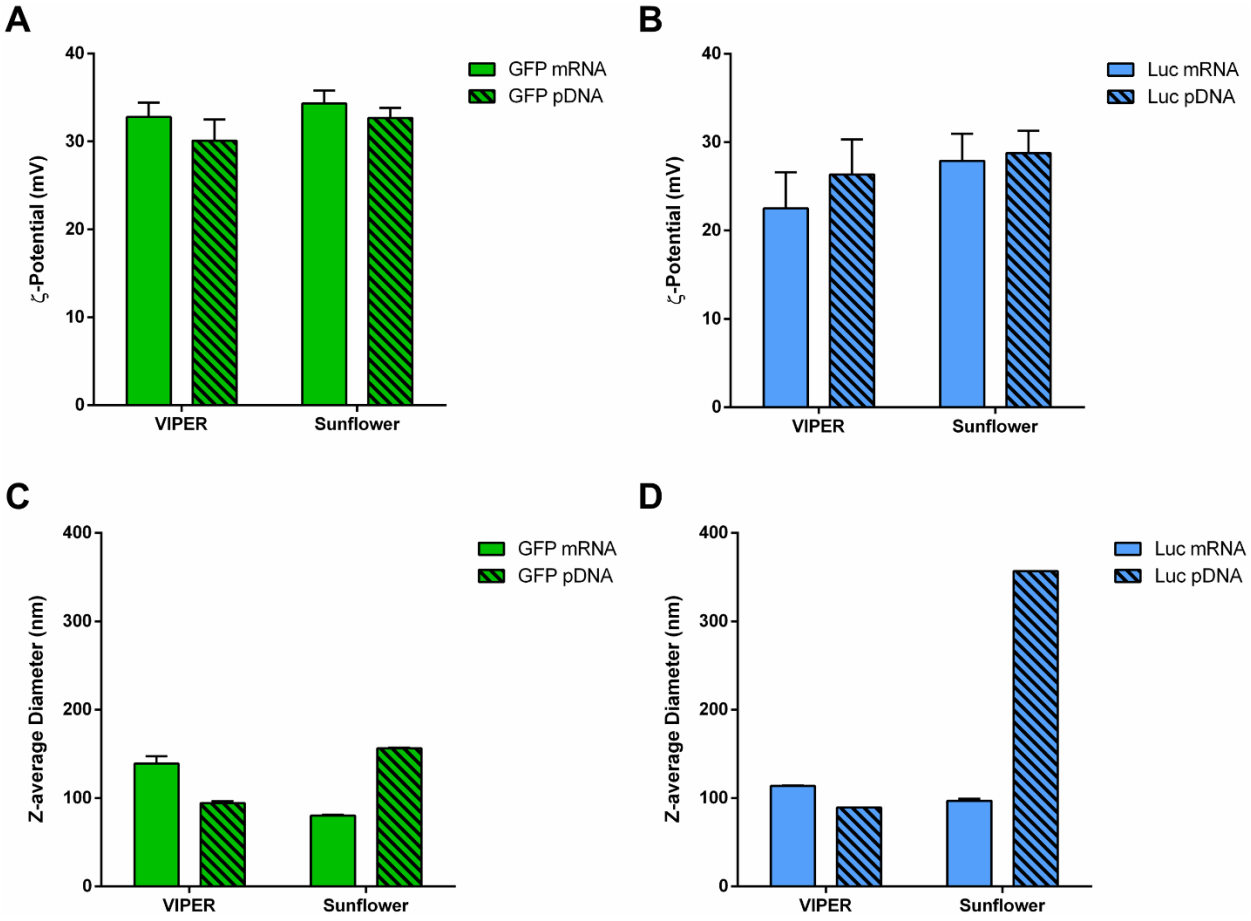

Supplemental Figure 2.3 **VIPER and sunflower polycation form mRNA polyplexes with defined ζ-potentials and hydrodynamic diameters. (A–B)** VIPER and sunflower mRNA polyplexes had mean ζ-potentials between 20–40 mV. These ζ-potentials were comparable to those of VIPER and sunflower pDNA polyplexes. **(C–D)** VIPER and sunflower mRNA polyplexes had Z-average hydrodynamic diameters between 80–140 nm. These hydrodynamic diameters were comparable to those of VIPER and sunflower pDNA polyplexes.

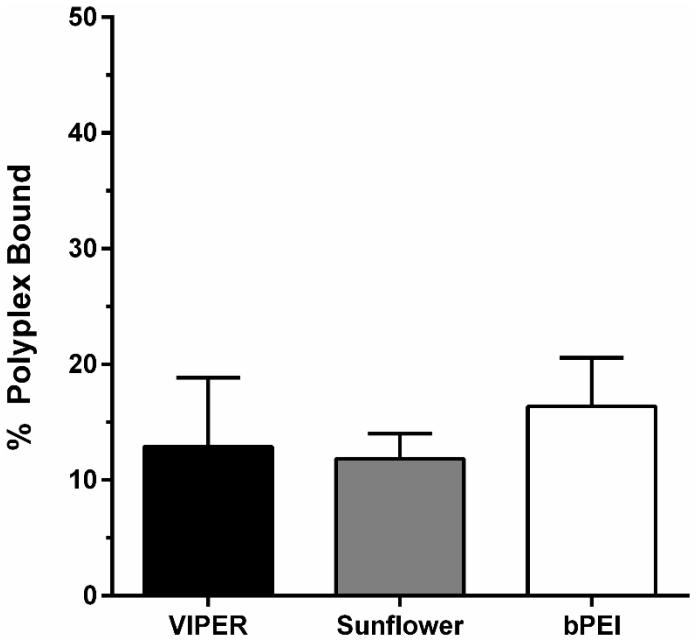

Supplemental Figure 2.4 **VIPER, sunflower, and bPEI mRNA polyplexes bind to HeLa cells.** HeLa cells were incubated with polyplexes packaging Cy5-labeled GFP mRNA for 30 min under serum-free conditions. After 30 min, the amount of polyplex remaining in the transfection media was measured and the percentage of polyplexes bound to cells was calculated. Approximately 13% of VIPER mRNA polyplexes, 12% of sunflower mRNA polyplexes, and 16% of bPEI mRNA polyplexes were bound to HeLa cells after 30 min of transfection in serum-free media. Error bars are expressed as mean + SD, $n = 3$.

Supplemental Table 2.1 **Polyplex formulations for in vitro mRNA transfections.**

Parameter	Serum-free OptiMEM	Complete Media
Quantity of mRNA per well	1 µg	2 µg
VIPER N/P	3	5
Sunflower N/P	5	5
bPEI N/P	5	5
Duration of transfection	1 hour	4 hours

2.7 References

(1) Kaczmarek, J. C.; Kowalski, P. S.; Anderson, D. G. Advances in the Delivery of RNA Therapeutics: From Concept to Clinical Reality. *Genome Med.* **2017**, *9*, 60.

(2) Jemielity, J.; Fowler, T.; Zuberek, J.; Stepinski, J.; Lewdorowicz, M.; Niedzwiecka, A.; Stolarski, R.; Darzynkiewicz, E.; Rhoads, R. E. Novel "Anti-Reverse" Cap Analogs with Superior Translational Properties. *RNA* **2003**, *9* (9), 1108–1122.

(3) Presnyak, V.; Alhusaini, N.; Chen, Y.-H.; Martin, S.; Morris, N.; Kline, N.; Olson, S.; Weinberg, D.; Baker, K. E.; Graveley, B. R.; et al. Codon Optimality Is a Major Determinant of mRNA Stability. *Cell* **2015**, *160* (6), 1111–1124.

(4) Holtkamp, S.; Kreiter, S.; Selmi, A.; Simon, P.; Koslowski, M.; Huber, C.; Türeci, O.; Sahin, U. Modification of Antigen-Encoding RNA Increases Stability, Translational Efficacy, and T-Cell Stimulatory Capacity of Dendritic Cells. *Blood* **2006**, *108* (13), 4009–4017.

(5) Andries, O.; Mc Cafferty, S.; De Smedt, S. C.; Weiss, R.; Sanders, N. N.; Kitada, T. N^1-Methylpseudouridine-Incorporated mRNA Outperforms Pseudouridine-Incorporated mRNA by Providing Enhanced Protein Expression and Reduced Immunogenicity in Mammalian Cell Lines and Mice. *J. Control. Release* **2015**, *217*, 337–344.

(6) Sahin, U.; Karikó, K.; Türeci, Ö. mRNA-Based Therapeutics — Developing a New Class of Drugs. *Nat. Rev. Drug Discov.* **2014**, *13* (10), 759–780.

(7) Kormann, M. S. D.; Hasenpusch, G.; Aneja, M. K.; Nica, G.; Flemmer, A. W.; Herber-Jonat, S.; Huppmann, M.; Mays, L. E.; Illenyi, M.; Schams, A.; et al. Expression of Therapeutic Proteins after Delivery of Chemically Modified mRNA in Mice. *Nat. Biotechnol.* **2011**, *29* (2), 154–159.

(8) Wang, Z.; Troilo, P. J.; Wang, X.; Griffiths, T. G.; Pacchione, S. J.; Barnum, A. B.; Harper, L. B.; Pauley, C. J.; Niu, Z.; Denisova, L.; et al. Detection of Integration of Plasmid DNA into Host Genomic DNA Following Intramuscular Injection and Electroporation. *Gene Ther.* **2004**, *11* (8), 711–721.

(9) Wang, P.; Na, J. Synthetic Messenger RNA and Cell Metabolism Modulation. *Methods Protoc.* **2013**, *969*, 221–233.

(10) Bettinger, T. Peptide-Mediated RNA Delivery: A Novel Approach for Enhanced Transfection of Primary and Post-Mitotic Cells. *Nucleic Acids Res.* **2001**, *29* (18), 3882–3891.

(11) Guan, S.; Rosenecker, J. Nanotechnologies in Delivery of mRNA Therapeutics Using Nonviral Vector-Based Delivery Systems. *Gene Ther.* **2017**, *24* (3), 133–143.

(12) Follenzi, A.; Ailles, L. E.; Bakovic, S.; Geuna, M.; Naldini, L. Gene Transfer by Lentiviral Vectors Is Limited by Nuclear Translocation and Rescued by HIV-1 Pol Sequences. *Nat. Genet.* **2000**, *25* (2), 217–222.

(13) Cohen, S.; Au, S.; Panté, N. How Viruses Access the Nucleus. *Biochim. Biophys. Acta - Mol. Cell Res.* **2011**, *1813* (9), 1634–1645.

(14) Deering, R. P.; Kommareddy, S.; Ulmer, J. B.; Brito, L. a; Geall, A. J. Nucleic Acid Vaccines: Prospects for Non-Viral Delivery of mRNA Vaccines. *Expert Opin. Drug Deliv.* **2014**, *11* (6), 885–899.

(15) Geall, A. J.; Verma, A.; Otten, G. R.; Shaw, C. A.; Hekele, A.; Banerjee, K.; Cu, Y.; Beard, C. W.; Brito, L. A.; Krucker, T.; et al. Nonviral Delivery of Self-Amplifying RNA Vaccines. *Proc. Natl. Acad. Sci.* **2012**, *109* (36), 14604–14609.

(16) Yin, H.; Kanasty, R. L.; Eltoukhy, A. A.; Vegas, A. J.; Dorkin, J. R.; Anderson, D. G. Non-Viral Vectors for Gene-Based Therapy. *Nat. Rev. Genet.* **2014**, *15* (8), 541–555.

(17) Dowdy, S. F. Overcoming Cellular Barriers for RNA Therapeutics. *Nat. Biotechnol.* **2017**, *35* (3), 222–229.

(18) Pack, D. W.; Hoffman, A. S.; Pun, S.; Stayton, P. S. Design and Development of Polymers

for Gene Delivery. *Nat. Rev. Drug Discov.* **2005**, *4* (7), 581–593.
(19) Hajj, K. A.; Whitehead, K. A. Tools for Translation: Non-Viral Materials for Therapeutic mRNA Delivery. *Nat. Rev. Mater.* **2017**, *2* (10), 17056.
(20) Wei, H.; Volpatti, L. R.; Sellers, D. L.; Maris, D. O.; Andrews, I. W.; Hemphill, A. S.; Chan, L. W.; Chu, D. S. H.; Horner, P. J.; Pun, S. H. Dual Responsive, Stabilized Nanoparticles for Efficient In Vivo Plasmid Delivery. *Angew. Chemie Int. Ed.* **2013**, *52* (20), 5377–5381.
(21) Cheng, Y.; Yumul, R. C.; Pun, S. H. Virus-Inspired Polymer for Efficient In Vitro and In Vivo Gene Delivery. *Angew. Chemie Int. Ed.* **2016**, *55* (39), 12013–12017.
(22) Cheng, Y.; Wei, H.; Tan, J.-K. Y.; Peeler, D. J.; Maris, D. O.; Sellers, D. L.; Horner, P. J.; Pun, S. H. Nano-Sized Sunflower Polycations As Effective Gene Transfer Vehicles. *Small* **2016**, *12* (20), 2750–2758.
(23) Debus, H.; Baumhof, P.; Probst, J.; Kissel, T. Delivery of Messenger RNA Using Poly(Ethylene Imine)–Poly(Ethylene Glycol)-Copolymer Blends for Polyplex Formation: Biophysical Characterization and In Vitro Transfection Properties. *J. Control. Release* **2010**, *148* (3), 334–343.
(24) Newland, B.; Abu-Rub, M.; Naughton, M.; Zheng, Y.; Pinoncely, A. V.; Collin, E.; Dowd, E.; Wang, W.; Pandit, A. GDNF Gene Delivery via a 2-(Dimethylamino)Ethyl Methacrylate Based Cyclized Knot Polymer for Neuronal Cell Applications. *ACS Chem. Neurosci.* **2013**, *4* (4), 540–546.
(25) Lallana, E.; Rios De La Rosa, J. M.; Tirella, A.; Pelliccia, M.; Gennari, A.; Stratford, I. J.; Puri, S.; Ashford, M.; Tirelli, N. Chitosan/Hyaluronic Acid Nanoparticles: Rational Design Revisited for RNA Delivery. *Mol. Pharm.* **2017**, *14* (7), 2422–2436.
(26) Nagy, J. A.; Chang, S.-H.; Dvorak, A. M.; Dvorak, H. F. Why Are Tumour Blood Vessels Abnormal and Why Is It Important to Know? *Br. J. Cancer* **2009**, *100* (6), 865–869.
(27) Lorenz, C.; Fotin-Mleczek, M.; Roth, G.; Becker, C.; Dam, T. C.; Verdurmen, W. P. R.; Brock, R.; Probst, J.; Schlake, T. Protein Expression from Exogenous mRNA: Uptake by Receptor-Mediated Endocytosis and Trafficking via the Lysosomal Pathway. *RNA Biol.* **2011**, *8* (4), 627–636.
(28) Burke, R. S.; Pun, S. H. Extracellular Barriers to In Vivo PEI and PEGylated PEI Polyplex-Mediated Gene Delivery to the Liver. *Bioconjug. Chem.* **2008**, *19* (3), 693–704.
(29) Üzgün, S.; Nica, G.; Pfeifer, C.; Bosinco, M.; Michaelis, K.; Lutz, J.-F.; Schneider, M.; Rosenecker, J.; Rudolph, C. PEGylation Improves Nanoparticle Formation and Transfection Efficiency of Messenger RNA. *Pharm. Res.* **2011**, *28* (9), 2223–2232.
(30) Cheng, C.; Convertine, A. J.; Stayton, P. S.; Bryers, J. D. Multifunctional Triblock Copolymers for Intracellular Messenger RNA Delivery. *Biomaterials* **2012**, *33* (28), 6868–6876.
(31) Wang, Y.; Su, H.-H.; Yang, Y.; Hu, Y.; Zhang, L.; Blancafort, P.; Huang, L. Systemic Delivery of Modified mRNA Encoding Herpes Simplex Virus 1 Thymidine Kinase for Targeted Cancer Gene Therapy. *Mol. Ther.* **2013**, *21* (2), 358–367.
(32) García, L.; Urbiola, K.; Düzgüneş, N.; Tros De Ilarduya, C. Lipopolyplexes as Nanomedicines for Therapeutic Gene Delivery. *Methods Enzymol.* **2012**, *509*, 327–338.
(33) Persano, S.; Guevara, M. L.; Li, Z.; Mai, J.; Ferrari, M.; Pompa, P. P.; Shen, H. Lipopolyplex Potentiates Anti-Tumor Immunity of mRNA-Based Vaccination. *Biomaterials* **2017**, *125*, 81–89.
(34) Kaczmarek, J. C.; Patel, A. K.; Kauffman, K. J.; Fenton, O. S.; Webber, M. J.; Heartlein, M. W.; DeRosa, F.; Anderson, D. G. Polymer-Lipid Nanoparticles for Systemic Delivery of mRNA to the Lungs. *Angew. Chemie Int. Ed.* **2016**, *55* (44), 13808–13812.
(35) Su, X.; Fricke, J.; Kavanagh, D. G.; Irvine, D. J. In Vitro and In Vivo mRNA Delivery Using Lipid-Enveloped pH-Responsive Polymer Nanoparticles. *Mol. Pharm.* **2011**, *8* (3), 774–787.
(36) Rezaee, M.; Oskuee, R. K.; Nassirli, H.; Malaekeh-Nikouei, B. Progress in the Development

of Lipopolyplexes as Efficient Non-Viral Gene Delivery Systems. *J. Control. Release* **2016**, *236*, 1–14.
(37) Kurosaki, T.; Kawakami, S.; Higuchi, Y.; Suzuki, R.; Maruyama, K.; Sasaki, H.; Yamashita, F.; Hashida, M. Development of Anionic Bubble Lipopolyplexes for Efficient and Safe Gene Transfection with Ultrasound Exposure in Mice. *J. Control. Release* **2014**, *176* (1), 24–34.
(38) Chung, Y. H.; Beiss, V.; Fiering, S. N.; Steinmetz, N. F. COVID-19 Vaccine Frontrunners and Their Nanotechnology Design. *ACS Nano* **2020**, *14* (10), 12522–12537.
(39) McKinlay, C. J.; Vargas, J. R.; Blake, T. R.; Hardy, J. W.; Kanada, M.; Contag, C. H.; Wender, P. A.; Waymouth, R. M. Charge-Altering Releasable Transporters (CARTs) for the Delivery and Release of mRNA in Living Animals. *Proc. Natl. Acad. Sci.* **2017**, *114* (4), E448–E456.
(40) Uchida, H.; Itaka, K.; Uchida, S.; Ishii, T.; Suma, T.; Miyata, K.; Oba, M.; Nishiyama, N.; Kataoka, K. Synthetic Polyamines to Regulate mRNA Translation through the Preservative Binding of Eukaryotic Initiation Factor 4E to the Cap Structure. *J. Am. Chem. Soc.* **2016**, *138* (5), 1478–1481.
(41) Gonçalves, C.; Akhter, S.; Pichon, C.; Midoux, P. Intracellular Availability of pDNA and mRNA after Transfection: A Comparative Study among Polyplexes, Lipoplexes, and Lipopolyplexes. *Mol. Pharm.* **2016**, *13* (9), 3153–3163.
(42) Chen, Q.; Qi, R.; Chen, X.; Yang, X.; Wu, S.; Xiao, H.; Dong, W. A Targeted and Stable Polymeric Nanoformulation Enhances Systemic Delivery of mRNA to Tumors. *Mol. Ther.* **2017**, *25* (1), 92–101.

CHAPTER 3

Lytic Polyplex Vaccines Enhance Antigen-Specific Cytotoxic T Cell Response through Induction of Local Cell Death[†,‡]

David J. Peeler*, Albert Yen*, Nicholas Luera, Patrick S. Stayton, and Suzie H. Pun

Synopsis. Endosomolytic vaccine nanocarriers can potentiate cellular immune responses by enhancing cross-presentation. We recently developed a cationic polymer–lytic peptide conjugate (VIPER) that greatly improves endosomal escape and intracellular activity of nucleic acid cargoes. We hypothesized that VIPER's unique mechanism of endosomal disruption can increase cytoplasmic delivery of other biomacromolecules (e.g., peptides). Herein, VIPER is formulated as a polyplex subunit vaccine composed of conjugated peptide antigens and electrostatically complexed poly(I:C) nucleic acid adjuvant. This polyplex vaccine is evaluated to determine whether conjugation of the lytic peptide melittin to the pH-responsive micelle core improves vaccination outcomes. Although VIPER delivers peptide antigens intracellularly, disrupts endosomes in antigen-presenting cells (APCs) in vitro, and generates strong antigen-specific cytotoxic T cell responses in vivo, significantly enhanced cross-presentation is only observed in conjunction with VIPER-induced local cell death. While these results demonstrate that VIPER is a useful platform technology for the study of vaccine delivery, full elucidation of how endosomal disruption by VIPER improves vaccination outcomes will require decoupling of endosomolysis from cytotoxicity, as well as precise targeting of VIPER vaccine formulations to APC populations in vivo.

[†]Adapted with permission from: Peeler, D. J.*; **Yen, A.***; Luera, N.; Stayton, P. S.; Pun, S. H. Lytic Polyplex Vaccines Enhance Antigen-Specific Cytotoxic T Cell Response through Induction of Local Cell Death. *Adv. Ther.* **2021**, 2100005.

[‡]An initial draft of the above publication appears as *Chapter 5* in the doctoral dissertation of David J. Peeler, an equally contributing author (URI: http://hdl.handle.net/1773/45109). The above publication is adapted for inclusion in this dissertation with permission from both David J. Peeler and Suzie H. Pun (Chair of the Supervisory Committee).

*Equally contributing authors.

3.1 Introduction

Peptide vaccines are a promising cancer immunotherapy because of their tolerability and customizability.[1–3] Through judicious selection of peptide epitopes, a peptide vaccine regimen can be tailored to patient-specific cancers.[1,2] Regardless of the cancer's epitope signature, an effective cancer peptide vaccine must induce antiviral-like responses from tumor-specific, $CD8^+$ cytotoxic T cells (CTCs).[2] Antigen-presenting cells (APCs) prime antitumor CTCs by taking up exogenous tumor antigens, processing them into peptide epitopes, and presenting these epitopes on MHC class I (MHCI) molecules to naïve $CD8^+$ T cells, a phenomenon known as cross-presentation.[1,4,5]

It is well established that processing of antigens by proteasomes in the APC cytosol is a primary pathway for cross-presentation.[6–8] For example, Moore and colleagues demonstrated that delivering ovalbumin-derived peptide antigens into the APC cytosol through osmotic lysis of pinosomes gives rise to APC populations that prime ovalbumin-specific CTCs.[9] However, delivery of tumor antigens alone is usually insufficient for durable antitumor immunity, as T cell priming is inefficient without concomitant stimulation of APC maturation by vaccine adjuvants (e.g., alum).[10] Most cancer vaccine formulations include adjuvants, but since many tumor antigens exhibit low immunogenicity and CTC effector function is often suppressed by tumor microenvironments, cancer peptide vaccines have achieved only modest treatment outcomes in clinical trials.[3,10–12]

Integrating adjuvants and tumor peptide antigens into nanoparticle-based formulations, or "nanovaccines," may improve the potency of cancer peptide vaccines.[13–16] Polymeric nanoparticles are particularly promising vaccine carriers because they can be synthetically designed to navigate biological barriers impeding vaccine delivery to APCs.[15–19] For instance, loading polymeric nanoparticles with antigen and adjuvant allows for simultaneous uptake of both cargoes by the same APC, which is difficult to realize with soluble vaccine formulations.[16] Furthermore, while most conventional subunit vaccines suffer from rapid clearance and poor

lymph node accumulation, the dimensions and surface chemistries of polymeric nanovaccines can be optimized for lymphatic transport and APC uptake, thereby reducing toxicity associated with systemic adjuvant biodistribution.[19,20] Once internalized by APCs, polymeric nanovaccines with endosomolytic properties may also enhance cross-presentation by improving the efficiency of cytoplasmic antigen delivery and/or by releasing inflammasome-activating molecules from endosomal compartments.[21–29]

A variety of technologies for cytosolic delivery of nucleic acid therapeutics have been described in the literature, and the same endosomal disruption mechanisms utilized by these technologies may be repurposed for vaccine delivery.[30–32] We recently reported a cationic polymer ("Virus-Inspired Polymer for Endosomal Release," or VIPER) that facilitates efficient endosomal escape of nucleic acid cargo through selective display of membrane-lytic peptides as a result of pH-triggered micelle disassembly.[33,34] We further demonstrated that VIPER micelles can encapsulate a wide variety of peptides regardless of the peptides' physicochemical properties.[35] Inspired by these observations and prior applications of cationic polymers for co-delivery of adjuvants and antigens, we hypothesized that VIPER polyplex formulations could increase cross-presentation efficiency by mediating endosomal escape of vaccine components.[27,36]

In this work, we synthesize VIPER polymers that co-deliver peptide antigen via a reversible disulfide bond and nucleic acid adjuvant via electrostatic complexation. We demonstrate that VIPER delivers its cargo intracellularly and that inclusion of a membrane-lytic peptide, melittin, within the VIPER formulation via covalent conjugation enhances endosomal disruption in APCs in vitro. However, this enhanced endosomal disruption does not correlate directly with increased cross-presentation, as APCs treated directly with VIPER do not cross-present more efficiently. Further investigation reveals that cross-presentation efficiency is increased only when APCs are co-cultured with "bystander" cell populations pre-treated with cytotoxic VIPER doses. These findings suggest that VIPER's lytic bioactivity augments cellular immune responses by inducing local cell death, upon which resident APCs process and cross-

present antigens from the apoptotic milieu.[37] Indeed, intradermal immunization of mice with VIPER generates strong antigen-specific T cell responses and prolongs survival in a subset of therapeutically vaccinated, melanoma-bearing mice, supporting the use of VIPER as a platform technology for further study of vaccine delivery.

3.2 Experimental Section

3.2.1 Materials

All chemicals used for polymer and peptide synthesis were purchased from either Sigma-Aldrich or Thermo Fisher Scientific and used without further purification as previously described.[35] All cell culture reagents were purchased from Gibco. Bovine serum albumin was purchased from Miltenyi Biotec. Endotoxin-free plasmid pmaxGFP, produced in *E. coli* using a pmaxCloning™ vector (Lonza), was purified with the Plasmid Giga Kit (Qiagen) according to manufacturer protocol. Incomplete Freund's adjuvant (InvivoGen) was stored at 4 °C until emulsification with antigen and adjuvant according to the manufacturer protocol. Endotoxin-free SIINFEKL peptide (InvivoGen) was dissolved in endotoxin-free 5% (w/v) glucose in water (Sigma-Aldrich) and stored at -20 °C until further use. Endotoxin-free high molecular weight poly(I:C) (InvivoGen) was annealed in sterile saline according to manufacturer protocol. Annealed poly(I:C) was then buffer exchanged into 5% (w/v) glucose in water via centrifugal filtration on a 10 kDa cutoff Amicon® centrifugal filter (EMD Millipore) before sterile filtration with a 0.22 μm pore filter (EMD Millipore) and storage at -20 °C until further use. The H-2K^b/SIINFEKL tetramer was a gift of the NIH Tetramer Core Facility at Emory University.

3.2.2 Peptide synthesis

Lytic (cysteine-melittin; GIGAVLKVLTTGLPALISWIKRKRQQC) and antigenic (CSSSIINFEKL) peptides were obtained through solid-phase peptide synthesis as previously described.[35] Briefly,

standard Fmoc amino acids and NovaPEG Rink Amide resin (EMD Millipore) were loaded onto a Liberty Blue™ microwave peptide synthesizer (CEM) at 0.25 mmol product scale. After synthesis, resin was immersed in trifluoroacetic acid (TFA) comprising 5% (v/v) dimethoxybenzene, 2.5% (v/v) triisopropylsilane, and 2.5% (v/v) ethanedithiol to cleave off peptides. For melittin, 2.5% (v/v) water was also added to the TFA. Crude peptide was recovered after two successive cold ether precipitations, and peptide product was purified to > 98% purity by reversed-phase HPLC with a mobile phase of water/acetonitrile + 0.1% (v/v) TFA and a gradient elution method. MALDI-TOF (University of Washington Department of Medicinal Chemistry Mass Spectrometry Center) was used to confirm molecular weights of purified peptides. To synthesize rhodamine-CSSSIINFEKL, 5/6-carboxy-tetramethyl-rhodamine succinimidyl ester (Thermo Fisher Scientific) was conjugated to deprotected peptide N-terminal amines on resin via reaction with 1-ethyl-3-(-3-dimethylaminopropyl) carbodiimide hydrochloride (Sigma-Aldrich), followed by peptide cleavage and purification.

3.2.3 Polymer synthesis, peptide conjugation, and micelle formation

Block copolymer (p(OEGMA$_{8.6}$-*co*-DMAEMA$_{50.0}$)-*b*-p(DIPAMA$_{25.3}$-*co*-PDSEMA$_{1.0}$) was synthesized by reversible addition–fragmentation chain-transfer (RAFT) polymerization, purified by dialysis, and characterized by ^{1}H NMR and size exclusion chromatography as previously described.[33,35] Peptides were conjugated to this polymer backbone via disulfide exchange between cysteine and PDSEMA as described in previous work, and reported methods were used to purify polymer-peptide conjugates.[33,35] Micelles were formed by mixing various polymer-peptide conjugates in acidic phosphate buffer before a rapid pH increase via addition of basic phosphate buffer as previously described.[33,35] After addition of basic phosphate buffer, polymer-peptide conjugate solution was rested overnight to form micelles. Micelles were then buffer exchanged into 5% (w/v) glucose in water on a 10 kDa cutoff Amicon® centrifugal filter,

sterile filtered through a 0.22 μm pore filter, and stored as a 0.5 μg CSSSIINFEKL/μL solution at 4 °C until use.

3.2.4 Preparation and characterization of polyplexes

To form polyplexes, micelle solution was added to either plasmid DNA or poly(I:C) solution, and the mixture was vigorously pipetted. Polyplexes were rested for 30 min at room temperature before characterization. Nucleic acid loading was confirmed by a gel retardation assay, where polyplexes formulated at various nitrogen to phosphate (N/P) ratios were loaded into a 1% (w/v) agarose gel made from 1× Tris-acetate-EDTA buffer (40 mM Tris-acetate and 1 mM EDTA) containing 0.5 μg/mL ethidium bromide. Gel electrophoresis was performed at 100V for 40 min. After electrophoresis, the gel was imaged on a UV transilluminator to visualize nucleic acid migration. Polyplex size and surface charge (ζ-potential) were also measured on a Zetasizer Nano ZS (Malvern Instruments). For each Zetasizer measurement, 20 μL of polyplex loaded with 1 μg of poly(I:C) were diluted in 10 mM NaCl to a final volume of 800 μL. Three independent measurements were taken for each polyplex formulation.

3.2.5 Cell culture

The DC2.4 mouse dendritic cell line (gift of Prof. Kim Woodrow) was cultured in RPMI 1640 supplemented with 10% heat-inactivated fetal bovine serum (HIFBS), L-glutamine, 1× penicillin/streptomycin (P/S), 10 mM HEPES buffer, 1× non-essential amino acids, and 55 μM β-mercaptoethanol (BME). The Gal8-DC2.4 cell line was generated by co-transfecting plasmids containing a transposable galectin 8–green fluorescent protein (Gal8-GFP) construct and PiggyBac transposon (gifts of Prof. Jordan Green) using Lipofectamine 2000 (Thermo Fisher Scientific) and then sorting for the top 5% brightest GFP^+ singlet cell events using a custom FACSAria™ sorter (BD). Transfected cells were expanded and sorted three times to yield a polyclonal population of Gal8-GFP^{high} cells. The B3Z mouse $CD8^+$ T cell hybridoma line (gift of

Prof. Nilabh Shastri) was cultured in RPMI 1640 supplemented with 10% HIFBS, L-glutamine, 1× P/S, 1 mM sodium pyruvate, and 50 μM BME. The NIH/3T3 mouse fibroblast line (ATCC) was cultured in DMEM supplemented with 10% HIFBS, L-glutamine, 4.5 g/L D-glucose, 1× P/S, and 110 mg/mL sodium pyruvate. The B16-OVA mouse melanoma line (gift of Prof. Amanda Lund) was cultured in DMEM supplemented with 10% FBS, L-glutamine, 4.5 g/L D-glucose, and 1× P/S. DC2.4, NIH/3T3, and B16-OVA cells were passaged every three days or when 75% confluent and seeded to reach 50–100% confluency at time of treatment or harvest. B3Z cells were passaged no more than 10 times and maintained at a cell density under 7×10^5 cells/mL.

3.2.6 Gal8 endosomal disruption assay

Gal8-DC2.4 cells were seeded in glass-bottom half-area 96-well plates at 10^4 cells/well and cultured overnight. Mixed micelles with varying molar ratios of antigen-conjugated polymer (AP) to either melittin-conjugated polymer (MP) or control polymer without peptide (CP) were formulated to yield 1:1, 1:2, 1:3, and 1:4 MP:AP (VIPER-Vax) micelles or CP:AP (Control-Vax) micelles. Micelles were mixed with poly(I:C) to form polyplexes (N/P = 10) and added to wells to a final antigen concentration of 2 μg/mL. After 8 h of incubation, culture media was removed and replaced with imaging media (FluoroBrite DMEM supplemented with 25 mM HEPES, 10% FBS, and Hoechst 33342). Live cell imaging was performed using a 20× objective on a custom Leica SP8X laser scanning confocal microscope to capture > 2×10^4 cells per condition. Summation of punctate Gal8 pixel area and normalization to cell count was performed using a slightly modified version of the original MATLAB code provided by Kilchrist et al.[38] (available upon request). Each experiment was repeated three times on different passages of the same cell line and data are presented as the mean of these three experiments.

3.2.7 In vitro dendritic cell transfection

DC2.4 cells were seeded in 24-well tissue culture plates at 2.5×10^4 cells/well and cultured for 16 h prior to transfection. Polyplexes loaded with 1 μg of pmaxGFP plasmid were formulated as described in *Section 3.2.4* by mixing micelle solution with 0.1 mg/mL plasmid solution at desired N/P ratios. Polyplexes were rested for at least 10 min at room temperature. Cells were then transfected with polyplex for 4 h, washed with phosphate-buffered saline (PBS), and resuspended in culture media. After 40 h more of culture, cells were lifted by scraping and stained with Zombie Violet™ viability dye (BioLegend). An Attune NxT Flow Cytometer (Thermo Fisher Scientific) was used to determine percent GFP expression in the viable cell population.

3.2.8 In vitro dendritic cell uptake

DC2.4 cells were incubated with 2 μg/mL rhodamine-CSSSIINFEKL delivered as soluble peptide, VIPER-Vax micelles, or VIPER-Vax polyplexes (N/P = 10) for various durations before uptake was quantified by flow cytometry as described in *Section 3.2.7*.

3.2.9 Dendritic cell cross-presentation and viability assays

DC2.4 cells were seeded in 96-well U-bottom tissue culture plates at 5×10^4 cells/well. Twenty four hours after seeding, DC2.4 cells were pulsed for 2 h with 2.5 μg/mL CSSSIINFEKL in 100 μL of culture media, administered as soluble peptide or as poly(I:C) polyplexes (N/P = 10). After the 2 h pulse, DC2.4 cells were washed two times with PBS and co-cultured for an additional 20–24 h with B3Z cells (mouse $CD8^+$ T cell hybridomas that produce β-galactosidase upon binding of SIINFEKL-MHCI complexes) at 10^5 B3Z cells/well in 200 μL of B3Z media.[27,39] After 20–24 h of co-culture, cells were centrifuged at 500 rcf for 7 min and culture media was removed. Cells were subsequently resuspended in 150 μL/well of CPRG lysis buffer (0.15 mM chlorophenol red-β-D-galactopyranoside [Roche], 0.1% [v/v] Triton X-100, 9 mM $MgCl_2$, and 100 μM BME in PBS) and incubated in the dark at 37 °C for 1.5 h.[27] After 1.5 h of incubation, cross-presentation levels were

quantified by measuring the absorbance of chlorophenol red at 570 nm (reference 650 nm) using a Tecan Infinite M200 plate reader. To assess DC2.4 cell viability after polyplex treatment, DC2.4 cells were first seeded in tissue culture plates and pulsed with vaccine formulations as described above. Cell viability was measured 20–24 h after pulsing with an MTS assay (Promega) according to manufacturer protocol.

3.2.10 Bystander cross-presentation and viability assays

NIH/3T3 cells were seeded in 96-well U-bottom tissue culture plates at 2.1×10^3 cells/well. Twenty four hours after seeding, NIH/3T3 cells were pulsed for 4 h with 0.625, 1.25, 2.5, or 5.0 μg/mL CSSSIINFEKL in 100 μL of culture media, administered as soluble peptide or as poly(I:C) polyplexes (N/P = 10). After the 4 h pulse, polyplex-containing media was removed and fresh culture media was added without any PBS washes. NIH/3T3 cells were subsequently co-cultured with DC2.4 cells (5×10^4 cells/well) in 100 μL of NIH/3T3 media supplemented with 10 mM HEPES buffer.[40] Note that DC2.4 cells were maintained in NIH/3T3 media supplemented with 10 mM HEPES buffer for at least three days prior to co-culture with NIH/3T3 cells. After 24 h of DC2.4 co-culture, cross-presentation levels were quantified using the same B3Z co-culture assay described in *Section 3.2.9*. To assess NIH/3T3 cell viability after polyplex treatment, NIH/3T3 cells were first seeded in tissue culture plates and pulsed with vaccine formulations as described above, with the addition of two PBS washes after pulsing. Cell viability was measured 24 h after pulsing with an MTS assay according to manufacturer protocol.

3.2.11 Immunization of mice. All animal procedures were conducted under protocols approved by the Institutional Animal Care and Use Committee at the University of Washington. Female C57BL/6 mice (Charles River Laboratories), 6–8 weeks old, were immunized via intradermal injection at the right base of the tail. In all studies comparing efficacy of polyplex formulations, mice were immunized with 10 μg of peptide antigen (SIINFEKL or CSSSIINFEKL)

and 17.5 μg of poly(I:C) in 50 μL of 5% (w/v) glucose. All formulations were prepared < 1 h prior to injection.

3.2.12 Tetramer staining and intracellular cytokine staining

Female C57BL/6 mice were immunized intradermally on D0 and D21 with either (i) vehicle (5% glucose), (ii) SIINFEKL + poly(I:C), (iii) CSSSIINFEKL + poly(I:C), (iv) Control-Vax polyplexes (N/P = 10), or (v) VIPER-Vax polyplexes (N/P = 10) using antigen and adjuvant doses listed in *Section 3.2.11* (n = 6 per treatment group).[27] On D28, mice were euthanized by Avertin overdose, and harvested spleens were placed on ice in RPMI 1640 supplemented with 10% FBS (cRPMI). Spleens were mechanically dissociated into a single cell suspensions using a syringe plunger and a 40 μm cell strainer, which was rinsed with media to collect single cells and replaced for each spleen. Splenocytes were pelleted by centrifugation at 800 rcf and resuspended in cRPMI with 100 U/mL DNase I (Worthington) for 5 min before lysis of red blood cells with ammonium-chloride-potassium (ACK) lysing buffer (Gibco). Following a PBS wash, splenocytes were split for either immediate surface staining or SIINFEKL restimulation followed by surface and intracellular cytokine staining (ICCS). Surface staining of 2×10^6 splenocytes per mouse (2×10^6 splenocytes per well, 96-well U-bottom plate) was conducted at room temperature beginning with Zombie NIR™ viability staining (1:500; BioLegend), two washes with PBS + 1% (v/v) bovine serum albumin (PBSA), 15 min room temperature incubation with PE H-2K^b/SIINFEKL tetramer (1:200; NIH Tetramer Core Facility), two washes with PBSA, 30 min incubation on ice with antibody cocktail (eFluor450 CD3ε [1:100; clone 145-2C11; Invitrogen], FITC CD8α [1:1000; clone KT-15; ProImmune], APC CD19 [1:1000; clone 1D3; Invitrogen]), and three final washes with PBSA before analysis by flow cytometry. For SIINFEKL restimulation, 2×10^6 splenocytes were plated per well (96-well U-bottom plate) in cRPMI with 20 μg/mL SIINFEKL peptide and incubated for 1 h at 37 °C and 5% CO_2, after which Protein Transport Inhibitor Cocktail (Thermo Fisher Scientific) was added to a 1× concentration. Cells were incubated an additional 8 h to

accumulate intracellular cytokines. Following a PBSA wash, cells were stained for viability, CD3ε, CD8α, and CD19 as described above and then fixed and permeabilized using the Cytofix/Cytoperm™ kit (BD) according to manufacturer protocol. Finally, ICCS was performed on ice for 30 min with PE-Cy7 IFN-γ antibody (1:50; clone XMG1.2; Invitrogen), followed by three washes with Perm/Wash™ buffer (BD) and analysis by flow cytometry.

3.2.13 Tumor inoculation and monitoring

Female C57BL/6 mice were inoculated subcutaneously with 10^5 B16-OVA cells in the right hind flank and randomized into treatment groups (n = 8 per treatment group), with immunization on D4 and D11 after inoculation. Animal weight was recorded immediately prior to inoculation and every two days thereafter. Once tumors were palpable, tumor dimensions were measured by caliper every two days, and tumor volumes were calculated using the equation $V = (L \times W^2)/2$. Mice were euthanized when tumor mass exceeded 10% of body weight, when body weight loss exceeded 20%, or when severe tumor ulceration was observed.

3.2.14 Tumor dissociation and analysis of tumor-infiltrating T cells

Mice were overdosed with Avertin upon reaching tumor volume criteria for euthanasia (n = 3; D42). Tumors were resected and minced with a scalpel in a dissociation cocktail of 1 mM L-cysteine, 0.5 mM EDTA, 20 U/mL papain, 20 U/mL collagenase D (Sigma-Aldrich), and 125 U/mL DNase I (Worthington) in 5 mL of RPMI 1640 per tumor. Each tumor was placed in a C-tube and subjected to two "imp_tumor" dissociations cycles performed by a gentleMACS™ Dissociator (Miltenyi Biotec) separated by a 40 min incubation at 37 °C before filtration through a 70 μm cell strainer into a 50 mL tube. Single cell suspensions were washed three times with 50 mL of PBS before 2×10^6 cells per tumor were stained for analysis by flow cytometry. Antibody staining and flow cytometry was performed as described in *Section 3.2.12* for splenocytes with the addition of mouse Fc block (1:100; clone 93; BioLegend) before staining with eFluor506 PD-1

(1:100; clone J43; Invitrogen) and PE CD45 (1:500; clone REA737; Miltenyi Biotec) antibodies in addition to eFluor450 CD3ε and FITC CD8α antibodies.

3.2.15 Statistical analyses

Statistical tests were performed with GraphPad Prism and included a two-tailed Student's t-test with Welch's correction, an one-way ANOVA with post-hoc Tukey HSD test, and a logrank test. All flow cytometry data were analyzed with FlowJo software.

3.3 Results and Discussion

3.3.1 Design of a nanocarrier for subunit antigen and nucleic acid adjuvant

We designed our VIPER nanovaccine with the goal of using an endosomolytic polymer to (i) improve cross-presentation via delivery of peptide antigens into APC cytosols and (ii) co-deliver a nucleic acid adjuvant to these cross-presenting cells (**Figure 3.1**). VIPER was synthesized as a block copolymer with a hydrophilic, cationic block for adjuvant loading and a pH-sensitive, hydrophobic block for either endosomal release or peptide antigen delivery.[33] The former block comprises 2-(dimethylamino)ethyl methacrylate (DMAEMA) copolymerized with oligo(ethylene glycol) monomethyl ether methacrylate (OEGMA). The pH-sensitive block consists primarily of 2-diisopropylaminoethyl methacrylate (DIPAMA) with copolymerized pyridyl disulfide ethyl methacrylate (PDSEMA) for conjugation to thiolated peptides.[41,42] This DIPAMA-rich block transitions sharply from hydrophobic to hydrophilic upon decreasing pH below 6.4.[33] Consequently, the block copolymers self-assemble into core-shell structures at physiological, extracellular pH (pH > 7.0) but disassemble into individual polymer chains in acidic environments (pH < 6.5). Peptides conjugated to the pH-sensitive block are thus protected by polymer micellization in extracellular environments but are exposed after cellular internalization into acidic endosomes.

The exogenous antigen ovalbumin is a popular model antigen for cancer vaccine research because of its high immunogenicity and well-characterized epitopes.[43] For our studies, we selected CSSSIINFEKL, a variant of the ovalbumin MCHI epitope SIINFEKL, as a model peptide antigen because it bore an N-terminal cysteine for conjugation and was cross-presented more efficiently than SIINFEKL in other reported work.[44,45] For endosomal release, the bee venom–derived peptide melittin was selected based on our results from our previous work, where we screened a panel of lytic peptides for endosomolytic activity.[35] The resulting polymers used for formulation of the VIPER nanovaccine were (i) control polymer (p(OEGMA$_{8.6}$-*co*-DMAEMA$_{50.0}$)-*b*-p(DIPAMA$_{25.3}$-*co*-PDSEMA$_{1.0}$) without conjugated peptide (CP), (ii) CSSSIINFEKL antigen-conjugated polymer (AP), and (iii) melittin-conjugated polymer (MP, also known as VIPER). Prior to micellization, polymers were mixed in acidic buffer at defined molar ratios of AP to MP or AP to CP (**Figure 3.1**). Neutralization of the acidic buffer triggered micellization of the polymer chains, forming mixed micelles with encapsulated melittin (VIPER-Vax) or without encapsulated melittin (Control-Vax).

Because the hydrophilic block of VIPER was designed for nucleic acid condensation, we selected poly(I:C) as an adjuvant.[33] Poly(I:C) is a synthetic viral RNA analog that triggers APC maturation and inflammatory cytokine production through agonism of Toll-like receptor 3.[11,46] Importantly, localized delivery of poly(I:C) via nanovaccines has been shown to limit its systemic toxicity while also amplifying on-target effects in APCs.[47,48] Poly(I:C) was incorporated into the VIPER nanovaccine by electrostatic complexation with VIPER's cationic micelle shell, similar to how polyethyleneimine and cationic liposomes were used for poly(I:C) complexation in previous work.[36,49,50] Complete adjuvant encapsulation was achieved at a polymer to adjuvant nitrogen to phosphate (N/P) ratio of five (polymer DMAEMA to adjuvant phosphate) (**Supplemental Figure 3.1**). VIPER-Vax and Control-Vax polyplexes (N/P = 10) shared similar physicochemical properties, exhibiting ζ-potentials of +10–12 mV and diameters of ~150 nm (**Supplemental Figure 3.2**). Based on our previous work with cationic polymer–nucleic acid complexes and

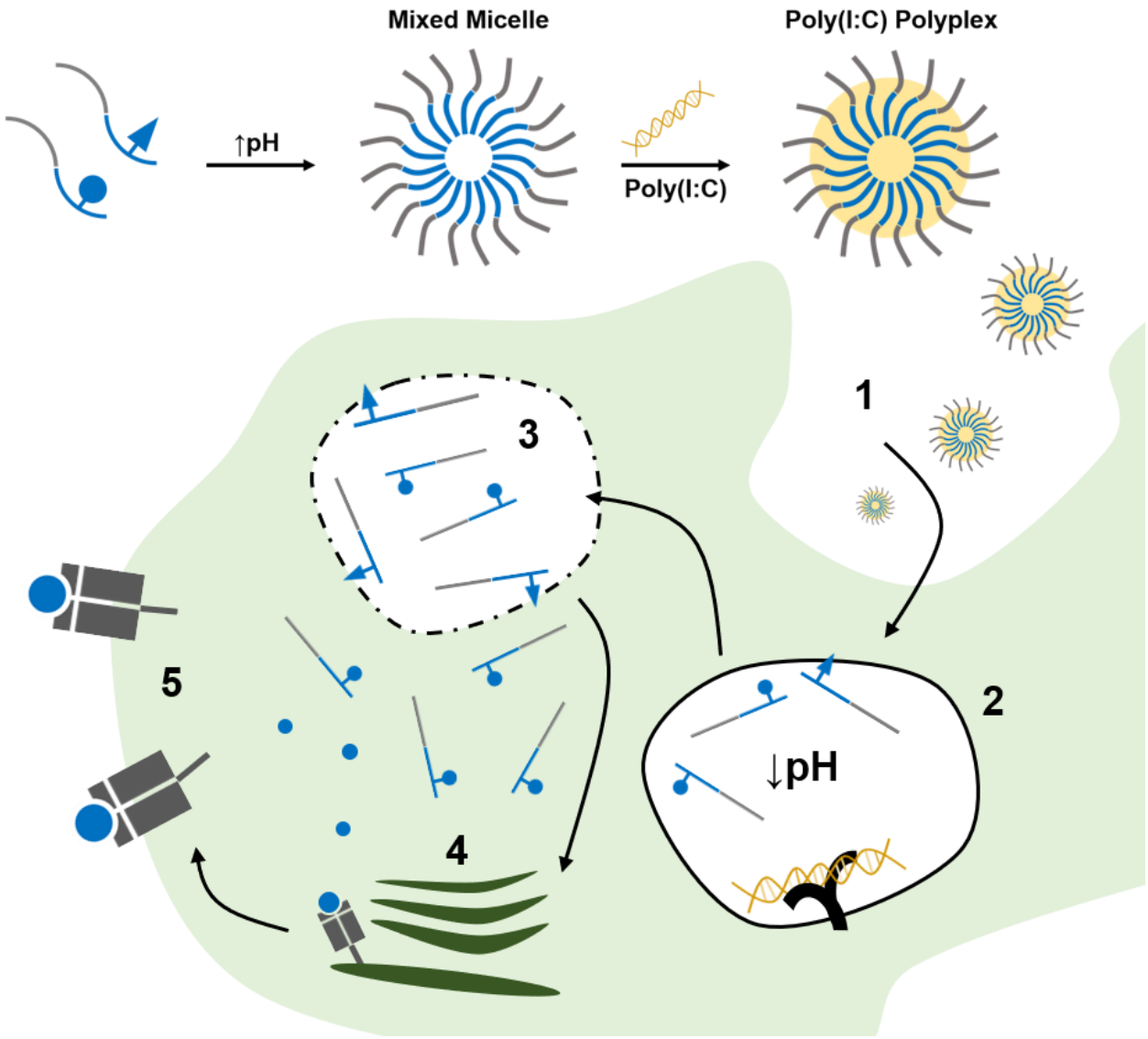

Figure 3.1 **Proposed mechanism for agonism of Toll-like receptor 3 and enhancement of cross-presentation by VIPER-Vax.** pH-sensitive polymers conjugated to lytic (triangle) or antigenic (circle) peptide persist as single polymer chains when stored under acidic conditions. At physiological pH, the polymer chains assemble into mixed micelles. Poly(I:C) vaccine polyplexes (VIPER-Vax) are formulated by simple mixing of micelles with naked poly(I:C). When delivered to an antigen-presenting cell, VIPER-Vax (1) undergoes endocytosis followed by (2) pH-triggered disassembly in the acidic endosome, allowing poly(I:C) to bind and activate Toll-like receptor 3. Lytic peptide–conjugated polymers also (3) disrupt the endosomal membrane, releasing peptide antigens into the cytosol for (4) processing in the endoplasmic reticulum and loading onto MHCI molecules. MHCI-antigen complexes are then transported to the cell membrane for (5) cross-presentation.

other reports of such work in the literature, we expected efficient cellular internalization of our positively charged poly(I:C) polyplexes.[51–53] Indeed, the size and surface charge of these

polyplexes allowed for uptake of rhodamine-labeled CSSSIINFEKL by DC2.4 mouse dendritic cells in vitro (**Supplemental Figure 3.3**).

3.3.2 Intracellular vaccine delivery and endosomal disruption

We first evaluated the ability of mixed micelle VIPER formulations to mediate endosomal disruption in Gal8-GFP–expressing DC2.4 cells. Kilchrist et al.[38] recently developed a high-throughput confocal microscopy–based assay that correlates endosomal release of intracellularly delivered cargoes with recruitment of galectin-8 (Gal8) to disrupted endosomal membranes. In this assay, the total pixel area of bright, punctate Gal8–green fluorescent protein (Gal8-GFP) signal in a given image is summed and divided by the number of cells in that image, such that greater GFP pixel area per cell correlates with a greater number of disrupted endosomes. We generated a Gal8-DC2.4 cell line and used it to determine the minimum ratio of MP to AP in micelle formulations required for efficient endosomal disruption.

Gal8-DC2.4 cells were treated with poly(I:C) polyplexes (N/P = 10) consisting of 1:1, 1:2, 1:3, or 1:4 MP:AP (VIPER-Vax) or CP:AP (Control-Vax) mixed micelles, and Gal8 signal was quantified by live cell imaging after an 8 h incubation (**Figure 3.2A,B**). Increased MP content in VIPER-Vax formulations correlated with increased endosomal disruption (ΣGal8/cell = 650 for 1:1 MP:AP vs. 102 for 1:4 MP:AP), and all Control-Vax formulations induced little detectable endosomal disruption (**Figure 3.2A**). Because treatment with both 1:1 and 1:2 VIPER-Vax formulations gave rise to significantly greater ΣGal8/cell than equivalent Control-Vax formulations, we proceeded with 1:2 MP:AP mixed micelles to maximize micellar antigen concentration (5% w/w) while retaining effective endosomal escape functionality.

After confirming that VIPER-Vax disrupts endosomes in DC2.4 cells, we investigated whether this increase in endosomal disruption would augment cytosolic delivery of biomacromolecule cargo. We substituted poly(I:C) with pmaxGFP, a GFP reporter transgene. Like poly(I:C), this plasmid is encapsulated by cationic polymers via electrostatic interactions.[35]

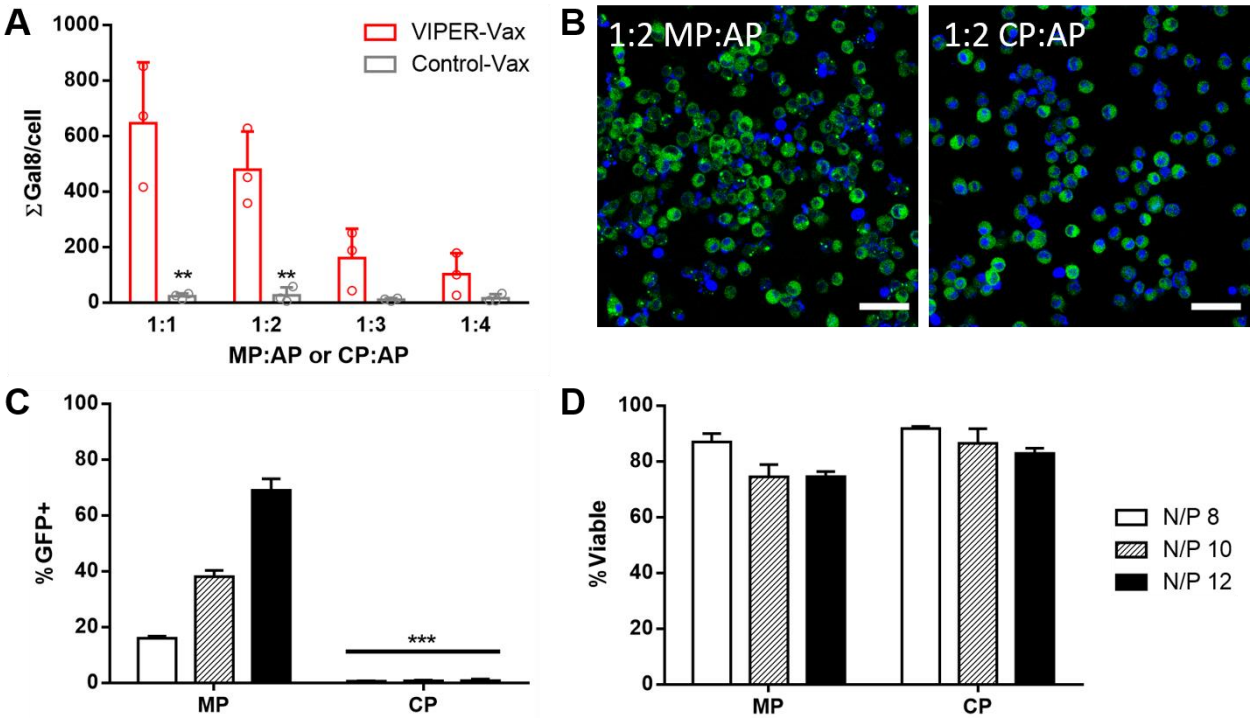

Figure 3.2 **Melittin is essential for endosomal disruption and plasmid transfection in DC2.4 cells. (A)** Gal8-DC2.4 cells were treated with poly(I:C) polyplexes (N/P = 10) consisting of 1:1, 2:1, 3:1, or 4:1 AP:MP (VIPER-Vax) or AP:CP (Control-Vax) mixed micelles, and Gal8 signal was quantified through live cell imaging after 8 h of incubation. Data are expressed as mean + SD, n = 3 independent experiments. Statistical significance is derived from Student's t-test comparing VIPER-Vax to Control-Vax at each mixed micelle AP:MP or AP:CP ratio (**p-value ≤ 0.01). **(B)** Representative images of Gal8-DC2.4 cells treated with the mixed micelle formulations carried forward in this work. Hoescht stained nuclei appear in blue and Gal8-GFP appears in green; punctate Gal8-GFP is localized to disrupted endosomes. Scale bar = 50 μm. **(C)** GFP expression and **(D)** cell viability were analyzed by flow cytometry 48 h after transfection of DC2.4 cells with polyplexes composed of pmaxGFP plasmid and either MP or CP. Data are expressed as mean + SD, n = 3 independent experiments. Statistical significance is derived from Student's t-test comparing MP and CP at each N/P ratio (***p-value ≤ 0.001).

Cytosolic delivery and subsequent nuclear translocation of the plasmid results in expression of GFP, and the percentage of transfected GFP$^+$ cells can be quantified by flow cytometry analysis.[35] We observed that MP polyplexes transfected more efficiently than CP polyplexes (69% GFP$^+$ cells vs. 0.77% GFP$^+$ cells at N/P = 12) in culture media, verifying that pH-dependent display of melittin facilitates cytosolic delivery of plasmids (**Figure 3.2C,D**).[33–35] For all subsequent experiments, we formulated VIPER-Vax and Control-Vax polyplexes at N/P = 10 to minimize polyplex

destabilization by anionic extracellular matrix components while maintaining poly(I:C) doses comparable to those used in previously reported in vivo studies.[47,49,50,54]

3.3.3 Cross-presentation

Given that VIPER-mediated endosomal disruption resulted in efficient cytosolic plasmid delivery in APCs, we then assessed whether this same endosomal disruption could improve cross-presentation efficiency via cytosolic peptide antigen delivery.[6,7] To measure cross-presentation and downstream T cell priming, we utilized the B3Z cell line, a mouse $CD8^+$ T cell hybridoma that produces β-galactosidase upon binding of its T cell receptor to the mouse SIINFEKL-MHCI complex.[39] Therefore, cross-presentation by mouse APCs can be indirectly quantified by co-culturing vaccine-pulsed APCs with B3Z cells and performing a colorimetric β-galactosidase assay (**Figure 3.3A**).[27,39] With this colorimetric assay, we surprisingly found that DC2.4 cells pulsed directly with VIPER-Vax polyplexes cross-presented at statistically similar levels to those pulsed with Control-Vax polyplexes and free CSSSIINFEKL (**Figure 3.3A**).

Interestingly, we achieved greater cross-presentation efficiency in this B3Z assay format by increasing VIPER-Vax dose to cytotoxic levels (data not shown). Based on this observation, we hypothesized that cross-presentation may be mediated (at least in part) by apoptotic "bystander" cells, where antigen-loaded apoptotic bodies from VIPER-pulsed APCs are processed by their viable counterparts for cross-presentation (**Figure 3.3C**).[37,55,56] This phenomenon has been reported for similar polyplex vaccine carriers complexed with antigen-encoding plasmid.[40] To explore our hypothesis, we pulsed NIH/3T3 fibroblasts with cytotoxic doses of polyplexes (0.625, 1.25, 2.5, and 5.0 μg/mL antigen doses) and subsequently co-cultured the fibroblasts with DC2.4 cells (**Supplemental Figure 3.3**).[40] We demonstrated ~7.3-, ~2.7-, and ~1.5-fold increases in cross-presentation when melittin was included in the polyplexes, at 1.25, 2.5, and 5 μg/mL antigen, respectively (**Figure 3.3B**). Note that NIH/3T3 fibroblasts express an MHC haplotype ($H\text{-}2^q$) incompatible for antigen presentation to $H\text{-}2K^b$–restricted B3Z cells, so any detectable

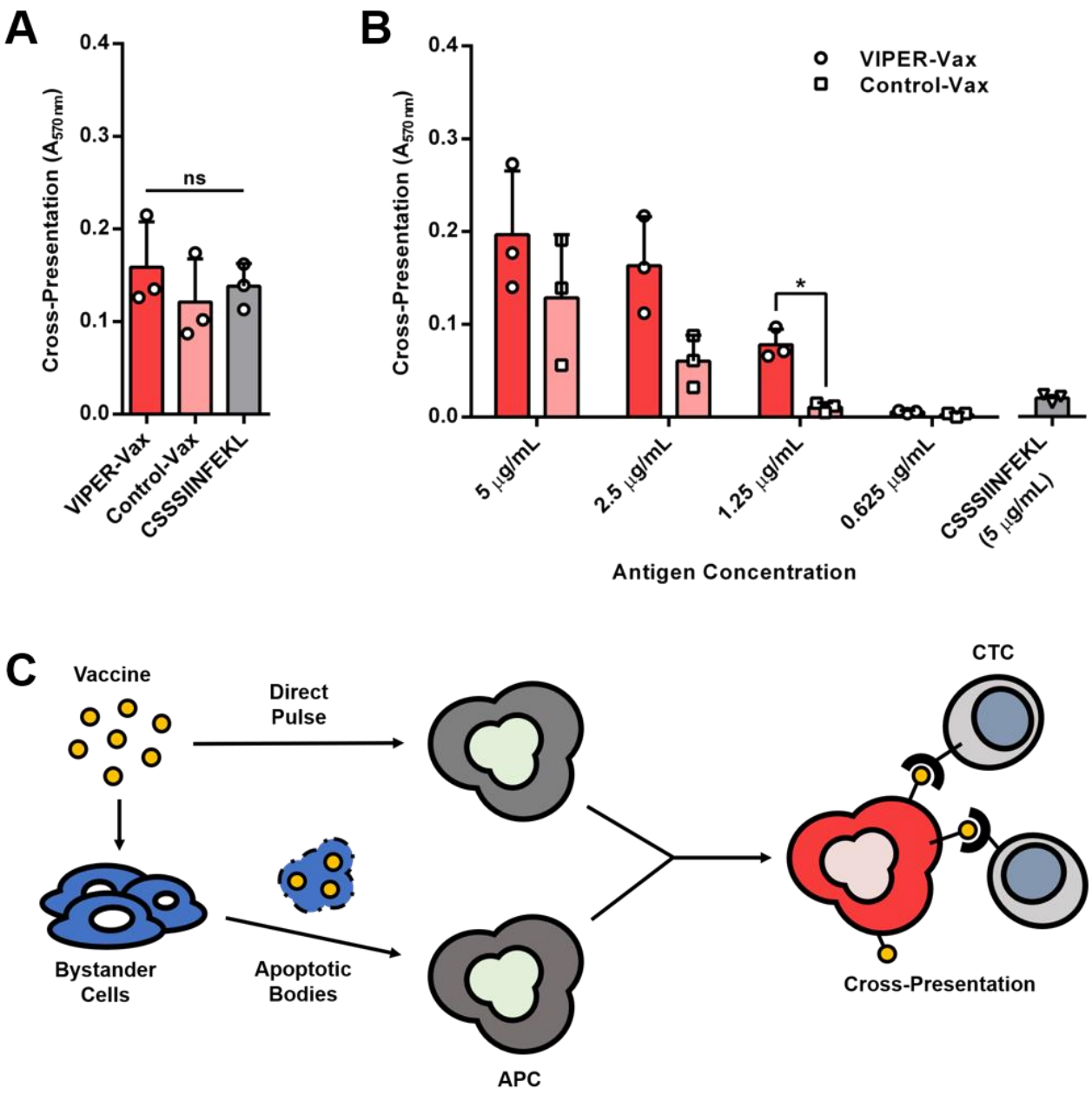

Figure 3.3 **Melittin potentiates cross-presentation via induction of local cell death.** **(A)** DC2.4 cells were pulsed with free CSSSIINFEKL, VIPER-Vax polyplex, or Control-Vax polyplex (2.5 μg/mL antigen) for 2 h and subsequently co-cultured for 20–24 h with B3Z cells. Recognition of MHCI-bound SIINFEKL by B3Z cells was detected using a colorimetric assay. Data expressed as mean + SD, $n = 3$ independent experiments. Statistical significance is derived from an one-way ANOVA with post-hoc Tukey HSD test (ns = no significance). **(B)** NIH/3T3 cells were pulsed with VIPER-Vax polyplex or Control-Vax polyplex for 4 h at cytotoxic polyplex doses. NIH/3T3 cells were subsequently co-cultured for 24 h with DC2.4 cells. B3Z cells were added after 24 h of NIH/3T3-DC2.4 co-culture, and the same colorimetric assay from (A) was used to quantify cross-presentation. Data are expressed as mean + SD, $n = 3$ independent experiments. Statistical significance is derived from a two-tailed Student's t-test with Welch's correction (*p-value ≤ 0.05). **(C)** Cross-presentation may occur after direct vaccine transfer into APCs or APC uptake of vaccine-loaded apoptotic bodies from bystander cells.

activation of B3Z cells may be directly attributed to DC2.4 cross-presentation and not NIH/3T3 antigen presentation.[57]

Taken altogether, these results suggest that our polyplex formulations stimulate cross-presentation through two distinct mechanisms: polyplexes may deliver vaccine cargo directly into APCs, or APCs may uptake vaccine-loaded apoptotic bodies produced by polyplex-pulsed bystander cells (**Figure 3.3C**).[40] Importantly, addition of melittin—which possesses cytolytic properties and has been utilized as a cancer immunotherapy agent—into the poly(I:C) polyplex formulation significantly increases cross-presentation through the latter mechanism.[58,59] In this way, VIPER-Vax behaves much like its virus namesake, "infecting" non-APC populations, killing them, and allowing local APCs to cross-present "viral" antigens of interest from apoptotic debris.[37,55] However, the degree to which melittin-mediated endosomal disruption affects cross-presentation remains unclear, as increasing melittin dose also increases cytotoxicity, resulting in cross-presentation associated with local cell death (**Supplemental Figure 3.3**). It is worth noting that MHCI loading may also take place within endosomes, and thus efficient endosomal peptide delivery alone may account for the cross-presentation observed in CSSSIINFEKL- and Control-Vax–treated DC2.4 cells, whereas cytosolic delivery of nucleic acid cargo is necessary for its bioactivity (**Figure 3.2, Figure 3.3A**).[7] Although cytocompatible VIPER-Vax doses are sufficiently endosomolytic for gene transfer in APCs, the corresponding quantity of cytosolically delivered antigen may be insufficient to enhance cross-presentation via cytosolic MHCI loading pathways (**Figure 3.2C,D**).[6,7]

An isolated investigation of how VIPER may augment cross-presentation through cytosolic peptide antigen delivery will require reduction of polymer cytotoxicity while preserving melittin's endosomal release properties. One possible approach for reducing VIPER cytotoxicity is the replacement of cationic DMAEMA in the polymer's hydrophilic block with neutrally charged monomers, as DMAEMA itself can lyse cell membranes and cause cell death.[60,61] Neutralizing VIPER's hydrophilic block may enable determination of a micellar melittin dose that potentiates

cross-presentation while minimizing cytotoxicity; furthermore, alternative vaccine adjuvant strategies may be explored, as neutral VIPER cannot electrostatically complex with nucleic acid adjuvants like poly(I:C).

3.3.4 Cytotoxic T cell responses in tumor-naïve mice

Armed with a vaccine nanocarrier capable of inducing efficient cross-presentation of peptide antigen cargo in vitro (albeit via a different mechanism than we expected), we sought to establish whether VIPER-Vax could elicit a therapeutically relevant, antigen-specific CTC response in mice. We hypothesized that our nanoformulation would prime a greater adaptive immune response than soluble vaccine formulations due to (i) enhanced co-delivery of antigens and adjuvants to APCs and (ii) reduced lymphatic clearance.[14–16] Based on our in vitro results, we further hypothesized that delivery of poly(I:C) in the context of VIPER-enhanced cross-presentation would result in greater expansion and functional maturation of anti-SIINFEKL CTCs. As a first step towards characterizing the cellular immune responses generated by VIPER-Vax, we intradermally vaccinated healthy mice with various antigen/poly(I:C) formulations on days 1 and 21 and analyzed splenic CTCs using tetramer staining and intracellular cytokine staining (ICCS) on day 28 (**Figure 3.4, Supplemental Figure 3.5**). We selected the dermis as the immunization site because it is rich in non-APC populations (e.g., fibroblasts) through which VIPER-induced cell death can mediate antigen transfer into skin-resident APCs.[62,63]

Compared to mice vaccinated with soluble CSSSIINFEKL/poly(I:C), mice vaccinated with VIPER-Vax had significantly more H-2K^b/SIINFEKL tetramer–bound CD8$^+$ T cells (4.57% vs. 2.55%) and significantly more SIINFEKL-specific, IFN-γ$^+$ CTCs (6.85% vs. 1.86%) (**Figure 3.4**). While mice treated with Control-Vax also exhibited an increased antigen-specific CTC response relative to mice treated with soluble CSSSIINFEKL/poly(I:C), this increase was not statistically significant. Surprisingly, vaccination with SIINFEKL/poly(I:C) yielded no detection of antigen-specific T cells beyond assay background established by vehicle-treated mice.

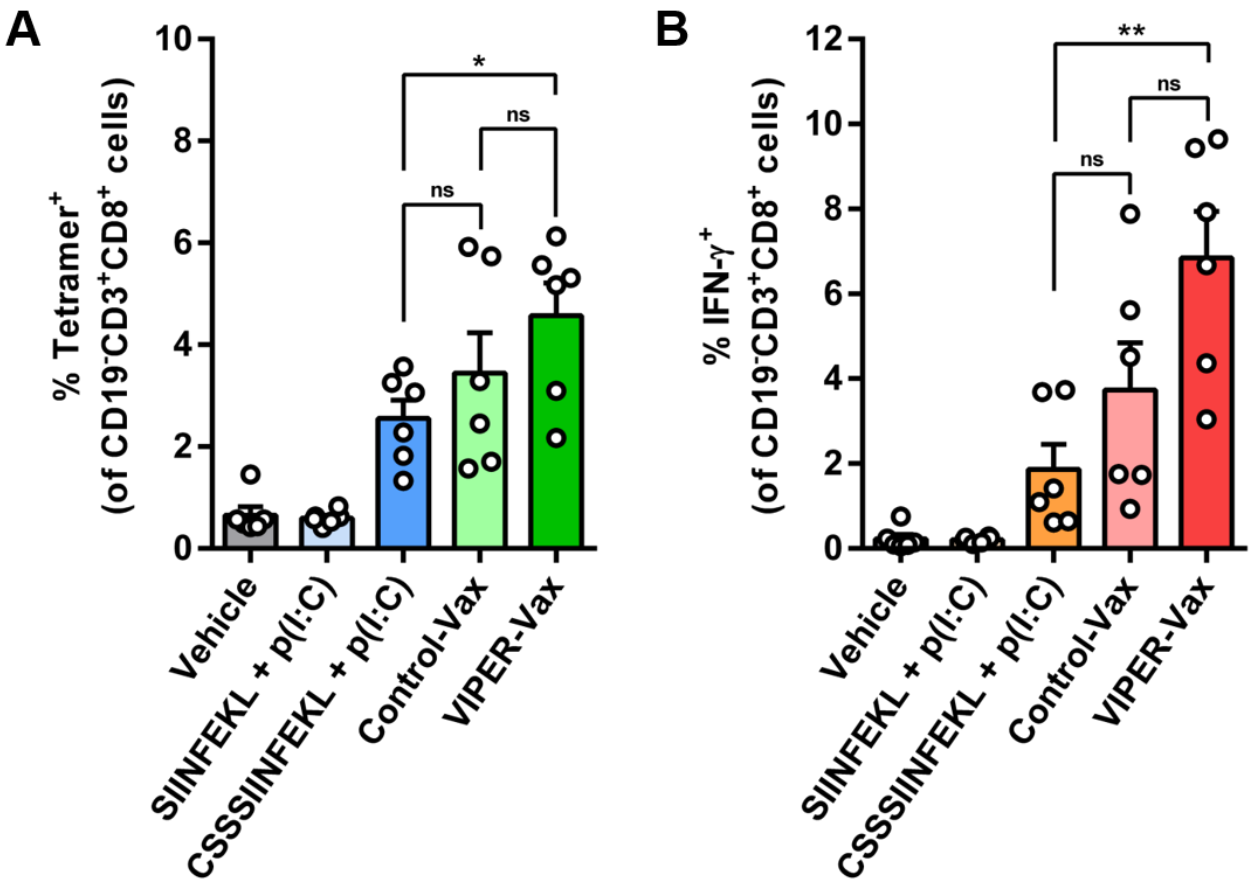

Figure 3.4 **Polyplex vaccination enhances the generation of antigen-specific cytotoxic T cells.** On days 1 and 21, female C57BL/6 mice were vaccinated intradermally at the base of the tail with various formulations containing 10 μg CSSSIINFEKL and 17.5 μg poly(I:C) in 50 μL of 5% glucose or with vehicle (5% glucose) alone. On day 28, spleens were harvested and dissociated splenocytes were either **(A)** directly stained with H-2K^b/SIINFEKL tetramer or **(B)** restimulated in culture with 20 μg/mL SIINFEKL for 8 h before intracellular staining of IFN-γ. Data are expressed as mean + SEM, n = 6. Statistical significance is derived from Student's t-test (*p-value ≤ 0.05; **p-value ≤ 0.01; ns = no significance).

These results demonstrate that VIPER-Vax can be used for subunit antigen delivery and further support the correlation between cross-presentation efficiency and antigen-specific CTC response levels.[27,44,64,65] As measured by tetramer staining and ICCS, vaccination with VIPER-Vax generated the largest number of anti-SIINFEKL CTCs of any formulation tested in this study. Furthermore, both VIPER-Vax and Control-Vax formulations generated a greater antigen-specific cellular immune response than either soluble antigen/adjuvant mixture, corroborating the importance of co-delivering antigens and adjuvants to APCs. The poor performance of

SIINFEKL/poly(I:C) relative to CSSSIINFEKL/poly(I:C) has been reported in a previous study and is attributed to less efficient MHCI loading in the absence of the CSS linker.[44,45] Overall, these data shows that VIPER-Vax immunization produces large quantities of antigen-specific CTCs with robust IFN-γ expression; inclusion of melittin in the VIPER formulation is also necessary to significantly enhance adaptive immune responses over those elicited by the control formulations.

3.3.5 Therapeutic cancer vaccination

Having validated that VIPER-Vax induces a strong anti-SIINFEKL CTC response, we sought to evaluate the therapeutic relevance of this response in mice bearing syngeneic B16-OVA flank tumors. B16 tumors grow rapidly after subcutaneous inoculation and undergo metastatic-like engraftment when injected intravenously.[66] This tumor line also expresses several well-defined endogenous neoantigens that render the tumor susceptible to vaccine-induced immunity.[66] Because B16 neoantigens are typically poorly immunogenic, B16 cells expressing exogenous, highly immunogenic ovalbumin (B16-OVA) are often used for initial screens of vaccine efficacy, where ovalbumin or its epitopes are administered as antigens to B16-OVA–bearing mice.[43]

Prophylactic immunization of mice with a sufficiently potent ovalbumin vaccine can prevent engraftment of B16-OVA tumors.[44] Nevertheless, we opted for a survival analysis of therapeutically vaccinated mice because most cancers occur spontaneously.[67] VIPER-Vax was administered on days 4 and 11 after B16-OVA tumor inoculation with dosing equivalent to our previous study in tumor-naïve mice (**Figure 3.5A**). Average tumor growth rates and the survival of VIPER-Vax–vaccinated mice were benchmarked against those of mice vaccinated with (i) a soluble mixture of SIINFEKL and poly(I:C), (ii) SIINFEKL and poly(I:C) emulsified in incomplete Freund's adjuvant (IFA), or (iii) vehicle (5% glucose). All vaccine formulations delayed tumor growth and statistically prolonged survival relative to vehicle (**Figure 3.5B,C**). However, survival rates between the three vaccine treatment groups were not statistically different (**Figure 3.5C**).

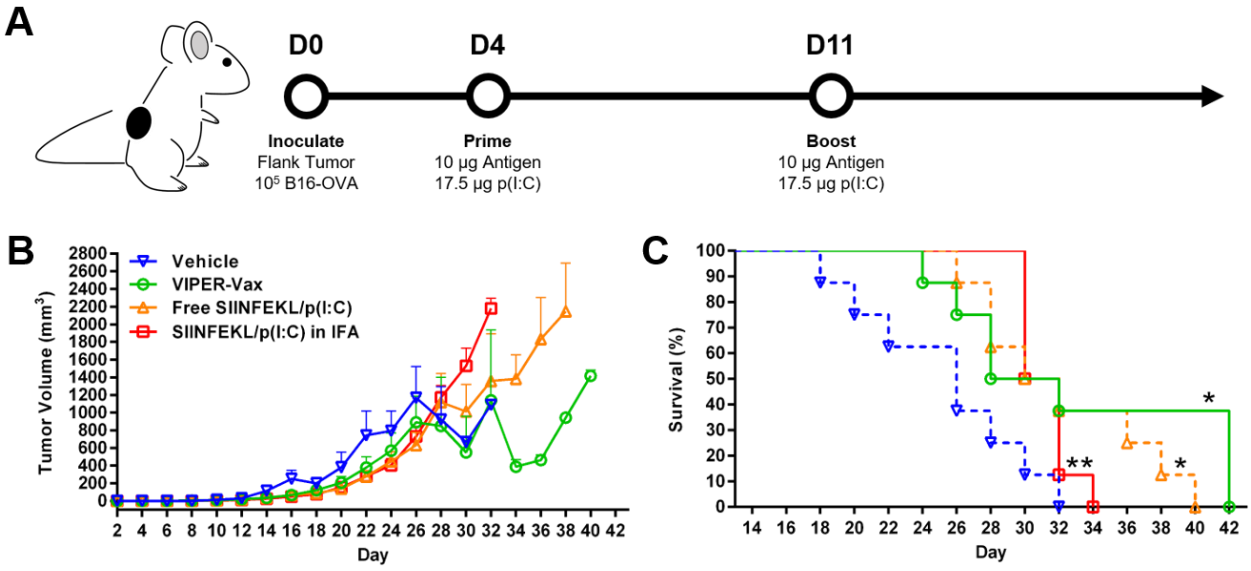

Figure 3.5 **Therapeutic polyplex vaccination delays tumor growth and prolongs survival in a subset of B16-OVA tumor–bearing mice. (A)** Female C57BL/6 mice were subcutaneously inoculated with 10^5 B16-OVA cells and randomized into various treatment groups**.** On days 4 and 11 after inoculation, mice were vaccinated intradermally at the right base of the tail with various formulations containing 10 μg CSSSIINFEKL and 17.5 μg poly(I:C). 5% glucose was used as a vehicle control. Tumor volume and animal weight were measured every other day. Animals were euthanized when tumor mass exceeded 10% body weight, when body weight loss exceeded 20%, or when severe tumor ulceration was observed. **(B)** Average tumor volumes as measured over the course of 42 days. Data are expressed as mean + SEM, n = 8. **(C)** Kaplan–Meier survival curves for mice immunized with various vaccine formulations. All vaccine formulations prolonged survival relative to vehicle. VIPER-Vax extended survival in 3/8 mice. Statistical significance is derived from a logrank test (*p-value ≤ 0.05; **p-value ≤ 0.01).

Although VIPER-Vax elicited strong anti-SIINFEKL CTC responses in tumor-naïve mice, therapeutic vaccination with VIPER-Vax in B16-OVA–bearing mice did not significantly improve survival outcomes over vaccination with conventional formulations. Notably, vaccination with VIPER-Vax delayed tumor growth in a subset of mice (3 of 8 mice) and extended their survival beyond all other mice in the study (**Figure 3.5C, Supplemental Figure 3.6**). We performed a terminal analysis of spleen- and tumor-resident cells from this subset of VIPER-Vax–treated mice and found that only 0.75% of $CD8^+$ splenocytes were IFN-γ^+ and that 44% of tumor-infiltrating $CD45^+CD8^+$ cells were PD-1^+ (**Supplemental Figure 3.7**). These data indicate T cell exhaustion, a hallmark of tumor immunosuppression.[2,4] Gradual immunosuppression of CTC effector

function by the tumor is a disappointing but not surprising outcome. Previously reported cancer nanovaccines—even those that statistically outperform soluble antigen/adjuvant formulations—required co-administration with immune checkpoint inhibitors for long-lasting antitumor immunity.[44,64]

Prior work has also shown that cationic polyplexes aggregate after injection into the dermis, likely because of charge interactions between cationic polymer side groups and anionic proteoglycans in extracellular matrix.[68,69] We suspect this aggregation may slow uptake of polyplexes by skin-resident APCs, reducing the rate of antigen transport to lymph nodes. Thus, intradermal vaccination with VIPER-Vax may not prime a sufficiently rapid immune response against aggressive cancers like B16 melanoma. The persistence of antigen in peripheral tissue may also result in antigen tolerance or CTC fratricide, a known disadvantage of slow-releasing vaccine formulations like IFA.[4] Indeed, immunization with an IFA emulsion of SIINFEKL and poly(I:C) provided the least therapeutic benefit of the vaccine formulations tested in the B16-OVA survival study. Given these results, we expect that VIPER-Vax would perform better as a prophylactic vaccine. Its therapeutic efficacy may also be improved by addition of MHC class II epitopes (to activate a T_H1 $CD4^+$ T cell response) or by co-administration of immune checkpoint inhibitors.[1,70] Future work in our laboratory will focus on altering the surface chemistry of VIPER micelles to enable rapid lymphatic trafficking. These surface chemistry modifications will also eliminate DMAEMA-associated toxicity as previously discussed, allowing direct investigation of how endosomal melittin exposure in APCs affects immune responses and therapeutic vaccination outcomes.

3.4 Conclusions

VIPER-Vax, a polymer micelle/poly(I:C) polyplex nanovaccine, disrupted endosome membranes via pH-sensitive exposure of encapsulated melittin, a lytic peptide. We hypothesized that VIPER-

Vax would enhance cross-presentation by efficiently delivering co-encapsulated peptide antigens into cytosolic MHCI loading pathways. However, we found that cross-presentation is enhanced only when VIPER-Vax induces lytic cell death, enabling resident APCs to cross-present antigens after uptake of vaccine-loaded apoptotic bodies. Despite the unexpected mechanism by which VIPER-Vax augments cross-presentation efficiency, intradermal immunization with VIPER-Vax generated larger numbers of antigen-specific CTCs in vivo than soluble antigen/adjuvant mixtures. While therapeutic vaccination with VIPER-Vax delayed B16-OVA tumor growth in a subset of mice, it did not consistently outperform traditional antigen/adjuvant formulations. This lack of therapeutic efficacy was likely due to slow T cell priming kinetics, which may be caused by polyplex depot formation after intradermal VIPER-Vax administration. In summary, we report a polyplex formulation for subunit antigen delivery that increases cross-presentation and improves antigen-specific CTC response. Future work will focus on new micelle surface chemistries that (i) decouple VIPER-Vax cytolysis from endosomolysis and (ii) facilitate rapid trafficking of VIPER-Vax to APCs in vivo, thereby enabling further investigation of how co-delivering lytic and antigenic peptides to APCs affects therapeutic CTC responses in aggressive cancer models.

3.5 Acknowledgements

This work was supported by NIH grants 1R01CA177272 and R01NS064404. Albert Yen was supported by a National Science Foundation Graduate Research Fellowship under grant DGE-1256082. We are grateful to Prof. Kim Woodrow (University of Washington) for kindly providing DC2.4 cells and for allowing the use of her lab's Zetasizer and plate reader. We are grateful to Prof. Jordan Green (Johns Hopkins University) for Gal8-GFP and PiggyBac transposon plasmids and to Prof. Craig Duvall (Vanderbilt University) for MATLAB code that enabled implementation of the Gal8 assay. We also acknowledge support from the National Institutes of Health (S10 OD016240) to the W.M. Keck Center for Advanced Studies in Neural Signaling and the assistance

of Keck Center manager Dr. Nathaniel Peters in performing the Gal8 assay. We are grateful to Prof. Nilabh Shastri (Johns Hopkins University) for kindly providing B3Z cells. We are grateful to Prof. Amanda Lund (Oregon Health & Science University) for kindly providing B16-OVA cells. We thank the NIH Tetramer Core Facility for providing H-2K^{b}/SIINFEKL tetramer. Finally, we acknowledge Dr. Hannah Frizzell (University of Washington) for many helpful discussions regarding study design.

3.6 Supporting Information

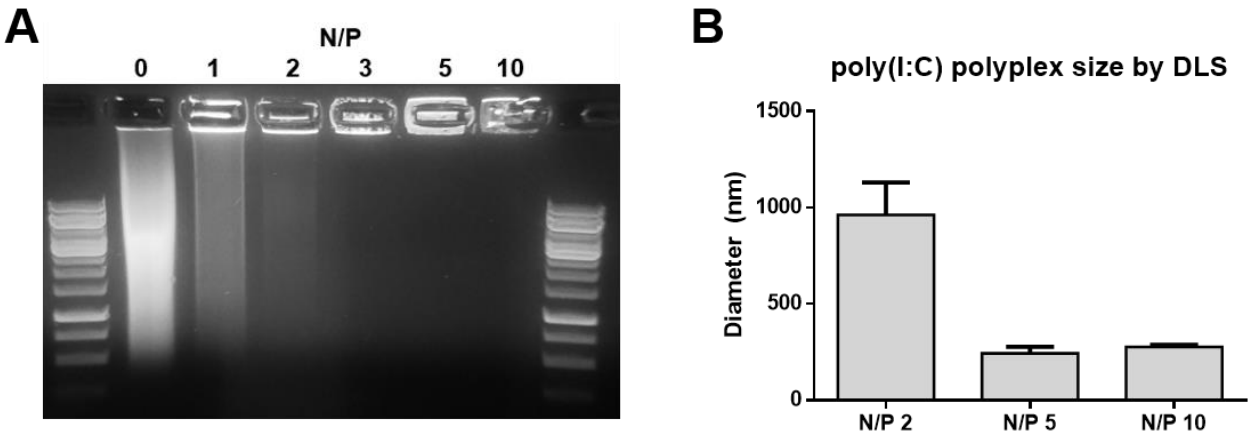

Supplemental Figure 3.1 **VIPER micelles form condensed polyplexes with poly(I:C).** Cationic polymer micelles were mixed with poly(I:C) nucleic acid adjuvant at various N/P ratios. **(A)** Nucleic acid packaging efficiency was characterized by a gel retardation assay. At higher N/P ratios, poly(I:C) was trapped within polyplexes and was unable to migrate through the gel during electrophoresis. **(B)** Polyplex size was evaluated by dynamic light scattering (DLS). Data are expressed as mean + SD, n = 3 independent measurements.

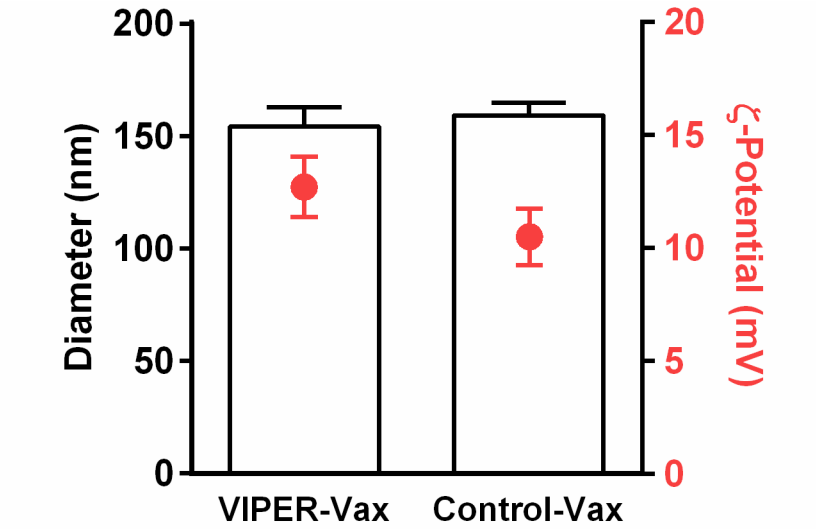

Supplemental Figure 3.2 **Characterization of VIPER-Vax and Control-Vax polyplexes at N/P = 10.** Cationic mixed micelles with (VIPER-Vax) or without (Control-Vax) melittin were mixed with poly(I:C) at N/P = 10 to form polyplexes. Polyplex diameter and surface charge were evaluated by dynamic light scattering and ζ-potential measurements, respectively. Data are expressed as mean + SD, n = 3 independent measurements.

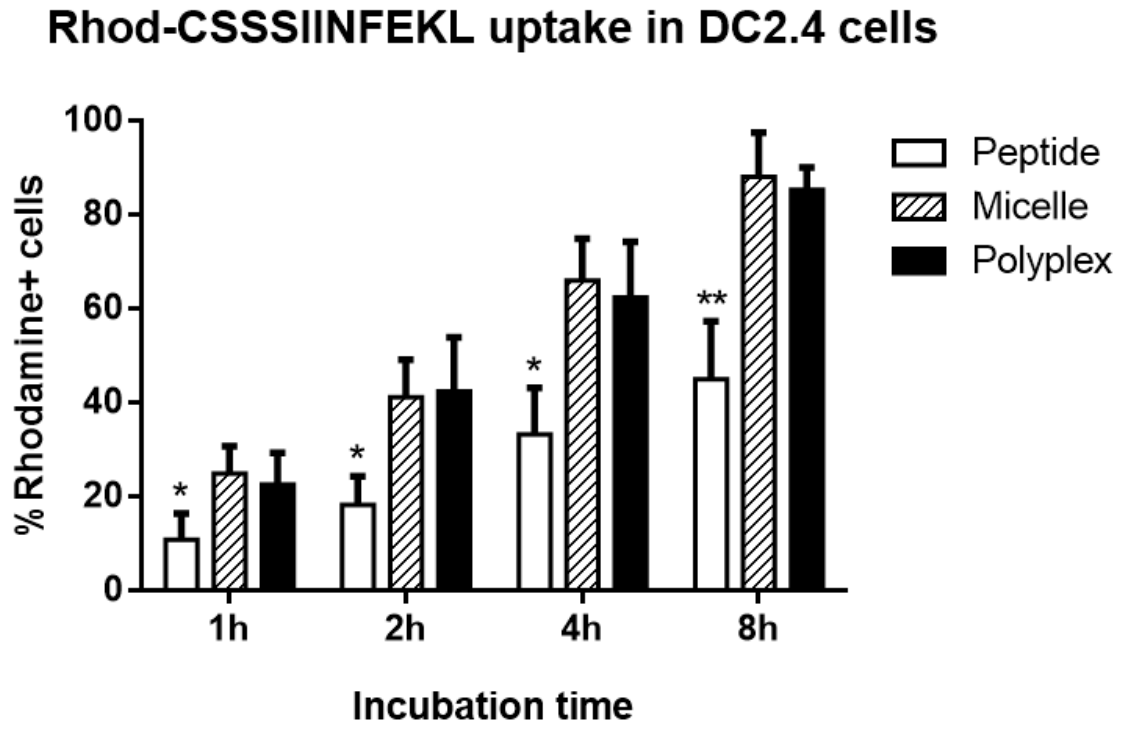

Supplemental Figure 3.3 **DC2.4 cells uptake fluorescently labeled peptide antigen.** DC2.4 cells were incubated with 2 μg/mL rhodamine-CSSSIINFEKL formulated as free peptide, cationic micelle, or N/P=10 poly(I:C) polyplex. Uptake was quantified by flow cytometry at various time points. Data are expressed as mean + SD, $n = 3$ independent experiments. Statistical significance is derived from Student's t-test (*p-value ≤ 0.05; **p-value ≤ 0.01).

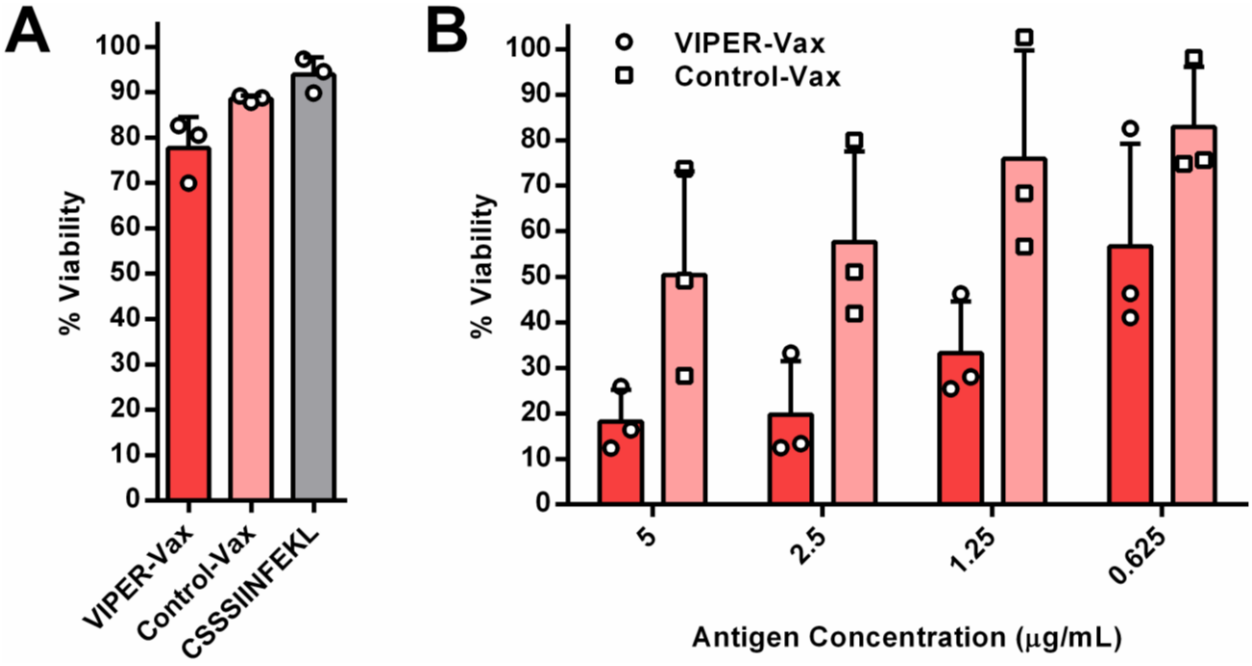

Supplemental Figure 3.4 **Cell viability corresponding to B3Z assays. (A)** DC2.4 cells were pulsed with 2.5 μg/mL CSSSIINFEKL delivered as either soluble peptide, VIPER-Vax polyplex, or Control-Vax polyplex for 2 h. An MTS assay was used to measure cell viability 20-24 h after pulsing. Data expressed as mean + SD; n = 3 independent experiments. **(B)** NIH/3T3 cells were pulsed with VIPER-Vax polyplexes or Control-Vax polyplexes for 4 h at the indicated antigen doses. An MTS assay was used to measure cell viability 24 h after pulsing. Data are expressed as mean + SD, n = 3 independent experiments.

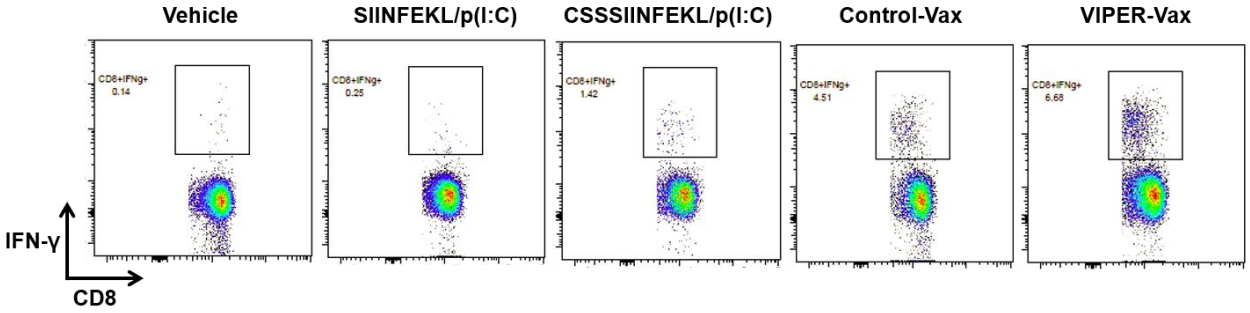

Supplemental Figure 3.5 **Flow cytometry gating strategy for intracellular cytokine staining.** Representative scatter plots showing $CD8^{+}IFN\text{-}\gamma^{+}$ T cells after SIINFEKL restimulation of harvested splenocytes from immunized mice.

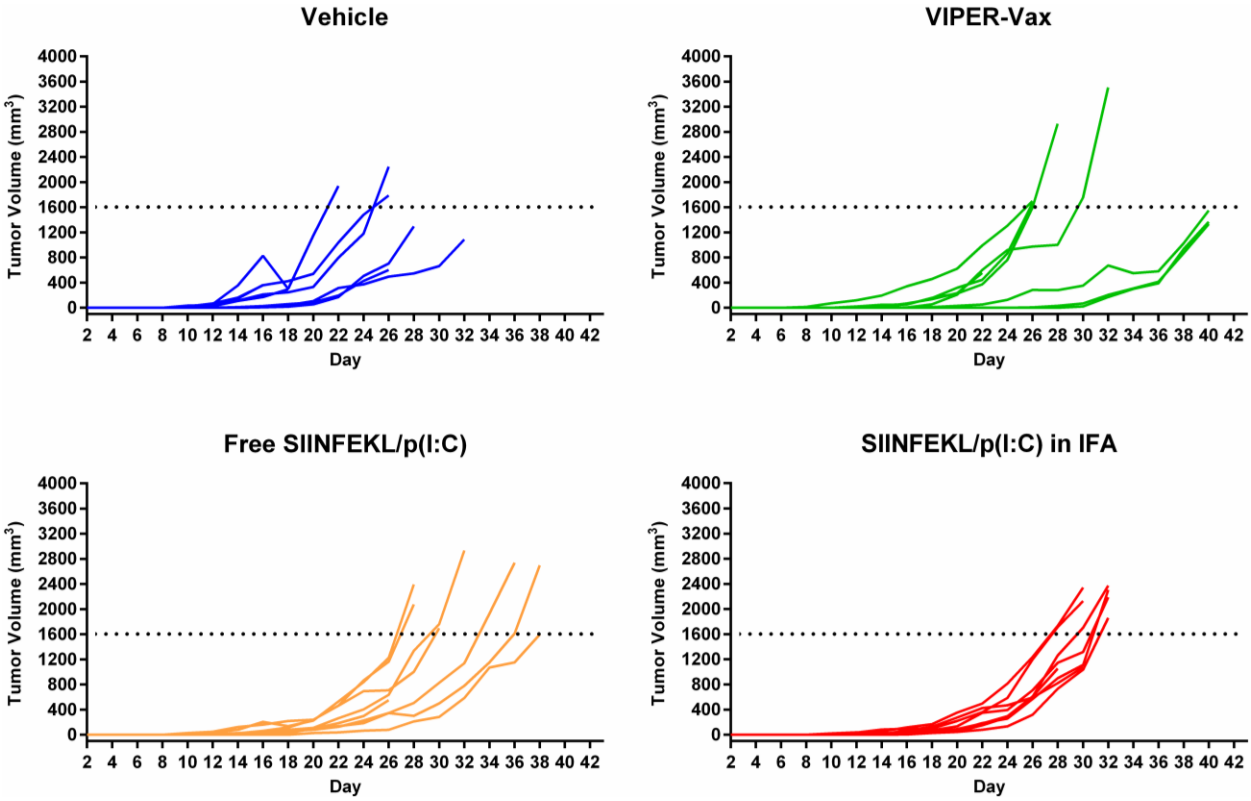

Supplemental Figure 3.6 **Spider plots of B16-OVA tumor growth in individual mice.** Mice were immunized with the formulations indicated. Note the subset of VIPER-Vax–immunized mice with extended survival duration relative to other mice.

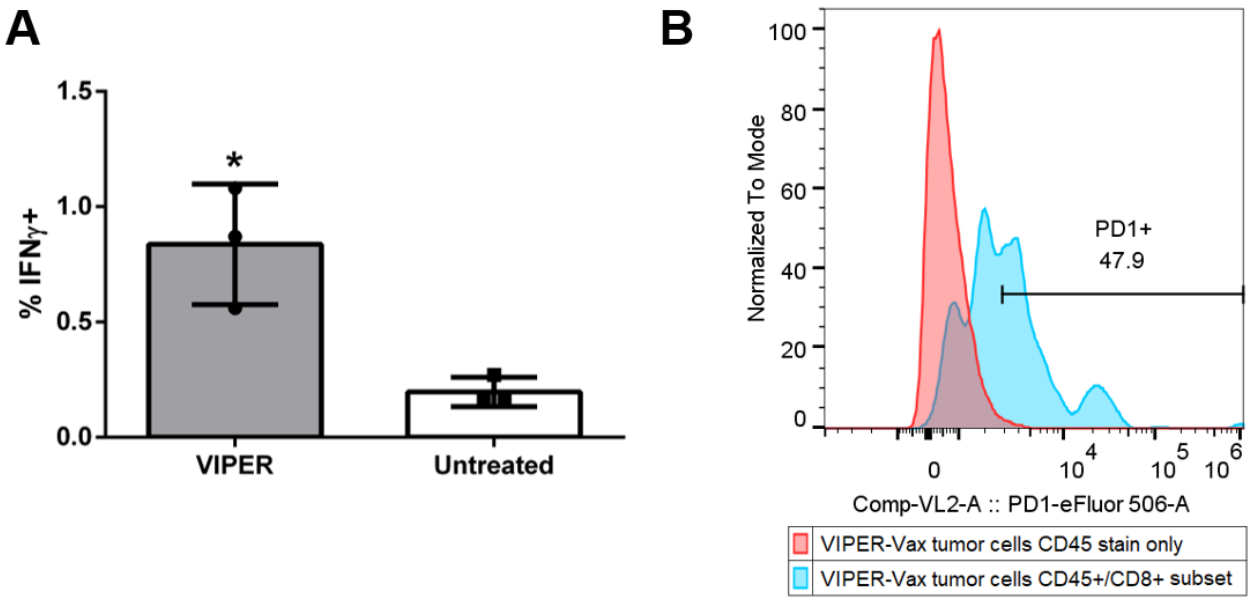

Supplemental Figure 3.7 **At time of sacrifice, tumor-bearing mice have relatively few cytotoxic T cells, and their tumor-infiltrating T cells express PD-1.** On D42 of the tumor study described in *Figure 3.5*, spleens were harvested from the surviving VIPER-Vax–immunized mice and tumor-naïve mice. **(A)** Dissociated splenocytes were restimulated in culture with 20 μg/mL SIINFEKL for 8 h before intracellular staining of IFN-γ in $CD8^+$ cells. Data are expressed as mean ± SD, $n = 3$. Statistical significance is derived from Student's t-test (*p-value ≤ 0.05). **(B)** On D42 of the tumor study described in *Figure 3.5*, tumors were harvested from the surviving VIPER-Vax–immunized mice ($n = 3$) and dissociated into single-cell suspensions for flow cytometry. Shown is a representative flow cytometry histogram of PD-1 expression in tumor-infiltrating $CD45^+CD8^+$ cells from a VIPER-Vax–immunized mouse.

Supplemental Table 3.1 **Staining panel used for flow cytometry analysis of T cells.**

Marker	Vendor	Clone (If Antibody)	Fluorophore
Viability	BioLegend	N/A	Zombie NIR™
CD3ε	Invitrogen	145-2C11	eFluor450
CD19	Invitrogen	1D3	APC
CD8α	ProImmune	KT-15	FITC
IFN-γ	Invitrogen	XMG1.2	PE-Cy7
SIINFEKL T Cell Receptor	NIH Tetramer Core Facility	N/A (H-2K^{b}/SIINFEKL Tetramer)	PE

3.7 References

(1) Hu, Z.; Ott, P. A.; Wu, C. J. Towards Personalized, Tumour-Specific, Therapeutic Vaccines for Cancer. *Nat. Rev. Immunol.* **2018**, *18* (3), 168–182.

(2) Chen, D. S.; Mellman, I. Oncology Meets Immunology: The Cancer-Immunity Cycle. *Immunity* **2013**, *39* (1), 1–10.

(3) Bezu, L.; Kepp, O.; Cerrato, G.; Pol, J.; Fucikova, J.; Spisek, R.; Zitvogel, L.; Kroemer, G.; Galluzzi, L. Trial Watch: Peptide-Based Vaccines in Anticancer Therapy. *OncoImmunology* **2018**, *7* (12), e1511506.

(4) Melief, C. J. M.; van der Burg, S. H. Immunotherapy of Established (Pre)Malignant Disease by Synthetic Long Peptide Vaccines. *Nat. Rev. Cancer* **2008**, *8* (5), 351–360.

(5) Deres, K.; Schild, H.; Wiesmüller, K.-H.; Jung, G.; Rammensee, H.-G. In Vivo Priming of Virus-Specific Cytotoxic T Lymphocytes with Synthetic Lipopeptide Vaccine. *Nature* **1989**, *342* (6249), 561–564.

(6) Sánchez-Paulete, A. R.; Teijeira, A.; Cueto, F. J.; Garasa, S.; Pérez-Gracia, J. L.; Sánchez-Arráez, A.; Sancho, D.; Melero, I. Antigen Cross-Presentation and T-Cell Cross-Priming in Cancer Immunology and Immunotherapy. *Ann. Oncol.* **2017**, *28* (suppl_12), xii44–xii55.

(7) Joffre, O. P.; Segura, E.; Savina, A.; Amigorena, S. Cross-Presentation by Dendritic Cells. *Nat. Rev. Immunol.* **2012**, *12* (8), 557–569.

(8) Mantegazza, A. R.; Magalhaes, J. G.; Amigorena, S.; Marks, M. S. Presentation of Phagocytosed Antigens by MHC Class I and II. *Traffic* **2013**, *14* (2), 135–152.

(9) Moore, M. W.; Carbone, F. R.; Bevan, M. J. Introduction of Soluble Protein into the Class I Pathway of Antigen Processing and Presentation. *Cell* **1988**, *54* (6), 777–785.

(10) Kratky, W.; Reis e Sousa, C.; Oxenius, A.; Sporri, R. Direct Activation of Antigen-Presenting Cells Is Required for $CD8^+$ T-Cell Priming and Tumor Vaccination. *Proc. Natl. Acad. Sci.* **2011**, *108* (42), 17414–17419.

(11) Hennessy, E. J.; Parker, A. E.; O'Neill, L. A. J. Targeting Toll-like Receptors: Emerging Therapeutics? *Nat. Rev. Drug Discov.* **2010**, *9* (4), 293–307.

(12) Bowen, W. S.; Svrivastava, A. K.; Batra, L.; Barsoumian, H.; Shirwan, H. Current Challenges for Cancer Vaccine Adjuvant Development. *Expert Rev. Vaccines* **2018**, *17* (3), 207–215.

(13) Hong, E.; Dobrovolskaia, M. A. Addressing Barriers to Effective Cancer Immunotherapy with Nanotechnology: Achievements, Challenges, and Roadmap to the next Generation of Nanoimmunotherapeutics. *Adv. Drug Deliv. Rev.* **2019**, *141*, 3–22.

(14) Zhang, R.; Billingsley, M. M.; Mitchell, M. J. Biomaterials for Vaccine-Based Cancer Immunotherapy. *J. Control. Release* **2018**, *292*, 256–276.

(15) Zhu, G.; Zhang, F.; Ni, Q.; Niu, G.; Chen, X. Efficient Nanovaccine Delivery in Cancer Immunotherapy. *ACS Nano* **2017**, *11* (3), 2387–2392.

(16) Irvine, D. J.; Swartz, M. A.; Szeto, G. L. Engineering Synthetic Vaccines Using Cues from Natural Immunity. *Nat. Mater.* **2013**, *12* (11), 978–990.

(17) Yoon, H. Y.; Selvan, S. T.; Yang, Y.; Kim, M. J.; Yi, D. K.; Kwon, I. C.; Kim, K. Engineering Nanoparticle Strategies for Effective Cancer Immunotherapy. *Biomaterials* **2018**, *178*, 597–607.

(18) Goldberg, M. S. Immunoengineering: How Nanotechnology Can Enhance Cancer Immunotherapy. *Cell* **2015**, *161* (2), 201–204.

(19) Hubbell, J. A.; Thomas, S. N.; Swartz, M. A. Materials Engineering for Immunomodulation. *Nature* **2009**, *462* (7272), 449–460.

(20) Ali, O. A.; Huebsch, N.; Cao, L.; Dranoff, G.; Mooney, D. J. Infection-Mimicking Materials to Program Dendritic Cells in Situ. *Nat. Mater.* **2009**, *8* (2), 151–158.

(21) Hornung, V.; Bauernfeind, F.; Halle, A.; Samstad, E. O.; Kono, H.; Rock, K. L.; Fitzgerald,

K. A.; Latz, E. Silica Crystals and Aluminum Salts Activate the NALP3 Inflammasome through Phagosomal Destabilization. *Nat. Immunol.* **2008**, *9* (8), 847–856.
(22) Demento, S. L.; Eisenbarth, S. C.; Foellmer, H. G.; Platt, C.; Caplan, M. J.; Mark Saltzman, W.; Mellman, I.; Ledizet, M.; Fikrig, E.; Flavell, R. A.; et al. Inflammasome-Activating Nanoparticles as Modular Systems for Optimizing Vaccine Efficacy. *Vaccine* **2009**, *27* (23), 3013–3021.
(23) Baljon, J. J.; Dandy, A.; Wang-Bishop, L.; Wehbe, M.; Jacobson, M. E.; Wilson, J. T. The Efficiency of Cytosolic Drug Delivery Using pH-Responsive Endosomolytic Polymers Does Not Correlate with Activation of the NLRP3 Inflammasome. *Biomater. Sci.* **2019**.
(24) Howland, S. W.; Wittrup, K. D. Antigen Release Kinetics in the Phagosome Are Critical to Cross-Presentation Efficiency. *J. Immunol.* **2008**, *180* (3), 1576–1583.
(25) Yuhua, H.; Litwin, T.; Nagaraja, A. R.; Kwong, B.; Katz, J.; Watson, N.; Irvine, D. J.; Hu, Y.; Litwin, T.; Nagaraja, A. R.; et al. Cytosolic Delivery of Membrane-Impermeable Molecules in Dendritic Cells Using pH-Responsive Core-Shell Nanoparticles. *Nano Lett.* **2007**, *7* (10), 3056–3064.
(26) Shen, H.; Ackerman, A. L.; Cody, V.; Giodini, A.; Hinson, E. R.; Cresswell, P.; Edelson, R. L.; Saltzman, W. M.; Hanlon, D. J. Enhanced and Prolonged Cross-Presentation Following Endosomal Escape of Exogenous Antigens Encapsulated in Biodegradable Nanoparticles. *Immunology* **2006**, *117* (1), 78–88.
(27) Wilson, J. T.; Keller, S.; Manganiello, M. J.; Cheng, C.; Lee, C. C.; Opara, C.; Convertine, A.; Stayton, P. S. pH-Responsive Nanoparticle Vaccines for Dual-Delivery of Antigens and Immunostimulatory Oligonucleotides. *ACS Nano* **2013**, *7* (5), 3912–3925.
(28) Lou, B.; De Koker, S.; Lau, C. Y. J.; Hennink, W. E.; Mastrobattista, E. mRNA Polyplexes with Post-Conjugated GALA Peptides Efficiently Target, Transfect, and Activate Antigen Presenting Cells. *Bioconjug. Chem.* **2018**.
(29) Liu, J.; Liu, X.; Han, Y.; Zhang, J.; Liu, D.; Ma, G.; Li, C.; Liu, L.; Kong, D. Nanovaccine Incorporated with Hydroxychloroquine Enhances Antigen Cross-Presentation and Promotes Antitumor Immune Responses. *ACS Appl. Mater. Interfaces* **2018**, *10* (37), 30983–30993.
(30) Varkouhi, A. K.; Scholte, M.; Storm, G.; Haisma, H. J. Endosomal Escape Pathways for Delivery of Biologicals. *J. Control. Release* **2011**, *151* (3), 220–228.
(31) Lönn, P.; Kacsinta, A. D.; Cui, X.-S.; Hamil, A. S.; Kaulich, M.; Gogoi, K.; Dowdy, S. F. Enhancing Endosomal Escape for Intracellular Delivery of Macromolecular Biologic Therapeutics. *Sci. Rep.* **2016**, *6* (1), 32301.
(32) Stewart, M. P.; Lorenz, A.; Dahlman, J.; Sahay, G. Challenges in Carrier-Mediated Intracellular Delivery: Moving beyond Endosomal Barriers. *Wiley Interdiscip. Rev. Nanomedicine Nanobiotechnology* **2016**, *8* (3), 465–478.
(33) Cheng, Y.; Yumul, R. C.; Pun, S. H. Virus-Inspired Polymer for Efficient In Vitro and In Vivo Gene Delivery. *Angew. Chemie Int. Ed.* **2016**, *55* (39), 12013–12017.
(34) Feldmann, D. P.; Cheng, Y.; Kandil, R.; Xie, Y.; Mohammadi, M.; Harz, H.; Sharma, A.; Peeler, D. J.; Moszczynska, A.; Leonhardt, H.; et al. In Vitro and In Vivo Delivery of siRNA via VIPER Polymer System to Lung Cells. *J. Control. Release* **2018**, *276*, 50–58.
(35) Peeler, D. J.; Thai, S. N.; Cheng, Y.; Horner, P. J.; Sellers, D. L.; Pun, S. H. pH-Sensitive Polymer Micelles Provide Selective and Potentiated Lytic Capacity to Venom Peptides for Effective Intracellular Delivery. *Biomaterials* **2019**, *192*, 235–244.
(36) Shir, A.; Ogris, M.; Wagner, E.; Levitzki, A. EGF Receptor-Targeted Synthetic Double-Stranded RNA Eliminates Glioblastoma, Breast Cancer, and Adenocarcinoma Tumors in Mice. *PLoS Med.* **2006**, *3* (1), 125–135.
(37) Blachère, N. E.; Darnell, R. B.; Albert, M. L. Apoptotic Cells Deliver Processed Antigen to Dendritic Cells for Cross-Presentation. *PLoS Biol.* **2005**, *3* (6), e185.
(38) Kilchrist, K. V.; Dimobi, S. C.; Jackson, M. A.; Evans, B. C.; Werfel, T. A.; Dailing, E. A.;

Bedingfield, S. K.; Kelly, I. B.; Duvall, C. L. Gal8 Visualization of Endosome Disruption Predicts Carrier-Mediated Biologic Drug Intracellular Bioavailability. *ACS Nano* **2019**, *13* (2), 1136–1152.
(39) Karttunen, J.; Sanderson, S.; Shastri, N. Detection of Rare Antigen-Presenting Cells by the LacZ T-Cell Activation Assay Suggests an Expression Cloning Strategy for T-Cell Antigens. *Proc. Natl. Acad. Sci. U. S. A.* **1992**, *89* (13), 6020–6024.
(40) Palumbo, R. N.; Zhong, X.; Wang, C. Polymer-Mediated DNA Vaccine Delivery via Bystander Cells Requires a Proper Balance between Transfection Efficiency and Cytotoxicity. *J. Control. Release* **2012**, *157* (1), 86–93.
(41) Li, Y.; Zhao, T.; Wang, C.; Lin, Z.; Huang, G.; Sumer, B. D.; Gao, J. Molecular Basis of Cooperativity in pH-Triggered Supramolecular Self-Assembly. *Nat. Commun.* **2016**, *7*, 13214.
(42) Zhou, K.; Wang, Y.; Huang, X.; Luby-Phelps, K.; Sumer, B. D.; Gao, J. Tunable, Ultrasensitive pH-Responsive Nanoparticles Targeting Specific Endocytic Organelles in Living Cells. *Angew. Chem. Int. Ed. Engl.* **2011**, *50* (27), 6109–6114.
(43) Bellone, M.; Cantarella, D.; Castiglioni, P.; Crosti, M. C.; Ronchetti, A.; Moro, M.; Garancini, M. P.; Casorati, G.; Dellabona, P. Relevance of the Tumor Antigen in the Validation of Three Vaccination Strategies for Melanoma. *J. Immunol.* **2000**, *165* (5), 2651–2656.
(44) Kuai, R.; Ochyl, L. J.; Bahjat, K. S.; Schwendeman, A.; Moon, J. J. Designer Vaccine Nanodiscs for Personalized Cancer Immunotherapy. *Nat. Mater.* **2017**, *16* (4), 489–496.
(45) Hirosue, S.; Kourtis, I. C.; van der Vlies, A. J.; Hubbell, J. A.; Swartz, M. A. Antigen Delivery to Dendritic Cells by Poly(Propylene Sulfide) Nanoparticles with Disulfide Conjugated Peptides: Cross-Presentation and T Cell Activation. *Vaccine* **2010**, *28* (50), 7897–7906.
(46) Furio, L.; Billard, H.; Valladeau, J.; Péguet-Navarro, J.; Berthier-Vergnes, O. Poly(I:C)-Treated Human Langerhans Cells Promote the Differentiation of $CD4^+$ T Cells Producing IFN-γ and IL-10. *J. Invest. Dermatol.* **2009**, *129* (8), 1963–1971.
(47) Hafner, A. M.; Corthésy, B.; Merkle, H. P. Particulate Formulations for the Delivery of Poly(I:C) as Vaccine Adjuvant. *Adv. Drug Deliv. Rev.* **2013**, *65* (10), 1386–1399.
(48) Jewell, C. M.; Bustamante Lopez, S. C.; Irvine, D. J. In Situ Engineering of the Lymph Node Microenvironment via Intranodal Injection of Adjuvant-Releasing Polymer Particles. *Proc. Natl. Acad. Sci.* **2011**, *108* (38), 15745–15750.
(49) Zaks, K.; Jordan, M.; Guth, A.; Sellins, K.; Kedl, R.; Izzo, A.; Bosio, C.; Dow, S. Efficient Immunization and Cross-Priming by Vaccine Adjuvants Containing TLR3 or TLR9 Agonists Complexed to Cationic Liposomes. *J. Immunol.* **2006**, *176* (12), 7335–7345.
(50) Schaffert, D.; Kiss, M.; Rödl, W.; Shir, A.; Levitzki, A.; Ogris, M.; Wagner, E. Poly(I:C)-Mediated Tumor Growth Suppression in EGF-Receptor Overexpressing Tumors Using EGF-Polyethylene Glycol-Linear Polyethylenimine as Carrier. *Pharm. Res.* **2011**, *28* (4), 731–741.
(51) Yen, A.; Cheng, Y.; Sylvestre, M.; Gustafson, H. H.; Puri, S.; Pun, S. H. Serum Nuclease Susceptibility of mRNA Cargo in Condensed Polyplexes. *Mol. Pharm.* **2018**, *15* (6), 2268–2276.
(52) Zuidam, N.; Posthumab, G.; de Vries, E.; Crommelin, D.; Hennink, W.; Storm, G. Effects of Physicochemical Characteristics of Poly(2-(Dimethylamino)Ethyl Methacrylate)-Based Polyplexes on Cellular Association and Internalization. *J. Drug Target.* **2000**, *8* (1), 51–66.
(53) Bishop, C. J.; Majewski, R. L.; Guiriba, T.-R. M.; Wilson, D. R.; Bhise, N. S.; Quiñones-Hinojosa, A.; Green, J. J. Quantification of Cellular and Nuclear Uptake Rates of Polymeric Gene Delivery Nanoparticles and DNA Plasmids via Flow Cytometry. *Acta Biomater.* **2016**, *37*, 120–130.
(54) Nordly, P.; Rose, F.; Christensen, D.; Nielsen, H. M.; Andersen, P.; Agger, E. M.; Foged, C.

Immunity by Formulation Design: Induction of High CD8+ T-Cell Responses by Poly(I:C) Incorporated into the CAF01 Adjuvant via a Double Emulsion Method. *J. Control. Release* **2011**, *150* (3), 307–317.
(55) Bosnjak, L.; Miranda-Saksena, M.; Koelle, D. M.; Boadle, R. A.; Jones, C. A.; Cunningham, A. L. Herpes Simplex Virus Infection of Human Dendritic Cells Induces Apoptosis and Allows Cross-Presentation via Uninfected Dendritic Cells. *J. Immunol.* **2005**, *174* (4), 2220–2227.
(56) Canton, J.; Blees, H.; Henry, C. M.; Buck, M. D.; Schulz, O.; Rogers, N. C.; Childs, E.; Zelenay, S.; Rhys, H.; Domart, M.-C.; et al. The Receptor DNGR-1 Signals for Phagosomal Rupture to Promote Cross-Presentation of Dead-Cell-Associated Antigens. *Nat. Immunol.* **2021**, *22* (2), 140–153.
(57) Dzierszinski, F.; Pepper, M.; Stumhofer, J. S.; LaRosa, D. F.; Wilson, E. H.; Turka, L. A.; Halonen, S. K.; Hunter, C. A.; Roos, D. S. Presentation of Toxoplasma Gondii Antigens via the Endogenous Major Histocompatibility Complex Class I Pathway in Nonprofessional and Professional Antigen-Presenting Cells. *Infect. Immun.* **2007**, *75* (11), 5200–5209.
(58) Liu, H.; Hu, Y.; Sun, Y.; Wan, C.; Zhang, Z.; Dai, X.; Lin, Z.; He, Q.; Yang, Z.; Huang, P.; et al. Co-Delivery of Bee Venom Melittin and a Photosensitizer with an Organic-Inorganic Hybrid Nanocarrier for Photodynamic Therapy and Immunotherapy. *ACS Nano* **2019**, *13* (11), 12638–12652.
(59) Yu, X.; Dai, Y.; Zhao, Y.; Qi, S.; Liu, L.; Lu, L.; Luo, Q.; Zhang, Z. Melittin-Lipid Nanoparticles Target to Lymph Nodes and Elicit a Systemic Anti-Tumor Immune Response. *Nat. Commun.* **2020**, *11*, 1110.
(60) van de Wetering, P.; Cherng, J.-Y.; Talsma, H.; Hennink, W. E. Relation between Transfection Efficiency and Cytotoxicity of Poly(2-(Dimethylamino)Ethyl Methacrylate)/Plasmid Complexes. *J. Control. Release* **1997**, *49* (1), 59–69.
(61) Richards, S.-J.; Jones, A.; Tomás, R. M. F.; Gibson, M. I. Photochemical "In-Air" Combinatorial Discovery of Antimicrobial Co-Polymers. *Chem. - A Eur. J.* **2018**, *24* (52), 13758–13761.
(62) Blakney, A. K.; McKay, P. F.; Ibarzo Yus, B.; Hunter, J. E.; Dex, E. A.; Shattock, R. J. The Skin You Are In: Design-of-Experiments Optimization of Lipid Nanoparticle Self-Amplifying RNA Formulations in Human Skin Explants. *ACS Nano* **2019**, *13* (5), 5920–5930.
(63) Depelsenaire, A. C. I.; Meliga, S. C.; McNeilly, C. L.; Pearson, F. E.; Coffey, J. W.; Haigh, O. L.; Flaim, C. J.; Frazer, I. H.; Kendall, M. A. F. Colocalization of Cell Death with Antigen Deposition in Skin Enhances Vaccine Immunogenicity. *J. Invest. Dermatol.* **2014**, *134* (9), 2361–2370.
(64) Luo, M.; Wang, H.; Wang, Z.; Cai, H.; Lu, Z.; Li, Y.; Du, M.; Huang, G.; Wang, C.; Chen, X.; et al. A STING-Activating Nanovaccine for Cancer Immunotherapy. *Nat. Nanotechnol.* **2017**, *12* (7), 648–654.
(65) Wilson, D. S.; Hirosue, S.; Raczy, M. M.; Bonilla-Ramirez, L.; Jeanbart, L.; Wang, R.; Kwissa, M.; Franetich, J.-F.; Broggi, M. A. S.; Diaceri, G.; et al. Antigens Reversibly Conjugated to a Polymeric Glyco-Adjuvant Induce Protective Humoral and Cellular Immunity. *Nat. Mater.* **2019**, *18* (2), 175–185.
(66) Overwijk, W. W.; Restifo, N. P. B16 as a Mouse Model for Human Melanoma. In *Current Protocols in Immunology*; NIH Public Access, 2001; Vol. Chapter 20, p Unit 20.1.
(67) Tomasetti, C.; Li, L.; Vogelstein, B. Stem Cell Divisions, Somatic Mutations, Cancer Etiology, and Cancer Prevention. *Science* **2017**, *355* (6331), 1330–1334.
(68) Zhong, X.; Han, W.; Wang, C.; Ji, W.; Palumbo, R. N.; Panus, D. Transgene Expression and Local Tissue Distribution of Naked and Polymer-Condensed Plasmid DNA after Intradermal Administration in Mice. *J. Control. Release* **2012**, *159* (2), 232–239.
(69) Burke, R. S.; Pun, S. H. Extracellular Barriers to In Vivo PEI and PEGylated PEI Polyplex-

Mediated Gene Delivery to the Liver. *Bioconjug. Chem.* **2008**, *19* (3), 693–704.
(70) Nam, J.; Son, S.; Park, K. S.; Zou, W.; Shea, L. D.; Moon, J. J. Cancer Nanomedicine for Combination Cancer Immunotherapy. *Nat. Rev. Mater.* **2019**, *4* (6), 398–414.

CHAPTER 4

Mannosylated Polymer Micelles Target Peptide Antigens to Dendritic Cells[†,‡]

Albert Yen*, David J. Peeler*, Selvi Srinivasan, Yunshi Zhou, Meilyn Sylvestre, Clinton M. Heinze, Lucy F. Yang, Nicholas Luera, Patrick S. Stayton, and Suzie H. Pun

Synopsis. Nonspecific biodistribution and poor antigen immunogenicity limits the efficacy of many subunit cancer vaccines. Activation of tumor-specific cellular immunity is mediated by dendritic cells (DCs). Cancer vaccine potency may be enhanced by targeting tumor antigens and vaccine adjuvants to these DCs. Here, we report mannosylated polymer micelles loaded with monomeric adjuvant prodrugs, or "drugamers," as well as covalently conjugated lytic peptides and peptide antigens. The mannosylated micelle corona targets vaccine cargo to DCs, but subsequent studies show that inclusion of lytic peptides in the micelle core may attenuate antigen-specific T cell responses. Nonetheless, in a model of mouse melanoma, our micelle formulation prolongs survival in comparison to soluble vaccine. Additional work is needed to elucidate how the bioactivities of drugamer, lytic peptide, and mannose combine to modulate antigen-specific immunity.

[†]All biomaterial synthesis schemes described in this chapter (and the next) are based on the foundational scheme reported in this seminal publication from our group: Cheng, Y.; Yumul, R. C.; Pun, S. H. Virus-Inspired Polymer for Efficient In Vitro and In Vivo Gene Delivery. *Angew. Chemie Int. Ed.* **2016**, *55* (39), 12013–12017.

[‡]A preliminary discussion of this research effort can be found in *Chapter 6* of David J. Peeler's doctoral dissertation (URI: http://hdl.handle.net/1773/45109).

*Equally contributing authors.

4.1 Introduction

Subunit vaccines are a cornerstone of modern medicine.[1] Long-lasting protective immunity against infectious diseases can be conferred by administration of antigens—unique protein or peptide "subunits" of pathogens—before an infectious disease ever manifests.[1] In addition, subunit vaccines are less toxic and cheaper to manufacture than attenuated or inactivated vaccines derived from whole pathogens.[2]

The main disadvantage of subunit vaccines is the low immunogenicity of most protein and peptide antigens.[1] Since attenuated and inactivated vaccines consist of whole pathogens, they contain both antigens and pathogen-associated molecular patterns (PAMPs), biomolecules that bind pattern recognition receptors (PRRs) expressed by immune cells, activating immunostimulatory signaling pathways.[3] Activation of these signaling pathways during antigen processing is necessary for disease clearance and protective immunity.[3] To compensate for the poor immunogenicity of subunit antigens, vaccine adjuvants are typically incorporated into subunit vaccine formulations.[1–5] These vaccine adjuvants are synthetic substances that act as antigen depots, increasing antigen bioavailability, or they may be designed to mimic PAMPs, triggering pathogen-specific immune responses in the absence of pathogen.[1,3,5]

The clinical success rates of subunit vaccines for infectious diseases has inspired development of similar vaccines for cancer. To date, however, clinical outcomes for subunit cancer vaccine regimens have been subpar.[6–8] Several biological barriers limit the efficacy of subunit cancer vaccines. First, cancer vaccines are typically administered after a tumor is already established, and strong immune responses are needed to fully eliminate the tumor.[6] Furthermore, tumor antigens are often identical to self-antigens from noncancerous tissue and do not elicit robust immunity.[9–11] Finally, tumor microenvironments are known to suppress the function of effector immune cells.[4,6] Administration of more potent adjuvants or combinatorial adjuvant

therapies may improve the efficacy of subunit cancer vaccines, but systemic toxicity caused by nonspecific adjuvant bioactivity is a major safety concern.[12,13]

The potency of subunit cancer vaccines may be safely enhanced through targeted delivery of tumor antigens and vaccine adjuvants to dendritic cells (DCs). Cellular immune responses are initiated by DCs.[14] When stimulated with adjuvant in the presence of antigen, immature DCs undergo maturation, process antigens into peptide epitopes, and present these epitopes on MHC molecules to naïve T cells.[14] Presentation of epitopes on MHC class I (MHCI) molecules primes $CD8^+$ cytotoxic T cells (CTCs) that destroy antigen-expressing cells (e.g., tumor cells), whereas presentation of epitopes on MHC class II (MHCII) molecules primes $CD4^+$ helper T cells that boost the function of DCs, CTCs, and other immune cells.[15] Primed T cells are key effector immune cells, and both $CD8^+$ and $CD4^+$ T cell immunity are crucial for tumor clearance.[7,16,17]

Since T cell priming occurs primarily in lymphatic organs, delivery strategies that localize vaccine components to lymph node–resident DCs are a subject of extensive research. One such strategy is the use of synthetic nanoparticles for DC-targeted vaccine delivery.[18–21] How nanoparticle vaccines, or "nanovaccines," traffic through the lymphatics is a function of particle size, shape, surface charge, and material.[19,21] The interplay between these design parameters is not fully understood, but prior research has shown that nanovaccines with 20–100 nm diameters drain passively to lymphoid DCs after injection into the interstitium.[19,22,23] Larger particles drain inefficiently into the lymphatics because they are often trapped by extracellular matrix, but they may still be taken up by migratory DCs, which transport peripheral antigens to lymph nodes for presentation to T cells.[19,24,25]

Active targeting mechanisms may further increase association of nanovaccines with DCs. Functionalization of vaccines with mannose ligands can improve vaccine uptake by DCs through binding of C-type lectins, a broad class of carbohydrate-binding proteins that interact with mannose moieties found on many pathogens.[26–28] Some C-type lectins are PRRs expressed by DCs (e.g., CD206) and facilitate receptor-mediated endocytosis of mannosylated vaccines.[28,29] Others

are soluble PRRs (e.g., mannose-binding lectin) that promote DC phagocytosis of mannosylated vaccines via opsonization.[28,30,31]

We draw upon these nanoparticle targeting principles to create nanovaccines that efficiently deliver cancer vaccine cargo to DCs. In *Chapter 3*, we reported "VIPER-Vax," the first subunit cancer nanovaccine based on our group's "Virus-Inspired Polymer for Endosomal Release," or VIPER.[32–34] VIPER-Vax is a cationic polyplex vaccine with co-encapsulated melittin, a membrane-lytic peptide, and peptide antigen.[32] Poly(I:C), a nucleic acid adjuvant, is loaded into VIPER-Vax via cation-driven condensation.[32,35] As discussed in *Chapter 3*, VIPER-Vax and its encapsulated cargo are readily internalized by DCs in vitro and potentiate antigen presentation via a bystander killing mechanism.[32,36,37] However, its cationic charge may hinder uptake by DCs after administration, limiting its therapeutic potential.[32] Indeed, prior research has shown that cationic polyplexes like VIPER-Vax may be trapped in anionic extracellular matrix, preventing DC uptake and lymphatic transport despite persistent depot formation at the injection site.[38,39] In this chapter, we build on our work with VIPER-Vax polyplexes and synthesize a neutrally charged, mannosylated VIPER-Vax for receptor-targeted delivery of cancer peptide vaccines to DCs.

4.2 Experimental Section

4.2.1 Materials

Resiquimod (R848) was purchased from InvivoGen. RPMI 1640 culture media (with L-glutamine) was purchased from Corning, fetal bovine serum (FBS) was purchased from Gibco, and bovine serum albumin was purchased from Miltenyi Biotec. Mannose ethyl methacrylate (MMA; MW = 292.72) and self-immolating R848 carbamate methacrylate (SRCMA; MW = 676.2) were synthesized by Selvi Srinivasan using reported methods from the Ratner and Stayton groups.[40,41] Chain transfer agents (CTAs) 4-((((2-carboxyethyl)thio)carbonothioyl)thio)-4-cyanopentanoic acid (CCC) and 4-cyano-4-[(dodecylsulfanylthiocarbonyl)sulfanyl]pentanoic acid

(CCP) for reversible addition–fragmentation chain-transfer (RAFT) polymerization were purchased from Sigma-Aldrich. Azo initiators V-60 (azobisisobutyronitrile, or AIBN), V-70, and V-501 were purchased from Wako Chemical. Pyridyl disulfide ethyl methacrylate (PDSEMA) was obtained with previously reported synthesis methods.[42] 2-Diisopropylaminoethyl methacrylate (DIPAMA), 2-(dimethylamino)ethyl methacrylate (DMAEMA), and oligo(ethylene glycol) monomethyl ether methacrylate (OEGMA, average M_n = 300, 4–5 pendent ethylene oxide units) were purchased from Sigma-Aldrich; polymerization inhibitors were removed by passing monomers stocks through a basic alumina column.[33,34] 2-N,N′-diisopropylcarbodiimide (DIC), 4-(dimethylamino)pyridine (DMAP), and polyethylene glycol methyl ether (mPEG-OH, average M_n = 5,000) were purchased from Sigma-Aldrich. Methanol (MeOH, HPLC grade, 99.9%), dichloromethane (DCM), anhydrous N,N'-dimethylacetamide (DMAc, HPLC grade, 99.9%), N,N'-dimethylformamide (DMF, HPLC grade, 99.9%), anhydrous N-methyl-2-pyrrolidone (NMP, 99.5%), and dimethylsulfoxide (DMSO, > 99%) were purchased from Sigma-Aldrich and stored with activated molecular sieves.

4.2.2 Cationic VIPER synthesis

Block copolymer p(OEGMA$_{8.6}$-*co*-DMAEMA$_{50.0}$)-*b*-p(DIPAMA$_{25.3}$-*co*-PDSEMA$_{1.0}$) was synthesized by RAFT polymerization as described in *Section 3.2.3*.[32] Additional synthesis details are reported in previous work from our group.[33,34]

4.2.3 Polyethylene glycolsylated VIPER synthesis

Block copolymer PEG5000-*b*-p(DIPAMA$_{35}$-*co*-PDSEMA$_{2}$) was synthesized by RAFT polymerization. First, a polyethylene glycol–CCP (mPEG-CCP) macroCTA was obtained through a coupling reaction between mPEG-OH (1 mol eq.) and CCP (1.1 mol eq.) mediated by DIC and DMAP (10 mol eq. each) in DCM (20 mg/ml final reaction concentration). After a 24 h incubation with stirring at room temperature, mPEG-CCP macroCTA was separated from unreacted CCP via

flash chromatography and dried in a rotary evaporator. Next, mPEG-CCP macroCTA (1 mol eq.), AIBN (0.1 mol eq.), DIPAMA (35 mol eq.), and PDSEMA (5 mol eq.) were dissolved in DMAc at 30% w/w in a round-bottom flask. The reaction mixture was purged with argon for 15 min before vigorous stirring at 70 °C for 20 h. The reaction was then terminated by air perfusion. Serial dialysis in MeOH and deionized (DI) water was used to purify the final polymer product prior to lyophilization. The polymer was dissolved in deuterated chloroform (Sigma-Aldrich) for ^{1}H NMR and block 2 degree of polymerization was confirmed relative to known block 1 PEG5000 content.

4.2.4 Mannosylated VIPER synthesis

Block copolymer pMMA$_{35}$-*b*-p(DIPAMA$_{26.8}$-*co*-PDSEMA$_{2.4}$) was synthesized by RAFT polymerization. First, a MMA-CCC macroCTA was polymerized from MMA (38 mol eq.) using V-501 (0.1 mol eq.) as the initiator and CCC (1 mol eq.) as the CTA. Reaction components were dissolved in DMSO at 25% w/w final concentration in a round-bottom flask. The reaction mixture was purged with argon for 15 min and vigorously stirred at 70 °C for 7 h. The reaction was then terminated by air perfusion. Degree of polymerization was calculated through ^{1}H NMR analysis of the reaction mixture in deuterated DMSO (Sigma-Aldrich). Dialysis in DI water was used to purify the MMA-CCC macroCTA before lyophilization. Next, the MMA-CCC macroCTA (1 mol eq.), AIBN (0.1 mol eq.), DIPAMA (200 mol eq.), and PDSEMA (20 mol eq.) were dissolved in NMP at 30% w/w in a round-bottom flask. The reaction mixture was purged with argon for 15 min and vigorously stirred at 70 °C for 3 h. The reaction was then terminated by air perfusion. Serial dialysis in NMP and DI water was used to purify the final polymer product before lyophilization. The final polymer product was dissolved in deuterated DMSO for ^{1}H NMR and block 2 degree of polymerization was confirmed relative to known block 1 MMA content.

4.2.5 Drugamer VIPER synthesis

Block copolymer p($MMA_{22.1}$-*co*-$SRCMA_{8.0}$)-*b*-p(DIPAMA27.3-*co*-$PDSEMA_{2.0}$) was synthesized by RAFT polymerization. First, a MMA-SRCMA-CCC macroCTA was polymerized from MMA (24 mol eq.) and SRCMA (8 mol eq.) using V-70 (0.1 mol eq) as the initiator and CCC (1 mol eq.) as the CTA. Reaction components were dissolved in DMSO at 25% w/w final concentration in a round-bottom flask. The reaction mixture was purged with argon for 15 min and vigorously stirred at 35 °C for 20 h. The reaction was then terminated by air perfusion. Dialysis in DI water was used to purify the MMA-SRCMA-CCC macroCTA before lyophilization. Degree of polymerization was calculated through ^{1}H NMR analysis of the reaction mixture and lyophilized product in deuterated DMSO. Next, MMA-SRCMA-CCC macroCTA (1 mol eq.), AIBN (0.1 mol eq.), DIPAMA (200 mol eq.), and PDSEMA (20 mol eq.) were dissolved in NMP at 30% w/w in a round-bottom flask. The reaction mixture was purged with argon for 15 min and vigorously stirred at 70 °C for 3 h. The reaction was then terminated by air perfusion. Serial dialysis in NMP and 4 °C DI water was used to purify the final polymer product before lyophilization. The polymer was dissolved in deuterated DMSO for ^{1}H NMR and block 2 degree of polymerization was confirmed relative to known block 1 MMA-SRCMA content.

4.2.6 Polymer characterization

As reported in previous work, polymer composition and dispersity ($Đ$) were determined by ^{1}H NMR and size exclusion chromatography, respectively.[33,34]

4.2.7 Peptide synthesis

As described in *Section 3.2.2* and previous work, cysteine-terminated melittin (GIGAVLKVLTTGLPALISWIKRKRQQC) and cysteine-serine-serine–terminated ovalbumin MHCI epitope (CSSSIINFEKL) were produced by solid-phase peptide synthesis and purified by reversed-phase HPLC.[32,34]

4.2.8 Polymer-peptide conjugation

As reported in *Section 3.2.3* and previous work, polymer-peptide conjugates were obtained through a disulfide exchange reaction.[32,34] Briefly, polymers and cysteine-terminated peptides were mixed in a compatible solvent at ≥ 20 mg/mL (MeOH for cationic and polyethyelene glycosylated VIPER conjugations, and DMF for mannosylated and drugamer VIPER conjugations). Reaction mixtures were incubated at room temperature, and disulfide exchange was confirmed by spectroscopic detection of pyridyl-2-thione byproduct.[32,34] For all polymers with ≥ 2 PDSEMA per chain (polyethylene glycolsylated, mannosylated, and drugamer VIPER), one melittin or two peptide antigens were conjugated per chain. Conjugates were dialyzed at 4 °C in DI water prior to lyophilization.

4.2.9 Micelle formation

Mixed VIPER micelles consisted of (i) peptide antigen–conjugated polymer (AP) mixed with (ii) melittin-conjugated polymer (MP) or (iii) unconjugated polymer (CP). As described in *Chapter 3*, a 2:1 molar ratio of AP:MP or AP:CP was used for all micelle formulations.[32] For cationic, polyethylene glycolsylated, and mannosylated VIPER, micelles were generated using the pH transition method described in *Section 3.2.3* and previous work.[32,34] For drugamer VIPER, micelles were generated by mixing the desired polymers in DMF before nanoprecipitation in pH 7.4 phosphate-buffered saline (PBS) with concurrent probe sonication (2.5 mg/mL final polymer concentration). DMF was removed by dialysis in PBS at 4 °C, and micelle aliquots were frozen at -20 °C to minimize drugamer degradation. Prior to use, micelle aliquots were thawed and re-sonicated to ensure monodisperse size distribution (data not shown).

4.2.10 Micelle size measurements

For size measurements, micelles were diluted in 150 mM PBS at pH 7.4 to a final polymer concentration of 0.1 mg/mL. After resting samples at room temperature for 30 min, micelle size was measured with a ZetaPlus instrument (Brookhaven Instruments).

4.2.11 Hemolysis assay

Human blood samples were collected according to guidelines from the University of Washington Institutional Review Board. The lytic bioactivity of drugamer VIPER micelles was quantified in vitro using a previously reported hemolysis assay.[33,34] Briefly, red blood cells (RBCs) were treated with test formulations (free melittin, drugamer VIPER micelles with melittin, or drugamer VIPER micelles without melittin) in phosphate buffer (pH 7.4 or 5.5) for 1 h at 37 °C. Melittin-free and melittin-loaded micelles were formulated at equimolar polymer concentrations. A range of melittin concentrations was tested (0.3125–50 μM) with 1% (v/v) Triton X-100 as a positive control. After treatment, RBC samples were centrifuged, and supernatant hemoglobin content was quantified via absorbance measurements at 541 nm. Percent hemolysis was calculated by standardizing absorbance values to that of the Triton X-100 sample.

4.2.12 Mice

All animal studies were conducted under protocols approved by the Institutional Animal Care and Use Committee at the University of Washington. Female C57BL/6 mice (Charles River Laboratories), 6–8 weeks old, were used for all studies.

4.2.13 Collection of lymph node–resident cells

Inguinal lymph nodes (ILNs) were harvested from euthanized mice. Each pair of ILNs from a mouse were stored at room temperature in 500 μL of RPMI 1640 + 10% FBS + 1 mg/mL collagenase D (Sigma-Aldrich) + 100 U/mL DNase I (Sigma-Aldrich) until homogenization. To

homogenize, ILNs were mashed against a 40 μm cell strainer with the end of a syringe plunger. Homogenized tissue was rinsed through the cell strainer into a conical tube with RPMI 1640 and stored on ice until analysis.

4.2.14 Vaccine localization to dendritic cells

VIPER micelle variants containing 20 μg of CSSSIINFEKL (10% rhodamine-labeled) were suspended in 40 μL of 5% (w/v) glucose. Mice were injected subcutaneously with micelles at the right tail base (n = 3 per treatment group). After 48 h, mice were euthanized and ILNs were harvested as described in *Section 4.2.13*. Bulk fluorescence of whole ILNs was visualized on a Xenogen IVIS-200 (Caliper Life Sciences). ILN–resident cells were then collected as described in *Section 4.2.13*. Collected cells were stained with Zombie Violet™ viability dye (1:500; BioLegend) for 15 min at room temperature. After viability staining, cells were blocked with CD16/CD32 antibody (1:100; clone 93; BioLegend) for 10 min at 4 °C. Cells were then stained for 30 min at 4 °C with the following antibodies: FITC CD45 (1:250; clone 30-F11; BioLegend), APC CD11c (1:250; clone N418; BioLegend), and PerCP-Cy5.5 MHCII (1:800; M5/114.15.2; BioLegend). After antibody staining, cells were washed with PBS + 1% (v/v) bovine serum albumin (PBSA) and resuspended in 250 μL of PBSA for analysis on an Attune NxT Flow Cytometer (Thermo Fisher Scientific). ILN–resident cells from untreated mice were used as assay baselines.

4.2.15 Analysis of antigen-specific T cells

On D0 and D21, mice were immunized with VIPER vaccine formulations (n = 6 per treatment group).[32,42] For each immunization, vaccines were suspended in 100 μL PBS, and 50 μL was administered subcutaneously on each side of the tail base (13 μg CSSSIINFEKL and 20 μg R848 per immunization). On D28, splenocytes were harvested for flow cytometry analysis as outlined in *Section 3.2.12* with the following modifications: (i) inclusion of a CD16/CD32 blocking step after viability staining as described in *Section 4.2.14*, (ii) a different vendor and dilution for the

FITC CD8α antibody (1:800; clone KT-15; Invitrogen), (iii) a 1:250 PE H-2K^b/SIINFEKL tetramer dilution (NIH Tetramer Core Facility), (iv) cell fixation in 200 μL of PBS + 0.5% (v/v) paraformaldehyde before flow cytometry analysis (tetramer staining only), and (v) exclusion of CD3ε and CD19 antibody stains.[32]

4.2.16 Tumor survival study

Mice were inoculated with 10^5 B16-OVA cells via subcutaneous flank injection as described in *Section 3.2.12* (n = 8 per treatment group).[32] Mice were immunized as described in *Section 4.2.15* on D4 and D11 after tumor inoculation. Every two days after inoculation, mice were weighed and tumor volumes were measured by caliper. Mice were euthanized if one or more of the following criteria were met: (i) tumor volume as measured by the equation $V = (L \times W^2)/2$ exceeds 1.5×10^3 mm^3, (ii) tumor weight exceeds 10% of body weight, (iii) over 20% of body weight is lost, and (iv) sever ulceration is observed.

4.2.17 Statistical analyses

FlowJo software was used to analyze flow cytometry data. GraphPad Prism was used to conduct statistical tests.

4.3 Results and Discussion

4.3.1 A mannosylated hydrophilic block

To synthesize a mannosylated VIPER vaccine carrier, we replaced the cationic first block of VIPER-Vax with a new block consisting of (i) mannose ethyl methacrylate (MMA) and (ii) R848 carbamate methacrylate, or "drugamer" (**Figure 4.1A**).[32,40,41] The drugamer was synthesized by conjugating R848—a small molecule agonist of Toll-like receptor 7/8, both endosomal pattern recognition receptors—to methacrylate with a self-immolating carbamate linker.[41,43,44] The

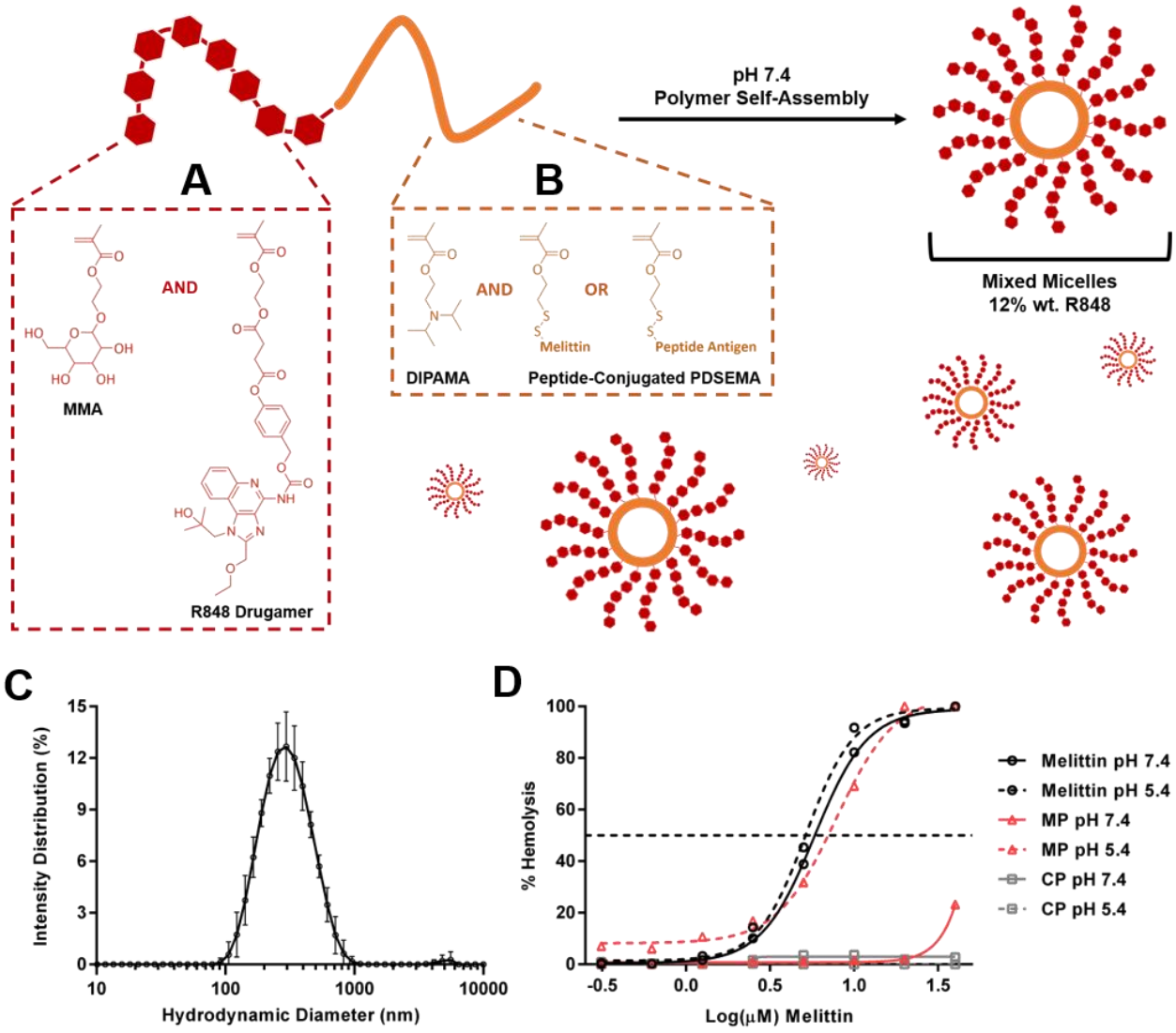

Figure 4.1 **Synthesis and characterization of mannosylated, adjuvant-loaded VIPER-Vax micelles. (A)** The hydrophilic block was composed of mannose ethyl methacrylate and a prodrug R848 carbamate methacrylate (drugamer).[40,41] Degradation of the drugamer's self-immolating carbamate linker releases free R848.[41] **(B)** The pH-switching hydrophobic block of this mannosylated polymer controlled micelle assembly and contained conjugation handles for thiolated melittin (a lytic peptide) and peptide antigen.[32,33] **(C)** The final micelle product (coined Drugamer-VIPER-Vax) exhibited a Z-average diameter of 269 nm (as measured by dynamic light scattering). **(D)** Micelle disassembly at acidic pH exposed melittin, lysing red blood cells. Melittin: free melittin; MP: melittin-loaded micelles; CP: melittin-free micelles. The polymer concentration of CP was matched to that of MP. This assay was conducted in triplicate.

composition of this new polymer's hydrophobic second block was the same as that of VIPER-Vax, with pH-switching 2-diisopropylaminoethyl methacrylate (DIPAMA) for modulation of micelle

formation and pyridyl disulfide ethyl methacrylate (PDSEMA) for loading of cysteine-terminated peptides (**Figure 4.1B**).[32,33] As with the original VIPER-Vax, the second block of the new polymer was conjugated to melittin or SIINFEKL (cysteine-serine-serine-SIINFEKL, abbreviated CSSSIINFEKL), the MHCI epitope of ovalbumin (**Figure 4.1B**).[32,45] Mixed micellization of CSSSIINFEKL-conjugated polymers and melittin-conjugated polymers at a 2:1 molar ratio produced mannosylated, drugamer-loaded micelles (denoted Drugamer-VIPER-Vax) roughly 270 nm in diameter (**Figure 4.1C, Supplemental Table 4.1, Supplemental Table 4.2**).

The two blocks of Drugamer-VIPER-Vax may act in concert to augment potency of conjugated vaccine cargo. Multivalent display of mannose ligands in the hydrophilic block may actively target both polymerized R848 and conjugated peptide antigen to DCs via C-type lectin binding, minimizing nonspecific adjuvant toxicity and maximizing antigen presentation efficiency.[29] The R848 drugamer—a prodrug monomer designed for slow adjuvant release—may sustain DC maturation and downstream T cell responses.[27,29,41,46] Furthermore, VIPER-induced lysis of DC endosomes may enhance antigen-specific CTC priming, as antigen presentation through the cytosolic MHCI pathway requires endosomal release of antigen.[42] Using a hemolysis assay, we confirmed that Drugamer-VIPER-Vax retained acid-responsive lytic bioactivity similar to that of the original cationic VIPER, with micelle disassembly and melittin-induced hemolysis observed only at acidic endosomal pH (**Figure 4.1C**).[33,34]

4.3.2 Targeting of mannosylated VIPER to dendritic cells

To assess whether mannose ligands target VIPER nanovaccines to DCs in vivo, we injected mice subcutaneously at the right tail base with VIPER-Vax micelles displaying (i) cationic p(OEGMA-*co*-DMAEMA) (Cationic-VIPER-Vax), (ii) neutrally charged, polyethylene glycolsylated (PEG-VIPER-Vax), or (iii) mannosylated (MMA-VIPER-Vax) coronas, all loaded with rhodamine-labeled CSSSIINFEKL (**Figure 4.2A, Supplemental Table 4.1, Supplemental Table 4.2**). Note that the hydrophilic block of MMA-VIPER-Vax contained no drugamer.

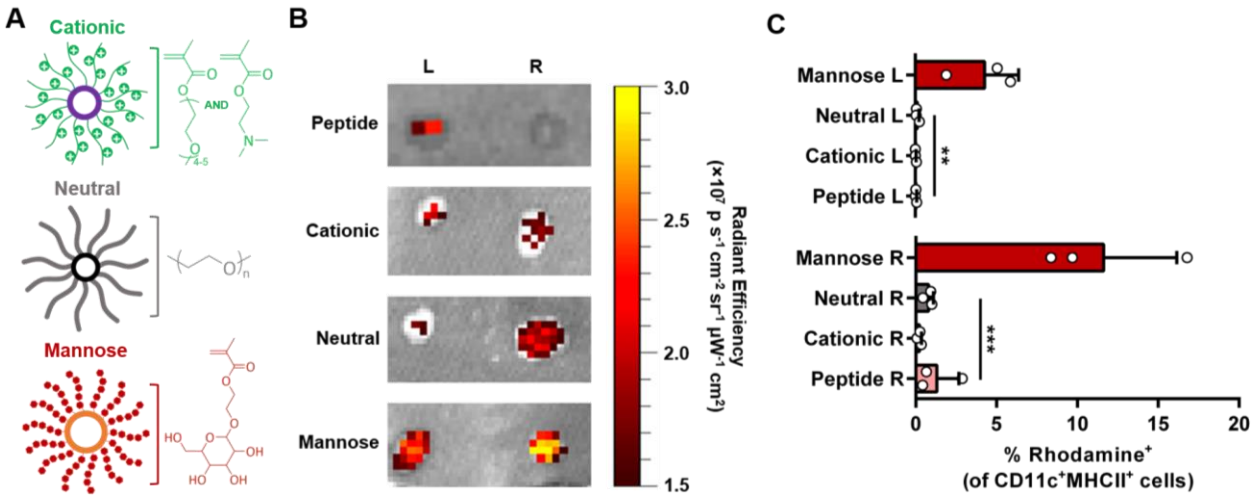

Figure 4.2 **Mannosylated VIPER-Vax is preferentially targeted to dendritic cells.** **(A)** VIPER-Vax micelles with cationic, polyethylene glycolylated (netural), or mannosylated coronas were loaded with rhodamine-labeled CSSSIINFEKL. **(B)** Micelles were administered subcutaneously at the right tail base of mice. Draining inguinal lymph nodes (ILNs) were harvested 48 h after administration. As visualized by Xenogen imaging of harvested ILNs, mannosylated VIPER-Vax drained most efficiently to ILNs after subcutaneous tail base administration (L = left ILN, R = right ILN). **(C)** Efficient ILN drainage of mannosylated VIPER-Vax correlated with preferential micelle accumulation in ILN-resident $CD11c^+MHCII^+$ DCs. Data are expressed as mean + SD, $n = 3$. Statistical significance is derived from an one-way ANOVA with post-hoc Fisher's LSD test (**p-value ≤ 0.01; ***p-value ≤ 0.001).

Fluorescent imaging of harvested inguinal lymph nodes (ILNs) 48 h after micelle injection showed that MMA-VIPER-Vax was transported more efficiently to draining ILNs than Cationic-VIPER-Vax and PEG-VIPER-Vax; preferential drainage of micelles into the right ILN corresponded with the chosen injection site (**Figure 4.2B**). Flow cytometry analysis of ILN-resident cells verified that MMA-VIPER-Vax and its antigen cargo were internalized more readily by $CD11c^+MHCII^+$ DCs than the other micelle variants (**Figure 4.2C**). The minimal accumulation of Cationic-VIPER-Vax in ILN-resident DCs—less than even that of free rhodamine-labeled CSSSIINFEKL—corroborated findings from *Chapter 3*, which suggested that retention of cationic VIPER-Vax polyplex at the injection site reduced its therapeutic efficacy.[32,38,39]

Although MMA-VIPER-Vax is targeted to DCs after subcutaneous administration, the exact mechanism through which this targeting occurs is unknown. Wilson et al.[29] found that

mannosylated unimer vaccines (i.e., free polymer chains) can target DCs via binding of CD206 and CD209, both cell membrane–bound C-type lectins. To date, we have been unable to demonstrate DC internalization of mannosylated VIPER-Vax micelles via similar surface receptor–mediated pathways (data not shown). However, mannose also binds soluble C-type lectins.[47] Therefore, opsonization by circulating C-type lectins and subsequent phagocytosis may also be a viable pathway for DC uptake of mannosylated VIPER nanovaccines.[28,30,31]

4.3.3 Antigen-specific T cell response

After verifying that mannosylation of the micelle corona targets VIPER-Vax to DCs, we investigated whether inclusion of melittin and drugamer in the micelle formulation would potentiate priming of antigen-specific CTC responses. Antigen-conjugated polymer was mixed with melittin-conjugated polymer at a 2:1 molar ratio to obtain Drugamer-VIPER-Vax micelles (**Figure 4.1A**). MMA-VIPER-Vax, the drugamer-free equivalent, was also prepared. Melittin-free equivalents of Drugamer-VIPER-Vax and MMA-VIPER-Vax—denoted Drugamer-Control-Vax and MMA Control-Vax, respectively—were formulated by mixing antigen-conjugated polymer with unconjugated polymer. Mice were immunized subcutaneously at the tail base on D0 and D21 with 13 μg of CSSSIINFEKL and 20 μg of R848 using the following formulations: (i) free CSSSIINFEKL + free R848, (ii) MMA-Control-Vax + free R848, (iii) MMA-VIPER-Vax + free R848, (iv) Drugamer-Control-Vax, and (v) Drugamer-VIPER-Vax (**Figure 4.3A**). All formulations were suspended in phosphate-buffered saline (PBS). The 20 μg R848 dose was based on those reported in previous studies with similar R848-loaded particulate vaccine systems.[29,46,48] Mice were euthanized on D28, and splenocytes were harvested for tetramer staining and intracellular cytokine staining of SIINFEKL-specific splenic CTCs as described in *Chapter 3* (**Figure 4.3A**).[32]

Surprisingly, immunization with MMA-Control-Vax + R848 and Drugamer-Control-Vax elicited stronger SIINFEKL-specific CTC responses than immunization with their melittin-loaded

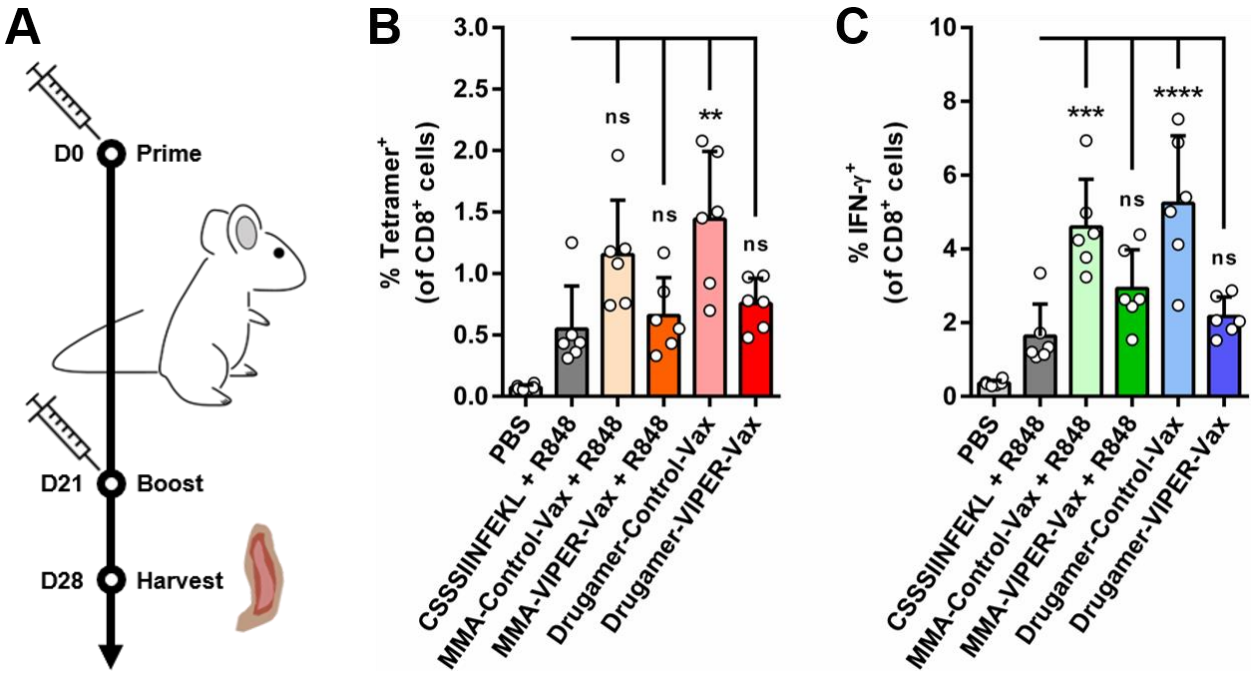

Figure 4.3 **Micellar melittin diminishes cytotoxic T cell activity. (A)** Mice were immunized on D0 and D21 via subcutaneous tail base injection. Splenic CTC responses were quantified on D28. Melittin-free vaccines (MMA-Control-Vax + R848 and Drugamer-Control-Vax) induced higher splenic levels of SIINFEKL-specific CTCs than melittin-containing vaccines (MMA-VIPER-Vax + R848 and Drugamer-VIPER-Vax), as indicated by differential **(B)** expression of SIINFEKL-specific T cell receptors (% $CD8^+Tetramer^+$) and **(C)** IFN-γ production by $CD8^+$ cells upon SIINFEKL restimulation (% $CD8^+IFN\text{-}\gamma^+$). Data are expressed as mean + SD, $n = 6$. Statistical significance is derived from an one-way ANOVA with post-hoc Tukey HSD test (**p-value ≤ 0.01; ***p-value ≤ 0.001; ****p-value ≤ 0.0001).

counterparts (**Figure 4.3**). MMA-Control-Vax + R848 and Drugamer-Control-Vax were also the only nanovaccine formulations to generate statistically greater CTC responses than the soluble vaccine formulation (CSSSIINFEKL + R848). At first glance, these findings contradict literature reporting the inflammatory effects of melittin.[49,50] However, there is a parallel body of literature that describes the opposite phenomenon—melittin may also suppress inflammation.[51] Incidentally, binding of mannose to C-type lectins expressed on innate immune cells (e.g., DCs) activates inflammatory cell signaling pathways.[52] Thus, the mannosylated VIPER-Vax corona may possess adjuvant properties that are attenuated by intracellular melittin bioactivity in DCs,

thereby reducing antigen-specific CTC responses. Additional studies are required to characterize DC maturation and cross-presentation after immunization with mannosylated VIPER-Vax.

While the aforementioned findings were perhaps the most prominent of this study, it is also important to note that inclusion of drugamer in the VIPER-Vax formulation did not affect CTC priming. We observed similar SIINFEKL-specific CTC responses in mice immunized with drugamer and those immunized with admixed R848 (**Figure 4.3**). Because no drugamer release studies were conducted, drugamer stability remains uncharacterized. The drugamer carbamate linker may have hydrolyzed during polymerization and/or storage, releasing free R848.[41,53] Nonetheless, covalent conjugation of adjuvant onto VIPER-Vax polymers—whether in prodrug form or as non-degradable units—is a worthwhile endeavor, as administration of free R848 may result in damaging systemic inflammation.[54–58] Loading of adjuvant into a targeted nanovaccine localizes adjuvant immunostimulation to immune cell populations of interest.[29,46,48]

4.4.4 B16-OVA tumor survival model

We moved forward with a tumor survival study to investigate whether VIPER-Vax–induced CTC responses would correlate with anticancer efficacy. Mice were immunized subcutaneously at the tail base on D4 and D11 after flank inoculation with B16-OVA, a murine melanoma tumor line that expresses ovalbumin (**Figure 4.4A**).[59] Although micellar vaccine formulations delayed tumor growth, all micelle-immunized mice showed similar tumor growth rates (**Figure 4.4B, Supplemental Figure 4.1**). Survival rates mirrored tumor growth rates. Mice immunized with micellar vaccine formulations exhibited statistically greater survival than mice immunized with soluble peptide vaccine (**Figure 4.4C–F**). However, all micelle-immunized mice died within 32–36 days after tumor inoculation, indicating little difference in therapeutic efficacy between the various micelle formulations. Moreover, the overall efficacy of these micellar vaccines was limited; in all micellar vaccine treatment groups, the last mouse succumbed to disease only 4–8 days after the last mouse immunized with soluble vaccine (**Figure 4.4C–F**).

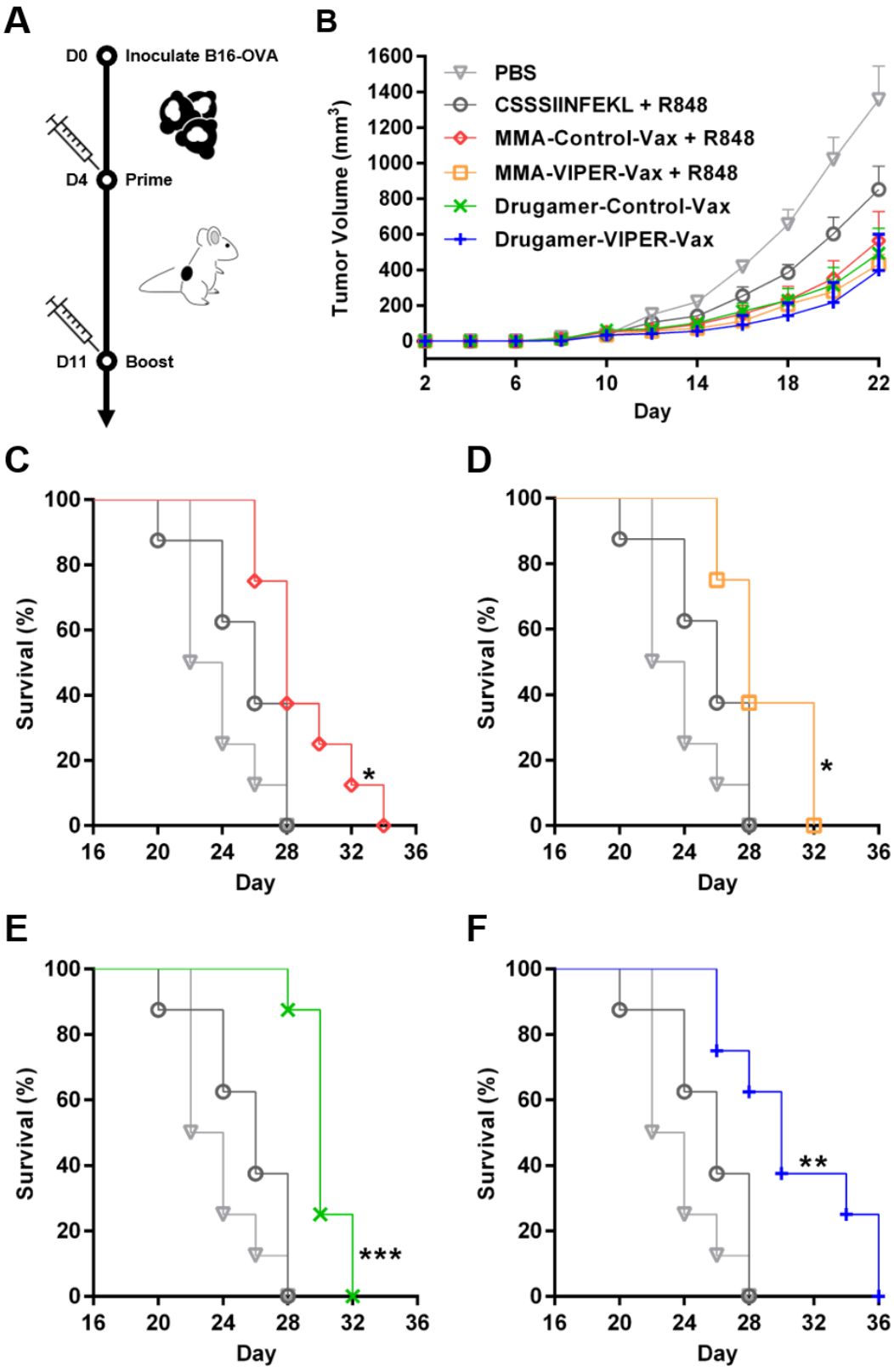

Figure 4.4 **Mannosylated nanovaccines slow progression of mouse melanoma. (A)** On D0, B16-OVA melanoma was inoculated into the subcutaneous hind flanks of mice. After

inoculation, mice were immunized on D4 and D11. **(B)** Mannosylated micelle vaccines slowed tumor growth. Data are expressed as mean + SEM, n = 8. **(C–F)** Micelle-immunized mice survived significantly longer than those immunized with soluble vaccine. All micelle vaccines showed similar efficacy regardless of melittin or drugamer content. Statistical significance is derived from a logrank test comparing survival of the micelle vaccine treatment group with that of the soluble vaccine treatment group (*p-value ≤ 0.05; **p-value ≤ 0.01; ***p-value ≤ 0.001).

Our survival data suggest that anticancer efficacy of mannosylated VIPER-Vax may not depend solely on direct priming of antigen-specific cellular immunity via the canonical DC-CTC axis. Since a variety of innate immune cells express C-type lectins, administration of mannosylated micelles may induce inflammation similar to that associated with acute infection, which can cause tumor regression.[52,60] Hence, any deleterious effect of micellar melittin on cross-presentation and CTC priming may be offset by inflammatory mannose bioactivity in non-DC innate immune cell populations, resulting in similar survival profiles across all micellar vaccine treatment groups (**Figure 4.4C–F**).

The overall efficacy of mannosylated VIPER-Vax may also be limited by other factors. First and foremost, no MHCII epitopes were included in this formulation. Durable tumor regression is dependent on $CD4^+$ helper T cell activity, so the lack of an MHCII ovalbumin epitope may have reduced vaccine potency (albeit the therapeutic efficacy of micellar vaccine against B16-OVA was still greater than that of soluble peptide vaccine).[7,17] Moreover, the true therapeutic benefit of mannosylated VIPER-Vax may remain unclear without parallel administration of immune checkpoint inhibitors (e.g., anti-PD-1 antibodies), as comparable nanovaccine systems cannot completely abrogate tumor growth without blockade of tumor immunosuppression mechanisms.[45,61,62]

4.4 Conclusions

We synthesized a new VIPER-Vax variant with a neutrally charged, mannosylated hydrophilic block. A prodrug R848 monomer, or “drugamer,” was also copolymerized into this hydrophilic

block. This mannosylated VIPER-Vax variant efficiently delivered conjugated peptide antigen cargo to DCs. Unexpectedly, inclusion of melittin in the VIPER-Vax formulation had deleterious effects on CTC priming. Future work with the VIPER-Vax platform will include (i) synthesis of multiantigen nanovaccine formulations, where combined libraries of MHCI and MHCII epitopes are covalently conjugated to VIPER-Vax polymers, and (ii) tumor survival studies with co-administration of immune checkpoint inhibitors. We anticipate that incorporation of multiantigen cargo and immune checkpoint inhibitors into mannosylated VIPER-Vax regimens will further improve their anticancer efficacy. However, it may be prudent to investigate cross-talk between mannose, melittin, and R848 bioactivities before adding more bioactive components to VIPER-Vax.

4.5 Acknowledgements

This work was supported by NIH grants 1R01CA177272 and R01NS064404. Albert Yen was supported by a National Science Foundation Graduate Research Fellowship under grant DGE-1256082. We thank the NIH Tetramer Core Facility for providing H-2K^b/SIINFEKL tetramer. We also thank Prof. Kim Woodrow (University of Washington) for allowing the use of her lab's plate reader. Finally, we thank Prof. Amanda Lund (Oregon Health & Science University) for her kind gift of B16-OVA cells.

4.6 Supporting Information

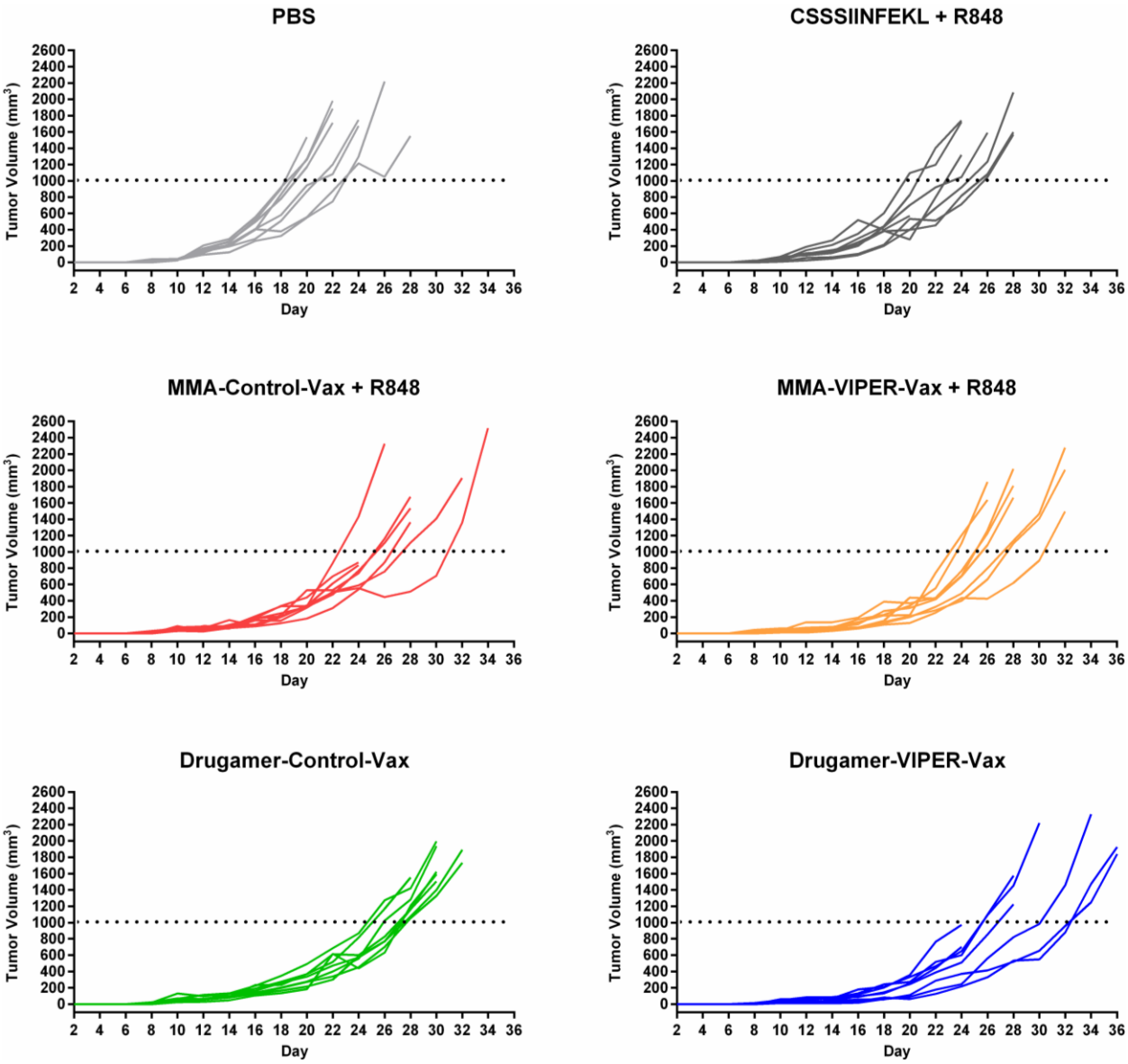

Supplemental Figure 4.1 **Spider plots showing progression of B16-OVA mouse melanoma.** Mice were immunized therapeutically with the indicated vaccine formulations.

Supplemental Table 4.1 **VIPER-Vax polymers, their chemical compositions, and other polymer characteristics.**

VIPER-Vax Polymer Variant	Chemical Composition (via ^{1}H NMR)	M_n (via ^{1}H NMR)	$Đ$ (via GPC)
Cationic-VIPER-Vax	p(OEGMA$_{8.6}$-*co*-DMAEMA$_{54.2}$)-*b*-p(DIPAMA$_{25}$-*co*-PDSEMA$_1$)	16,072	1.19
PEG-VIPER-Vax	PEG5000-*b*-p(DIPAMA$_{35}$-*co*-PDSEMA$_2$)	12,977	1.24
MMA-VIPER-Vax	pMMA$_{35}$-*b*-p(DIPAMA$_{26.8}$-*co*-PDSEMA$_{2.4}$)	19,106	1.23
Drugamer-VIPER-Vax	p(MMA$_{22.1}$-*co*-SRCMA$_{8.0}$)-*b*-p(DIPAMA$_{27.3}$-*co*-PDSEMA$_{2.0}$)	18,506	1.26

Supplemental Table 4.2 **VIPER-Vax micelle sizes.**

VIPER-Vax Polymer Variant	Z-Average Diameter* (nm)
Cationic-VIPER-Vax	22.7 ± 1.9
PEG-VIPER-Vax	96.0 ± 12.4
MMA-VIPER-Vax	120.9 ± 16.0
Drugamer-VIPER-Vax	268.9 ± 4.8

*Mean ± SD of three independent measurements.

Supplemental Table 4.3 **Staining panels used for flow cytometry.**

Dendritic Cell Panel

Marker	Vendor	Clone (If Antibody)	Fluorophore
Viability	BioLegend	N/A	Zombie Violet™
CD16/CD32	BioLegend	93	N/A
CD45	BioLegend	30-F11	FITC
CD11c	BioLegend	N418	APC
MHCII (I-A/I-E)	BioLegend	M5/114.15.2	PerCP-Cy5.5

T Cell Panel

Marker	Vendor	Clone (If Antibody)	Fluorophore
Viability	BioLegend	N/A	Zombie NIR™
CD16/CD32	BioLegend	93	N/A
CD8	Invitrogen	KT-15	FITC
IFN-γ	Invitrogen	XMG1.2	PE-Cy7
SIINFEKL T Cell Receptor	NIH Tetramer Core Facility	N/A (H-2K^{b}/SIINFEKL Tetramer)	PE

4.7 References

(1) Vetter, V.; Denizer, G.; Friedland, L. R.; Krishnan, J.; Shapiro, M. Understanding Modern-Day Vaccines: What You Need to Know. *Ann. Med.* **2018**, *50* (2), 110–120.

(2) Li, W.; Joshi, M.; Singhania, S.; Ramsey, K.; Murthy, A. Peptide Vaccine: Progress and Challenges. *Vaccines* **2014**, *2* (3), 515–536.

(3) Black, M.; Trent, A.; Tirrell, M.; Olive, C. Advances in the Design and Delivery of Peptide Subunit Vaccines with a Focus on Toll-like Receptor Agonists. *Expert Rev. Vaccines* **2010**, *9* (2), 157–173.

(4) Malonis, R. J.; Lai, J. R.; Vergnolle, O. Peptide-Based Vaccines: Current Progress and Future Challenges. *Chem. Rev.* **2020**, *120* (6), 3210–3229.

(5) Khong, H.; Overwijk, W. W. Adjuvants for Peptide-Based Cancer Vaccines. *J. Immunother. Cancer* **2016**, *4*, 56.

(6) Hollingsworth, R. E.; Jansen, K. Turning the Corner on Therapeutic Cancer Vaccines. *npj Vaccines* **2019**, *4*, 7.

(7) Knutson, K. L.; Schiffman, K.; Cheever, M. A.; Disis, M. L. Immunization of Cancer Patients with a HER-2/Neu, HLA-A2 Peptide, P369–377, Results in Short-Lived Peptide-Specific Immunity. *Clin. Cancer Res.* **2002**, *8* (5), 1014–1018.

(8) Bezu, L.; Kepp, O.; Cerrato, G.; Pol, J.; Fucikova, J.; Spisek, R.; Zitvogel, L.; Kroemer, G.; Galluzzi, L. Trial Watch: Peptide-Based Vaccines in Anticancer Therapy. *OncoImmunology* **2018**, *7* (12), e1511506.

(9) Töpfer, K.; Kempe, S.; Müller, N.; Schmitz, M.; Bachmann, M.; Cartellieri, M.; Schackert, G.; Temme, A. Tumor Evasion from T Cell Surveillance. *J. Biomed. Biotechnol.* **2011**, 918471.

(10) Bright, R. K.; Bright, J. D.; Byrne, J. A. Overexpressed Oncogenic Tumor-Self Antigens. *Hum. Vaccines Immunother.* **2014**, *10* (11), 3297–3305.

(11) Houghton, A. N.; Guevara-Patiño, J. A. Immune Recognition of Self in Immunity against Cancer. *J. Clin. Invest.* **2004**, *114* (4), 468–471.

(12) Bowen, W. S.; Svrivastava, A. K.; Batra, L.; Barsoumian, H.; Shirwan, H. Current Challenges for Cancer Vaccine Adjuvant Development. *Expert Rev. Vaccines* **2018**, *17* (3), 207–215.

(13) Batista-Duharte, A.; Martínez, D. T.; Carlos, I. Z. Efficacy and Safety of Immunological Adjuvants. Where Is the Cut-Off? *Biomed. Pharmacother.* **2018**, *105* (May), 616–624.

(14) Nierkens, S.; Tel, J.; Janssen, E.; Adema, G. J. Antigen Cross-Presentation by Dendritic Cell Subsets: One General or All Sergeants? *Trends Immunol.* **2013**, *34* (8), 361–370.

(15) Rincon-Restrepo, M.; Mayer, A.; Hauert, S.; Bonner, D. K.; Phelps, E. A.; Hubbell, J. A.; Swartz, M. A.; Hirosue, S. Vaccine Nanocarriers: Coupling Intracellular Pathways and Cellular Biodistribution to Control CD4 vs CD8 T Cell Responses. *Biomaterials* **2017**, *132*, 48–58.

(16) Disis, M. L.; Gad, E.; Herendeen, D. R.; Lai, V. P.-; Park, K. H.; Cecil, D. L.; O'Meara, M. M.; Treuting, P. M.; Lubet, R. A. A Multiantigen Vaccine Targeting Neu, IGFBP-2, and IGF-IR Prevents Tumor Progression in Mice with Preinvasive Breast Disease. *Cancer Prev. Res.* **2013**, *6* (12), 1273–1282.

(17) Kreiter, S.; Vormehr, M.; Van De Roemer, N.; Diken, M.; Löwer, M.; Diekmann, J.; Boegel, S.; Schrörs, B.; Vascotto, F.; Castle, J. C.; et al. Mutant MHC Class II Epitopes Drive Therapeutic Immune Responses to Cancer. *Nature* **2015**, *520* (7549), 692–696.

(18) Wang, H.; Mooney, D. J. Biomaterial-Assisted Targeted Modulation of Immune Cells in Cancer Treatment. *Nat. Mater.* **2018**, *17* (9), 761–772.

(19) Irvine, D. J.; Hanson, M. C.; Rakhra, K.; Tokatlian, T. Synthetic Nanoparticles for Vaccines and Immunotherapy. *Chem. Rev.* **2015**, *115* (19), 11109–11146.

(20) Park, J. H.; Um, W.; Shin, J. M.; Lee, J. A.; Song, S. H.; Ko, H.; Son, S.; Lee, E. S. Recent Advances in Polymeric Nanomedicines for Cancer Immunotherapy. *Adv. Healthc. Mater.* **2019**, *8* (4), 1801320.
(21) Ke, X.; Howard, G. P.; Tang, H.; Cheng, B.; Saung, M. T.; Santos, J. L.; Mao, H. Q. Physical and Chemical Profiles of Nanoparticles for Lymphatic Targeting. *Adv. Drug Deliv. Rev.* **2019**, *151–152*, 72–93.
(22) Keller, S.; Wilson, J. T.; Patilea, G. I.; Kern, H. B.; Convertine, A. J.; Stayton, P. S. Neutral Polymer Micelle Carriers with pH-Responsive, Endosome-Releasing Activity Modulate Antigen Trafficking to Enhance CD8+ T Cell Responses. *J. Control. Release* **2014**, *191*, 24–33.
(23) Reddy, S. T.; Rehor, A.; Schmoekel, H. G.; Hubbell, J. A.; Swartz, M. A. In Vivo Targeting of Dendritic Cells in Lymph Nodes with Poly(Propylene Sulfide) Nanoparticles. *J. Control. Release* **2006**, *112* (1), 26–34.
(24) De Koker, S.; Cui, J.; Vanparijs, N.; Albertazzi, L.; Grooten, J.; Caruso, F.; De Geest, B. G. Engineering Polymer Hydrogel Nanoparticles for Lymph Node-Targeted Delivery. *Angew. Chemie - Int. Ed.* **2016**, *55* (4), 1334–1339.
(25) Merad, M.; Sathe, P.; Helft, J.; Miller, J.; Mortha, A. The Dendritic Cell Lineage: Ontogeny and Function of Dendritic Cells and Their Subsets in the Steady State and the Inflamed Setting. *Annu. Rev. Immunol.* **2013**, *31* (1), 563–604.
(26) Keler, T.; Ramakrishna, V.; Fanger, M. W. Mannose Receptor-Targeted Vaccines. *Expert Opin. Biol. Ther.* **2004**, *4* (12), 1953–1962.
(27) Patil, T. S.; Deshpande, A. S. Mannosylated Nanocarriers Mediated Site-Specific Drug Delivery for the Treatment of Cancer and Other Infectious Diseases: A State of the Art Review. *J. Control. Release* **2020**, *320*, 239–252.
(28) Kerrigan, A. M.; Brown, G. D. C-Type Lectins and Phagocytosis. *Immunobiology* **2009**, *214* (7), 562–575.
(29) Wilson, D. S.; Hirosue, S.; Raczy, M. M.; Bonilla-Ramirez, L.; Jeanbart, L.; Wang, R.; Kwissa, M.; Franetich, J.-F.; Broggi, M. A. S.; Diaceri, G.; et al. Antigens Reversibly Conjugated to a Polymeric Glyco-Adjuvant Induce Protective Humoral and Cellular Immunity. *Nat. Mater.* **2019**, *18* (2), 175–185.
(30) Tokatlian, T.; Read, B. J.; Jones, C. A.; Kulp, D. W.; Menis, S.; Chang, J. Y. H.; Steichen, J. M.; Kumari, S.; Allen, J. D.; Dane, E. L.; et al. Innate Immune Recognition of Glycans Targets HIV Nanoparticle Immunogens to Germinal Centers. *Science* **2019**, *363* (6427), 649–654.
(31) Nauta, A. J.; Castellano, G.; Xu, W.; Woltman, A. M.; Borrias, M. C.; Daha, M. R.; van Kooten, C.; Roos, A. Opsonization with C1q and Mannose-Binding Lectin Targets Apoptotic Cells to Dendritic Cells. *J. Immunol.* **2004**, *173* (5), 3044–3050.
(32) Peeler, D. J.; Yen, A.; Luera, N.; Stayton, P. S.; Pun, S. H. Lytic Polyplex Vaccines Enhance Antigen-Specific Cytotoxic T Cell Response through Induction of Local Cell Death. *Adv. Ther.* **2021**, 2100005.
(33) Cheng, Y.; Yumul, R. C.; Pun, S. H. Virus-Inspired Polymer for Efficient In Vitro and In Vivo Gene Delivery. *Angew. Chemie Int. Ed.* **2016**, *55* (39), 12013–12017.
(34) Peeler, D. J.; Thai, S. N.; Cheng, Y.; Horner, P. J.; Sellers, D. L.; Pun, S. H. pH-Sensitive Polymer Micelles Provide Selective and Potentiated Lytic Capacity to Venom Peptides for Effective Intracellular Delivery. *Biomaterials* **2019**, *192*, 235–244.
(35) Yen, A.; Cheng, Y.; Sylvestre, M.; Gustafson, H. H.; Puri, S.; Pun, S. H. Serum Nuclease Susceptibility of mRNA Cargo in Condensed Polyplexes. *Mol. Pharm.* **2018**, *15* (6), 2268–2276.
(36) Palumbo, R. N.; Zhong, X.; Wang, C. Polymer-Mediated DNA Vaccine Delivery via Bystander Cells Requires a Proper Balance between Transfection Efficiency and Cytotoxicity. *J. Control. Release* **2012**, *157* (1), 86–93.

(37) Bosnjak, L.; Miranda-Saksena, M.; Koelle, D. M.; Boadle, R. A.; Jones, C. A.; Cunningham, A. L. Herpes Simplex Virus Infection of Human Dendritic Cells Induces Apoptosis and Allows Cross-Presentation via Uninfected Dendritic Cells. *J. Immunol.* **2005**, *174* (4), 2220–2227.
(38) van den Berg, J. H.; Oosterhuis, K.; Hennink, W. E.; Storm, G.; van der Aa, L. J.; Engbersen, J. F. J.; Haanen, J. B. A. G.; Beijnen, J. H.; Schumacher, T. N.; Nuijen, B. Shielding the Cationic Charge of Nanoparticle-Formulated Dermal DNA Vaccines Is Essential for Antigen Expression and Immunogenicity. *J. Control. Release* **2010**, *141* (2), 234–240.
(39) Zhong, X.; Han, W.; Wang, C.; Ji, W.; Palumbo, R. N.; Panus, D. Transgene Expression and Local Tissue Distribution of Naked and Polymer-Condensed Plasmid DNA after Intradermal Administration in Mice. *J. Control. Release* **2012**, *159* (2), 232–239.
(40) Chen, J.; Son, H.-N.; Hill, J. J.; Srinivasan, S.; Su, F.-Y.; Stayton, P. S.; Convertine, A. J.; Ratner, D. M. Nanostructured Glycopolymer Augmented Liposomes to Elucidate Carbohydrate-Mediated Targeting. *Nanomedicine* **2016**, *12* (7), 2031–2041.
(41) Srinivasan, S.; Roy, D.; Chavas, T. E. J.; Vlaskin, V.; Ho, D.-K.; Pottenger, A.; LeGuyader, C. L. M.; Maktabi, M.; Strauch, P.; Jackson, C.; et al. Liver-Targeted Polymeric Prodrugs of 8-Aminoquinolines for Malaria Radical Cure. *J. Control. Release* **2021**, *331*, 213–227.
(42) Wilson, J. T.; Keller, S.; Manganiello, M. J.; Cheng, C.; Lee, C. C.; Opara, C.; Convertine, A.; Stayton, P. S. pH-Responsive Nanoparticle Vaccines for Dual-Delivery of Antigens and Immunostimulatory Oligonucleotides. *ACS Nano* **2013**, *7* (5), 3912–3925.
(43) Hennessy, E. J.; Parker, A. E.; O'Neill, L. A. J. Targeting Toll-like Receptors: Emerging Therapeutics? *Nat. Rev. Drug Discov.* **2010**, *9* (4), 293–307.
(44) Hung, Y.-F.; Chen, C.-Y.; Shih, Y.-C.; Liu, H.-Y.; Huang, C.-M.; Hsueh, Y.-P. Endosomal TLR3, TLR7, and TLR8 Control Neuronal Morphology through Different Transcriptional Programs. *J. Cell Biol.* **2018**, *217* (8), 2727–2742.
(45) Kuai, R.; Ochyl, L. J.; Bahjat, K. S.; Schwendeman, A.; Moon, J. J. Designer Vaccine Nanodiscs for Personalized Cancer Immunotherapy. *Nat. Mater.* **2017**, *16* (4), 489–496.
(46) Lynn, G. M.; Laga, R.; Darrah, P. A.; Ishizuka, A. S.; Balaci, A. J.; Dulcey, A. E.; Pechar, M.; Pola, R.; Gerner, M. Y.; Yamamoto, A.; et al. In Vivo Characterization of the Physicochemical Properties of Polymer-Linked TLR Agonists That Enhance Vaccine Immunogenicity. *Nat. Biotechnol.* **2015**, *33* (11), 1201–1210.
(47) Turner, M. . The Role of Mannose-Binding Lectin in Health and Disease. *Mol. Immunol.* **2003**, *40* (7), 423–429.
(48) Lynn, G. M.; Sedlik, C.; Baharom, F.; Zhu, Y.; Ramirez-Valdez, R. A.; Coble, V. L.; Tobin, K.; Nichols, S. R.; Itzkowitz, Y.; Zaidi, N.; et al. Peptide–TLR-7/8a Conjugate Vaccines Chemically Programmed for Nanoparticle Self-Assembly Enhance CD8 T-Cell Immunity to Tumor Antigens. *Nat. Biotechnol.* **2020**, *38* (3), 320–332.
(49) Yu, X.; Dai, Y.; Zhao, Y.; Qi, S.; Liu, L.; Lu, L.; Luo, Q.; Zhang, Z. Melittin-Lipid Nanoparticles Target to Lymph Nodes and Elicit a Systemic Anti-Tumor Immune Response. *Nat. Commun.* **2020**, *11*, 1110.
(50) Lee, E. Y.; Zhang, C.; Di Domizio, J.; Jin, F.; Connell, W.; Hung, M.; Malkoff, N.; Veksler, V.; Gilliet, M.; Ren, P.; et al. Helical Antimicrobial Peptides Assemble into Protofibril Scaffolds That Present Ordered dsDNA to TLR9. *Nat. Commun.* **2019**, *10*, 1012.
(51) Lee, G.; Bae, H. Anti-Inflammatory Applications of Melittin, a Major Component of Bee Venom: Detailed Mechanism of Action and Adverse Effects. *Molecules* **2016**, *21* (5), 616.
(52) Kingeter, L. M.; Lin, X. C-Type Lectin Receptor-Induced NF-κB Activation in Innate Immune and Inflammatory Responses. *Cell. Mol. Immunol.* **2012**, *9* (2), 105–112.
(53) Ghosh, A. K.; Brindisi, M. Organic Carbamates in Drug Design and Medicinal Chemistry. *J. Med. Chem.* **2015**, *58* (7), 2895–2940.
(54) Nuhn, L.; Vanparijs, N.; De Beuckelaer, A.; Lybaert, L.; Verstraete, G.; Deswarte, K.; Lienenklaus, S.; Shukla, N. M.; Salyer, A. C. D.; Lambrecht, B. N.; et al. pH-Degradable

Imidazoquinoline-Ligated Nanogels for Lymph Node-Focused Immune Activation. *Proc. Natl. Acad. Sci.* **2016**, *113* (29), 8098–8103.
(55) Scott, E. A.; Stano, A.; Gillard, M.; Maio-Liu, A. C.; Swartz, M. A.; Hubbell, J. A. Dendritic Cell Activation and T Cell Priming with Adjuvant- and Antigen-Loaded Oxidation-Sensitive Polymersomes. *Biomaterials* **2012**, *33* (26), 6211–6219.
(56) Pockros, P. J.; Guyader, D.; Patton, H.; Tong, M. J.; Wright, T.; McHutchison, J. G.; Meng, T.-C. Oral Resiquimod in Chronic HCV Infection: Safety and Efficacy in 2 Placebo-Controlled, Double-Blind Phase IIa Studies. *J. Hepatol.* **2007**, *47* (2), 174–182.
(57) Gunzer, M.; Riemann, H.; Basoglu, Y.; Hillmer, A.; Weishaupt, C.; Balkow, S.; Benninghoff, B.; Ernst, B.; Steinert, M.; Scholzen, T.; et al. Systemic Administration of a TLR7 Ligand Leads to Transient Immune Incompetence Due to Peripheral-Blood Leukocyte Depletion. *Blood* **2005**, *106* (7), 2424–2432.
(58) Wang, B.; Van Herck, S.; Chen, Y.; Bai, X.; Zhong, Z.; Deswarte, K.; Lambrecht, B. N.; Sanders, N. N.; Lienenklaus, S.; Scheeren, H. W.; et al. Potent and Prolonged Innate Immune Activation by Enzyme-Responsive Imidazoquinoline TLR7/8 Agonist Prodrug Vesicles. *J. Am. Chem. Soc.* **2020**, *142* (28), 12133–12139.
(59) Bellone, M.; Cantarella, D.; Castiglioni, P.; Crosti, M. C.; Ronchetti, A.; Moro, M.; Garancini, M. P.; Casorati, G.; Dellabona, P. Relevance of the Tumor Antigen in the Validation of Three Vaccination Strategies for Melanoma. *J. Immunol.* **2000**, *165* (5), 2651–2656.
(60) Hoption Cann, S. A.; Van Netten, J. P.; Van Netten, C. Acute Infections as a Means of Cancer Prevention: Opposing Effects to Chronic Infections? *Cancer Detect. Prev.* **2006**, *30* (1), 83–93.
(61) Luo, M.; Wang, H.; Wang, Z.; Cai, H.; Lu, Z.; Li, Y.; Du, M.; Huang, G.; Wang, C.; Chen, X.; et al. A STING-Activating Nanovaccine for Cancer Immunotherapy. *Nat. Nanotechnol.* **2017**, *12* (7), 648–654.
(62) Shae, D.; Becker, K. W.; Christov, P.; Yun, D. S.; Lytton-Jean, A. K. R.; Sevimli, S.; Ascano, M.; Kelley, M.; Johnson, D. B.; Balko, J. M.; et al. Endosomolytic Polymersomes Increase the Activity of Cyclic Dinucleotide STING Agonists to Enhance Cancer Immunotherapy. *Nat. Nanotechnol.* **2019**, *14* (3), 269–278.

CHAPTER 5

Immunization with Mannosylated Melittin Micelles Attenuates Dendritic Cell Maturation

Albert Yen*, Shixian Lv*, Kefan Song, David J. Peeler, Selvi Srinivasan,
Patrick S. Stayton, and Suzie H. Pun

Synopsis. Herein, we offer a retrospective critique of our research approach to date and discuss experiments that explore unanswered questions raised throughout the previous chapters of this dissertation. Our key finding is that mannose-decorated, melittin-loaded micelle vaccines attenuate dendritic cell maturation, providing a possible explanation for the diminished antigen-specific T cell responses observed in mice immunized with these vaccines (see *Chapter 4*).

*Equally contributing authors.

5.1 Introduction

Thus far, our work on vaccine variants (VIPER-Vax) of the "Virus-Inspired Polymer for Endosomal Release" (VIPER) has been driven by two core hypotheses. In *Chapter 3*, we hypothesized that VIPER-Vax–enhanced endosomal release of peptide antigens would increase cross-presentation by dendritic cells (DCs) via cytosolic pathways.[1,2] In *Chapter 4*, we hypothesized that mannosylation of VIPER-Vax would improve DC targeting through mannose-directed binding of C-type lectins, thereby augmenting T cell immunity.[3,4] Unexpected biological phenomena subverted both hypotheses.

We approached the first of these hypotheses from the perspective of a gene delivery scientist (after all, VIPER was originally designed as a gene carrier).[5,6] Genes encoding protein are non-functional in the endosome; when such genes are delivered intracellularly, endosomal escape is a hard prerequisite for protein expression.[7–9] On the other hand, protein and peptide antigens initiate immune responses even if trapped in endosomes, as DCs are capable of cross-presenting antigens through vacuolar pathways independent of the cytosol.[2] While studies with other endosomolytic polymer vaccines show that endosomal escape of antigen can increase cross-presentation efficiency, it is not a prerequisite for cross-presentation.[10,11] In *Chapter 3* of this dissertation and in previously published works, we conclusively demonstrated that VIPER is endosomolytic and efficiently delivers condensed nucleic acid into the cytosol.[1,5,12] However, as evidenced by data reported in *Chapter 3*, peptide antigens bound to VIPER-Vax are not cross-presented more efficiently in vitro than soluble peptide antigens or those bound to melittin-free carrier.[1] We only enhance cross-presentation at cytotoxic VIPER-Vax doses, but under such cytotoxic treatment conditions, corpse-associated antigen transfer becomes a dominant mechanism for induction of cross-presentation.[1,13,14]

Our second hypotheses was subverted by happenstance. Targeting ligands that guide bioactive compounds to specific cell populations in vivo through receptor binding (e.g., antibodies

conjugated to drugs) are well-reported throughout the literature.[15,16] Mannose, in particular, serves as an effective targeting ligand for vaccine delivery, as DCs express a variety of C-type lectins, or carbohydrate-binding receptors.[17–19] What differentiates our mannosylated VIPER vaccine (reported in *Chapter 4*) from similar polymer vaccines is the covalent loading of both melittin and peptide antigen into a mannosylated micelle formulation, which unexpectedly suppresses cytotoxic T cell priming instead of augmenting it. Since both melittin and mannose possess immunostimulatory properties, it is surprising that combining the two biomolecules within a micellar vaccine mitigates T cell responses after immunization.[20–22] Interestingly, however, melittin may also inhibit activation of nuclear factor kappa B (NF-κB), a transcription factor that plays a key role in inflammatory cell signaling pathways.[23–26] Because binding of C-type lectins on innate immune cells (e.g., DCs) stimulates inflammatory signaling mechanisms dependent on NF-κB, co-delivery of melittin and mannose in micellar form to DCs may abrogate DC maturation and subsequent cross-presentation.[21,25] Elucidation of intracellular signaling cross-talk triggered by combined melittin and mannose bioactivities is beyond the scope of this dissertation. Nevertheless, further investigation of how mannosylated VIPER vaccines affect DC maturation may inform improvements to our vaccine design.

Taken together, the findings presented throughout this dissertation raise two important questions:

1. Is "[decoupling] VIPER-Vax cytolysis from endosomolysis"[1] possible? In other words, can VIPER vaccines enhance cross-presentation via endosomolysis without killing the antigen-presenting cell?[1]
2. What is the effect of mannosylated VIPER vaccines on DC maturation phenotype?

This chapter discusses results from a series of experiments that answer (at least in part) the above questions.

5.2 Experimental Section

5.2.1 Materials

Concanavalin A was purchased from InvivoGen. All other materials are listed in *Section 4.2.1*.

5.2.2 Synthesis of a new mannosylated VIPER

The reversible addition–fragmentation chain-transfer (RAFT) polymerization scheme described in *Section 4.2.4* was modified for synthesis of a new mannosylated VIPER. The first block of this new copolymer, composed of mannose ethyl methacrylate (MMA), was the same as that of the original mannosylated VIPER and was synthesized as described in *Section 4.2.4*.[27] For synthesis of the second block, feed quantities of 2-diisopropylaminoethyl methacrylate (DIPAMA) and pyridyl disulfide ethyl methacrylate (PDSEMA) were decreased to 60 mol eq. (from 200 mol eq.) and 10 mol eq. (from 20 mol eq.), respectively. In addition, the reaction time for second block synthesis was increased to 18 h (from 3 h). Reaction conditions were otherwise identical to those reported in *Section 4.2.4*. The final copolymer product, $pMMA_{35}$-*b*-p($DIPAMA_{43}$-*co*-$PDSEMA_{3.4}$), M_w ~24,000, had a higher DIPAMA and PDSEMA content than its previous iteration.

5.2.3 Polymer characterization

^{1}H NMR and size exclusion chromatography were used to measure polymer composition, M_w, and dispersity (*Đ*) as detailed in previous work from our group.[5,12]

5.2.4 Peptide synthesis

Ovalbumin (OVA) MHC class I (MHCI) epitope (CSSSIINFEKL), and OVA MHC class II (MHCII) epitope (CSSISQAVHAAHAEINEAGR), both functionalized with a terminal cysteine-serine-serine linker, were prepared using synthesis and purification protocols outlined in *Section 3.2.2*

and previous work.[1,12,28] A cysteine-terminated melittin (GIGAVLKVLTTGLPALISWIKRKRQQC) was also prepared.[1,12]

5.2.5 Conjugation of peptides to polymers

Purified peptides were conjugated to mannosylated VIPER following a protocol similar to those described in *Section 3.2.3*, *Section 4.2.8*, and previous work, with conjugation reactions performed in deionized (DI) water containing 2% (v/v) trifluoroacetic acid (Sigma-Aldrich), at a 3:5 molar ratio of peptide to polymer, and at a ≥ 20 mg/mL reaction concentration.[1,5,12] After dialysis in DI water and lyophilization, the following polymer-peptide conjugates were obtained: (i) melittin-conjugated polymer (MP) with two peptides per polymer, (ii) OVA MHCI epitope–conjugated polymer (1P) with two peptides per polymer, and (iii) OVA MHCII epitope–conjugated polymer (2P) with 1.5 peptides per polymer.

5.2.6 Formation of mannosylated VIPER micelles

Mannosylated VIPER micelles comprised some combination of MP, 1P, 2P, or unconjugated polymer and were formulated according to (i) the target dose of antigen and melittin, as well as (ii) the target molar ratio of antigen to melittin. Micelles were formulated using the pH transition protocol reported in *Section 3.2.3* and previous work.[1,5,12] In brief, polymers were dissolved in acidic phosphate buffer (pH 4.4). To form micelles, basic phosphate buffer (pH 10) was then slowly added until a final solution pH of 7.4.

5.2.7 Measurement of micelle size

Micelles were diluted in pH 7.4 phosphate-buffered saline (PBS) to a 0.2 mg/mL polymer concentration. A ZetaPlus instrument (Brookhaven Instruments) was used to measure micelle size.

5.2.8 Lectin binding assay

Binding of mannosylated VIPER micelles to concanavalin A was assessed using an agglutination assay described in a previous doctoral dissertation published at the University of Washington.[29] Briefly, micelles at a 50 μg/mL polymer concentration were mixed by pipetting with 100 μg/mL concanavalin A in 1× PBS + Ca^{2+} + Mg^{2+} (Corning). Immediately after mixing, micelle agglutination was quantified via optical density measurements at 350 nm.

5.2.9 Cell culture

DC2.4 cells (gift of Prof. Kim Woodrow) were maintained in RPMI 1640 (with L-glutamine) + 10% heat-inactivated fetal bovine serum (HIFBS; Gibco) + 1× non-essential amino acids (Gibco) + 10 mM HEPES buffer (Gibco) + 1× penicillin/streptomycin (Gibco) + 55 μM β-mercaptoethanol (Bio-Rad). B3Z $CD8^+$ T hybridoma cells (gift of Prof. Nilabh Shastri) were maintained below 7×10^5 cells/mL in RPMI 1640 (with L-glutamine) + 10% HIFBS + 1 mM sodium pyruvate + 1× penicillin/streptomycin + 50 μM β-mercaptoethanol. After 10 passages, B3Z cells were discarded.

5.2.10 DC2.4–B3Z T cell cross-presentation assay

This assay protocol was adapted from the one outlined in *Section 3.2.9*.[1,11] DC2.4 cells were seeded in 96-well U-bottom tissue culture plates at 10^4 cells/well. Immediately after seeding, DC2.4 cells were treated with micelle vaccine formulations at 37 °C and 5% CO_2 for 24 h (final volume of 100 μL/well). After 24 h, DC2.4 cells were co-cultured with B3Z cells for 24 h as described in *Section 3.2.9*.[1,11] Cells were then treated in the dark for 1.5 h at 37 °C with 150 μL per well of lysis buffer made from PBS (no Ca^{2+} or Mg^{2+}) + 0.15 mM chlorophenol red-β-D-galactopyranoside (Roche) + 0.1% (v/v) Triton X-100 + 9 mM $MgCl_2$ + 100 μM β-mercaptoethanol. The absorbance of chlorophenol red byproduct at 570 nm (reference 650 nm) was then measured to determine cross-presentation efficiency. To quantify cell viability, DC2.4 cells were treated with vaccine

formulations as described above. Cells were then washed twice with PBS, and an MTS assay (Promega) was performed according to manufacturer protocol.

5.2.11 Immunization of mice

All animal studies were conducted under protocols approved by the Institutional Animal Care and Use Committee at the University of Washington. Female C57BL/6 mice (Charles River Laboratories), 8–9 weeks old, were used for all studies. Mice were immunized by subcutaneous administration of vaccine in 50 μL PBS at both sides of the tail base (total volume of 100 μL per immunization).

5.2.12 Preparing a single cell suspension from lymph node tissue

Immunized mice were euthanized 24 or 48 h after immunization. Inguinal lymph nodes (ILNs) were harvested and stored on ice in Eppendorf tubes filled with RPMI 1640 + 10% FBS until further processing. ILNs were then incubated for 30 min at 37 °C in a tissue digest solution consisting of RPMI 1640 + 10% FBS + 1 mg/mL collagenase type IV (Worthington Biochemical) + 100 U/mL DNase I (Sigma-Aldrich). To quench enzyme activity after incubation, UltraPure™ 0.5M EDTA, pH 8.0 (Thermo Fisher Scientific) was added to a final concentration of 10 mM EDTA.[30] The end of a syringe plunger was then used to homogenize lymph nodes against a 70 μm cell strainer. Single cell suspensions were obtained by flushing strainers with PBS + 1% (v/v) bovine serum albumin (Miltenyi Biotec) + 2 mM EDTA (PBSA/EDTA). Cell suspensions were deposited in conical tubes and kept on ice until analysis.

5.2.13 Dendritic cell maturation and cross-presentation

ILN-resident cells from immunized mice were collected as described in *Section 5.2.12* and stained with Zombie NIR™ viability dye (1:500; BioLegend) for 15 min at room temperature. Cells were then washed with PBSA/EDTA and blocked with CD16/CD32 antibody (1:100; clone 93;

BioLegend) for 10 min at 4 °C. Cells were subsequently stained for 30 min at 4 °C with the following antibody panel: Alexa Fluor 488 CD8α (1:50, clone 53-6.7, BioLegend), Brilliant Violet 421™ CD11b (1:100; clone M1/70; BioLegend), Super Bright 600 CD103 (1:50, clone B-Ly7; Invitrogen), APC CD11c (1:200; clone N418; BioLegend), PerCP-Cy5.5 MHCII (1:500; M5/114.15.2; BioLegend), Brilliant Violet 510™ CD86 (1:50; clone GL-1; BioLegend), and PE H-2K^b bound to SIINFEKL (1:50; clone 25-D1.16; BioLegend). Once stained, cells were washed twice with PBSA/EDTA and suspended in 200 µL of fixation buffer (PBS + 0.5% [v/v] paraformaldehyde) prior to analysis on an Attune NxT Flow Cytometer (Thermo Fisher Scientific). For fluorescence compensation, UltraComp eBeads™ (Thermo Fisher Scientific) were used according to manufacturer protocol for antibody fluorophores, and single-stained cells were used for Zombie NIR™.

5.2.14 Statistical analyses

To analyze flow cytometry data, FlowJo software was used. Statistical tests for all data sets were performed with GraphPad Prism.

5.3 Results and Discussion

5.3.1 Resynthesis of mannosylated VIPER-Vax

In *Chapter 4*, we synthesized MMA-VIPER-Vax and Drugamer-VIPER-Vax, two VIPER vaccine variants with a mannosylated hydrophilic block. In short, the hydrophilic block of the former consisted entirely of mannose ethyl methacrylate (MMA), whereas the hydrophilic block of the latter was derived from copolymerization of MMA and a resiquimod (R848) prodrug monomer.[27,31] Based on dynamic light scattering measurements, both MMA-VIPER-Vax and Drugamer-VIPER-Vax micelles were greater than 100 nm in size, with Drugamer-VIPER-Vax close to 300 nm. Due to colloidal stability issues encountered during use of both micelle

formulations, we resynthesized MMA-VIPER-Vax by following a modified reaction scheme and increased 2-diisopropylaminoethyl methacrylate (DIPAMA) content in the hydrophobic block to improve micelle stability.[5] We obtained a new polymer with composition $pMMA_{35}$-*b*-p(**$DIPAMA_{43}$**-*co*-$PDSEMA_{3.4}$) instead of the original composition $pMMA_{35}$-*b*-p(**$DIPAMA_{26.8}$**-*co*-$PDSEMA_{2.4}$) reported in *Chapter 4*.

This new MMA-VIPER-Vax polymer was conjugated with (i) two cysteine-terminated melittins per polymer, (ii) two OVA MHCI epitopes (SIINFEKL) per polymer, or (iii) 1.5 OVA MHCII epitopes (ISQAVHAAHAEINEAGR) per polymer via its pyridyl disulfide side groups.[5,32] As in *Chapter 3* and *Chapter 4*, OVA epitopes were synthesized with an N-terminal cysteine-serine-serine linker for conjugation.[1,28] Epitope-conjugated and melittin-conjugated polymers combined to form mixed VIPER-Vax micelles between ~20–30 nm in size (data not shown). Notably, homogeneous micelles comprised solely of unconjugated polymers or melittin-conjugated polymers were ~40–50 nm in size (data not shown), indicating that peptide cargo content modulated VIPER micelle assembly in some way.[33]

Although this new MMA-VIPER-Vax micelle was smaller than its previous iteration, we did not anticipate any loss in lymphatic trafficking or DC targeting. Particles 20–100 nm in size drain readily into lymph nodes after subcutaneous administration, and the new micelle falls within this size range regardless of cargo content.[34,35] Moreover, this micelle was the first dual epitope VIPER-Vax formulation, and its efficacy may have predicted that of VIPER-Vax formulations with more diverse antigen cargo.

5.3.2 Binding of mannosylated VIPER-Vax to soluble lectins

After formulating dual epitope micelles with a newly synthesized MMA-VIPER-Vax polymer, we assessed whether these micelles could bind C-type lectins. To model this binding interaction, we mixed MMA-VIPER-Vax micelles with concanavalin A (ConA)—a soluble plant lectin with four mannose binding sites—in phosphate-buffered saline (PBS) and assayed for lectin-mediated

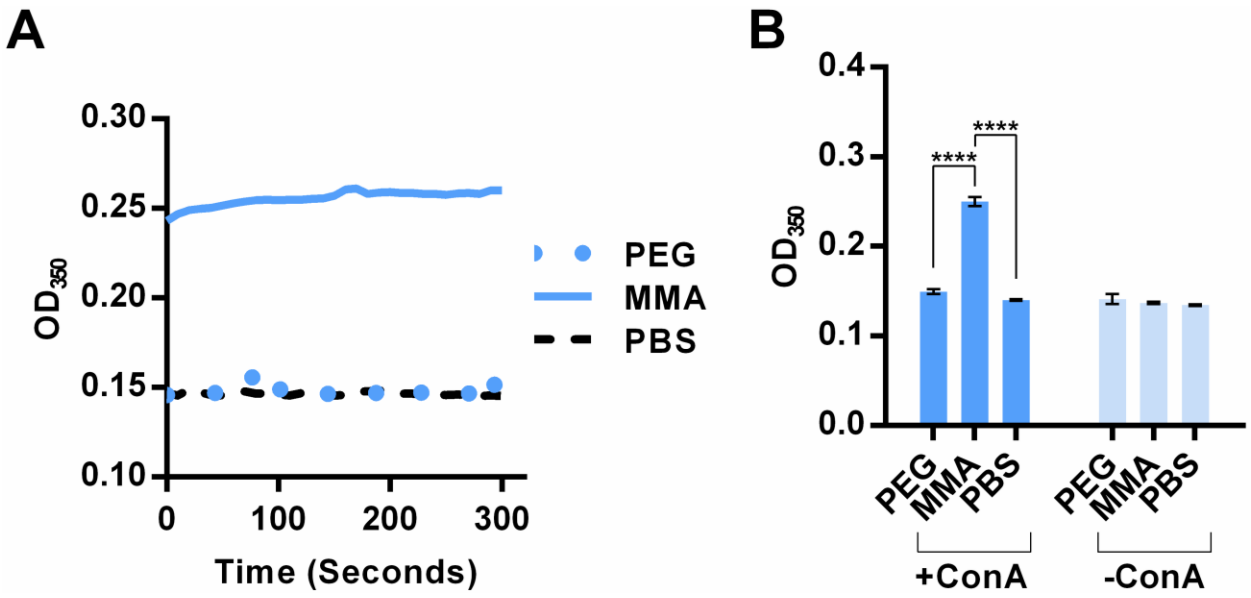

Figure 5.1 **Soluble lectins agglutinate mannosylated VIPER-Vax micelles. (A)** Mannosylated VIPER-Vax micelles (MMA) agglutinated immediately upon mixing with concanavalin A (ConA), a soluble plant lectin with multiple mannose binding sites.[29,36] A VIPER micelle variant with a polyethylene glycol (PEG) corona did not agglutinate in the presence of ConA.[22] Optical density measurements (350 nm) were taken every 10 seconds over a 5 min interval. Singlicate data shown. **(B)** Optical density was measured immediately after mixing micelles with ConA. MMA agglutinated only in the presence of ConA. Data are represented as mean ± SD, n = 3 independent measurements. Statistical significance is derived from an one-way ANOVA with post-hoc Tukey HSD test (****p-value ≤ 0.0001).

micelle agglutination via measurement of optical density.[29,36] MMA-VIPER-Vax micelles agglutinated instantly after mixing with ConA, whereas a VIPER micelle variant with a polyethyelene glycol (PEG) corona did not agglutinate (**Figure 5A**).[22] In the absence of ConA, no agglutination was observed with either micelle variant (**Figure 5B**).

Note that ConA is a soluble lectin, and agglutination of MMA-VIPER-Vax by ConA does not necessarily mean similar binding activity will be observed with cell membrane–bound C-type lectins.[21] Separate cell uptake studies are needed to confirm that MMA-VIPER-Vax micelles can be internalized by DCs through interaction with mannose-binding surface receptors (e.g., CD206).[3] Nonetheless, MMA-VIPER-Vax may still be phagocytosed by DCs if opsonized by soluble C-type lectins of the complement system.[37,38]

5.3.3 Preliminary analysis of dendritic cell maturation phenotype

Encouraged by our ConA agglutination assay results, we revisited the T cell suppression phenomenon observed in *Chapter 4*. In summary, mice immunized with Drugamer-VIPER-Vax or the previous iteration of MMA-VIPER-Vax (admixed with soluble R848) presented with markedly weaker antigen-specific T cell responses than mice immunized with melittin-free micelles. Using formulation parameters from *Chapter 4* as a starting point, we prepared mixed micelles with our new MMA-VIPER-Vax polymer. Mixed VIPER-Vax micelles were formulated at a 4:1 molar ratio of OVA epitope to melittin, and equivalent melittin-free micelles were prepared by combining epitope-conjugated and unconjugated polymers. Final micelle formulations, whether melittin-loaded (MMA-VIPER-Vax) or not (MMA-Control-Vax), contained 10 μg each of OVA MHCI epitope and OVA MHCII epitope. As we were interested in analyzing SIINFEKL cross-presentation efficiency of DCs in situ, we also prepared an antigen-free, melittin-loaded vehicle (MMA-VIPER-Vehicle) with unconjugated polymers in place of epitope-conjugated polymers. All formulations (except a PBS control) were admixed with 20 μg of soluble R848. We then immunized mice subcutaneously at the tail base and harvested draining inguinal lymph nodes (ILNs) 24 h after immunization to evaluate DC maturation levels (**Figure 5.2**).

DCs are typically identified by co-expression of CD11c and MHCII.[39–41] For flow cytometry analysis of ILN-resident DCs, we further partitioned the $CD11c^+MHCII^+$ DC population by expression of CD8, CD11b, or CD103 (**Supplemental Figure 5.1**). In general, $CD8^+$ DCs are lymphoid-resident, whereas $CD103^+$ DCs are of nonlymphoid origin and migrate to lymphatic tissue after antigen uptake; $CD11b^+$ DCs may be of either lymphoid or nonlymphoid backgrounds.[39–41] All three DC subtypes are critical for induction of adaptive immunity, and analysis of their maturation phenotypes may provide additional insight into how MMA-VIPER-Vax affects DC activation (e.g., MMA-VIPER-Vax is more bioactive in lymphoid DCs than in nonlymphoid DCs).[3,39–41] The expression level of CD86, a costimulatory receptor necessary for priming of antigen-specific T cell responses, was utilized as a maturation metric.[42,43] In mice

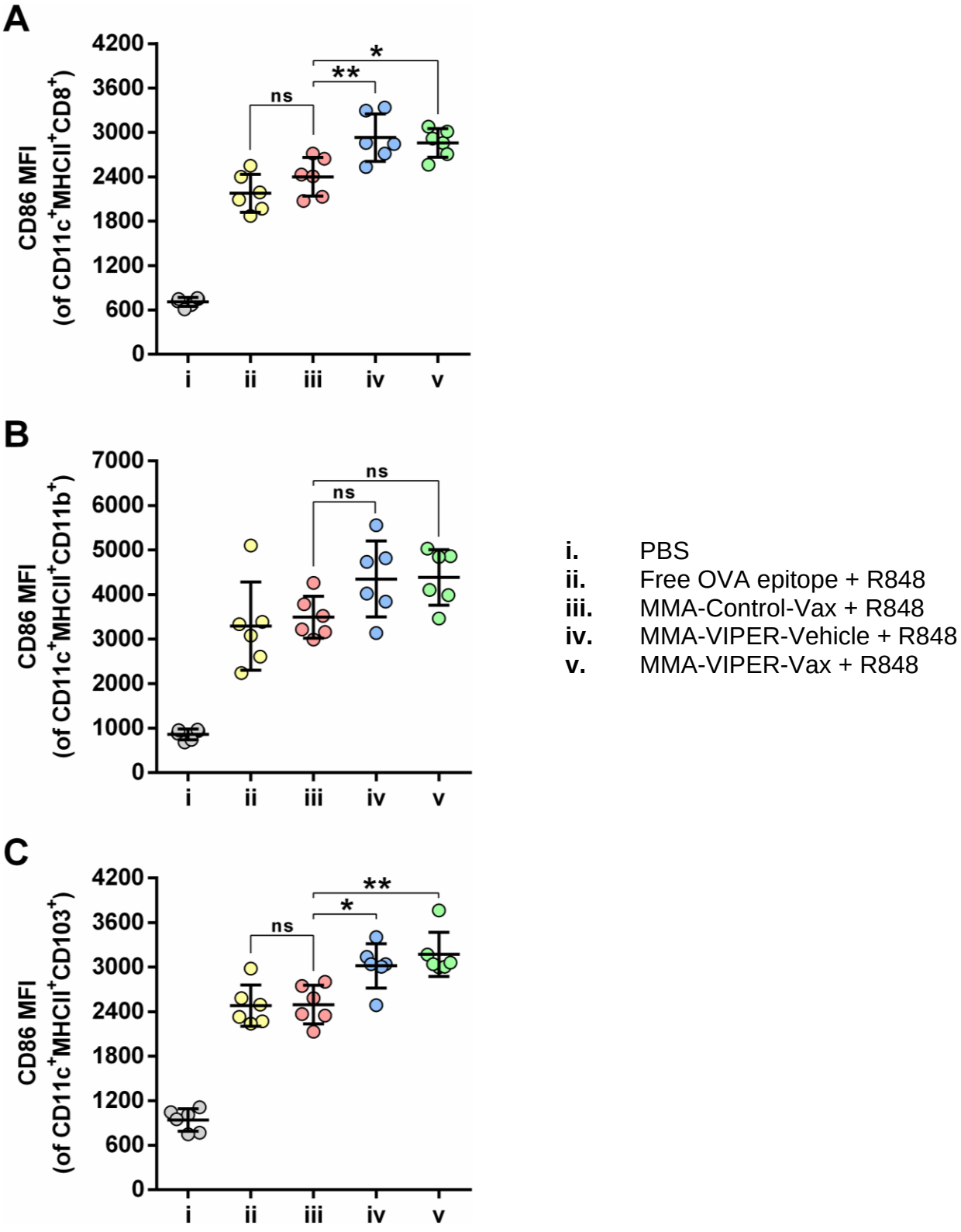

Figure 5.2 **Dendritic cell maturation is marginally increased by a low dose of micellar melittin.** Mannosylated micelles were formulated at a 4:1 molar ratio of OVA epitope to melittin, with 10 μg per OVA epitope and 20 μg of admixed soluble R848. Formulation

parameters corresponded to a ~3 nmol (~8.8 μg) melittin dose. Maturation of **(A)** $CD8^+$, **(B)** $CD11b^+$, and **(C)** $CD103^+$ DCs from inguinal lymph nodes of mice immunized at the tail base with (i) PBS, (ii) free OVA epitope + R848, (iii) MMA-Control-Vax + R848, (iv) MMA-VIPER-Vehicle + R848, or (v) MMA-VIPER-Vax + R848 was quantified by flow cytometry analysis of CD86 median fluorescence intensity (MFI) 24 h after immunization. Micellar melittin increased CD86 expression by a statistically significant (albeit marginal) amount over immunization with melittin-free formulations. Data are expressed as mean ± SD, n = 6. Statistical significance is derived from an one-way ANOVA with post-hoc Tukey HSD test (*p-value ≤ 0.05; **p-value ≤ 0.01; ns = no significance).

immunized with MMA-VIPER-Vax or MMA-VIPER-Vehicle, $CD8^+$ and $CD103^+$ DCs expressed statistically greater levels of CD86 (but only marginally so) than the same DCs from mice immunized with MMA-Control-Vax (**Figure 5.2A,C**). Similar trends were observed in $CD11b^+$ DCs, but no statistical difference in CD86 expression was achieved (**Figure 5.2B**). Furthermore, MMA-Control-Vax and free OVA epitope stimulated comparable levels of DC maturation. Unfortunately, no SIINFEKL cross-presentation (as quantified by antibody staining of SIINFEKL-bound MHCI) was detected in any treatment group (**Supplemental Figure 5.2**).[44]

5.3.4 Decoupling cytolysis from endosomolysis

At a 4:1 molar ratio of OVA epitope to melittin and a dose of 10 μg per OVA epitope, the new MMA-VIPER-Vax had no deleterious effect on DC maturation phenotype (**Figure 5.2**). Encouraged by this finding, we sought to increase the overall potency of the vaccine, as inclusion of melittin in the VIPER-Vax micelle in accordance with the aforementioned formulation parameters (corresponding to ~3 nmol of melittin, or ~8.8 μg) only marginally increased DC maturation.

In previous work with cationic VIPER-Vax polyplexes (see *Chapter 3*), we were unable to ascertain whether melittin-induced endosomal disruption could improve cross-presentation of antigen cargo through cytosolic pathways, as the formulation was cytotoxic in cultured DCs at high melittin doses.[1] Although endosomal disruption at tolerable doses was adequate for cytosolic plasmid transfer, such doses did not increase cross-presentation beyond what could be achieved

with melittin-free formulations.[1] We conjectured that the outer corona of VIPER-Vax polyplexes—partially composed of lytic cationic monomers—compounded the cytolytic bioactivity of melittin, rendering it difficult to study melittin endosomolysis and its effect on cross-presentation efficiency without also killing the DC.[1,12,45–47] The synthesis of mannosylated VIPER-Vax presented an opportunity for renewed study of melittin endosomolysis, as the lytic cationic monomers of the original VIPER-Vax were replaced with the non-charged MMA.[1]

Because MMA-VIPER-Vax formulated at a 4:1 molar ratio of antigen to melittin was not particularly potent, with no cross-presentation detected after immunization, we surmised that increasing melittin content would improve formulation potency and increase cross-presentation levels (**Figure 5.2, Supplemental Figure 5.2**). We prepared MMA-VIPER-Vax micelles at 1:1, 2:1, and 3:1 molar ratios of melittin-conjugated polymer to CSSSIINFEKL-conjugated polymer (1:1, 2:1, and 3:1 molar ratios of melittin to antigen, respectively) along with the melittin-free equivalents of these formulations (MMA-Control-Vax). To evaluate formulation potency, we conducted a DC2.4–B3Z T cell cross-presentation assay as described in *Chapter 3* and in other nanovaccine publications.[1,28,48,49] We expected MMA-VIPER-Vax to be less cytotoxic than VIPER-Vax polyplexes, so we incubated DC2.4 cells for 24 h with MMA-VIPER-Vax to maximize DC uptake, whereas a 2 h pulse was used in *Chapter 3* to minimize polyplex cytotoxicity.[1,50] It is important to note that this assay format does not offer any conclusive information about receptor-mediated uptake. DCs are phagocytic cells, and extended culture with MMA-VIPER-Vax may result in micelle uptake via receptor-independent mechanisms (e.g., macropinocytosis).[50–53]

Though we only completed one replicate of this assay, DC2.4 cells treated with MMA-VIPER-Vax cross-presented SIINFEKL more efficiently than cells treated with MMA-Control-Vax at all tested molar ratios of melittin to antigen, across a range of antigen concentrations (**Figure 5.3**). This trend was most prominent at a 1:1 molar ratio of melittin to antigen, where little decrease in viability was observed even at the highest antigen concentration tested (2 μM). In fact, higher molar ratios of melittin to antigen decreased viability without further increase in cross-

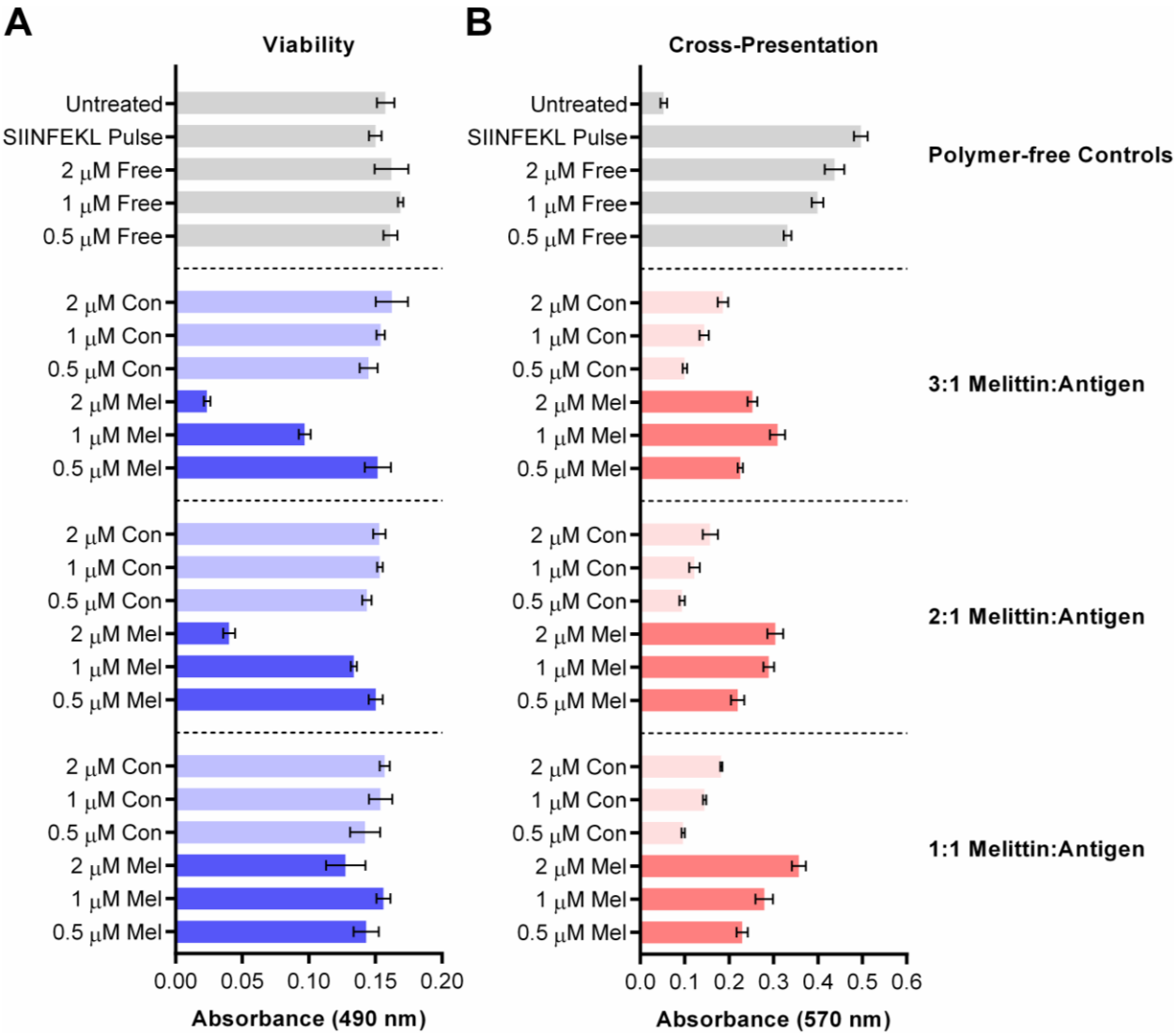

Figure 5.3 **Mannosylated VIPER-Vax enhances cross-presentation in vitro. (A)** Viability and **(B)** cross-presentation efficiency of DC2.4 cells pulsed for 24 h with the indicated vaccine formulations. Concentration values on the y-axis denote antigen dose. Molar ratios of melittin to CSSSIINFEKL are listed on the right side of the figure. DC2.4 cells pulsed for 4 h with 30 μM SIINFEKL (SIINFEKL Pulse) were included in this assay as a positive control. Mel: MMA-VIPER-Vax, Con: MMA-Control-Vax, Free: free CSSSIINFEKL. Data are represented as mean ± SD, n = 3 technical replicates.

presentation efficiency. Interestingly, free CSSSIINFEKL outperformed micelle formulations at equivalent antigen doses. Proteolytic processing of CSSSIINFEKL into the MHCI-bound SIINFEKL epitope may occur immediately after DC uptake in both cytosolic and endosomal compartments.[2] In contrast, micelles must disassemble and antigen-polymer disulfide linkages

must be reduced before antigen processing and MHCI loading can proceed.[54] Therefore, in an artificial culture environment where DCs are in direct contact with antigen, free CSSSIINFEKL may be presented more quickly than micelle-encapsulated CSSSIINFEKL. However, soluble peptide antigens are unstable in serum, and thus encapsulation of peptide antigens within a micelle carrier may be more beneficial in vivo, where peptide antigens must be transported to DCs before they can be presented.[55]

5.3.5 Suppression of dendritic cell maturation

Motivated by results from the latest DC2.4–B3Z T cell cross-presentation assay, we resumed in vivo investigation of vaccine efficacy and reformulated mannosylated VIPER-Vax micelles at a 1:1 molar ratio of OVA epitope to melittin. Following a review of similar nanovaccine work reported by Shae et al.[43], we increased antigen loading in mannosylated VIPER-Vax formulations to 25 μg per OVA epitope. To accommodate the target 1:1 molar ratio of OVA epitope to melittin, we concurrently loaded ~32 nmol (~94.4 μg) of melittin into our micelle formulation. Incidentally, this melittin dose closely matched that reported in a study by Yu et al.[20], where lipid nanoparticles were loaded with 35 nmol of melittin for lymph node delivery.

Since a 35 nmol dose of nanoparticulate melittin was found by Yu et al.[20] to stimulate DC maturation in lymph nodes after subcutaneous administration, we also investigated whether mannosylated VIPER-Vax at a ~32 nmol melittin dose could act as a self-adjuvant. Due to the systemic toxicity associated with administration of soluble R848, an “all-in-one” VIPER-Vax micelle formulation with self-adjuvant properties may be more clinically applicable.[56–59] As in our preliminary study of post-immunization DC maturation phenotype, we prepared MMA-Control-Vax, MMA-VIPER-Vax, and MMA-Vehicle-Vax formulations admixed with soluble R848. We also formulated MMA-Control-Vax and MMA-VIPER-Vax without admixed R848 to assess the self-adjuvant bioactivity of these mannosylated micelles. Mice were then immunized subcutaneously at the tail base. A flow cytometry analysis of DCs in the ILNs 24 h after immunization returned

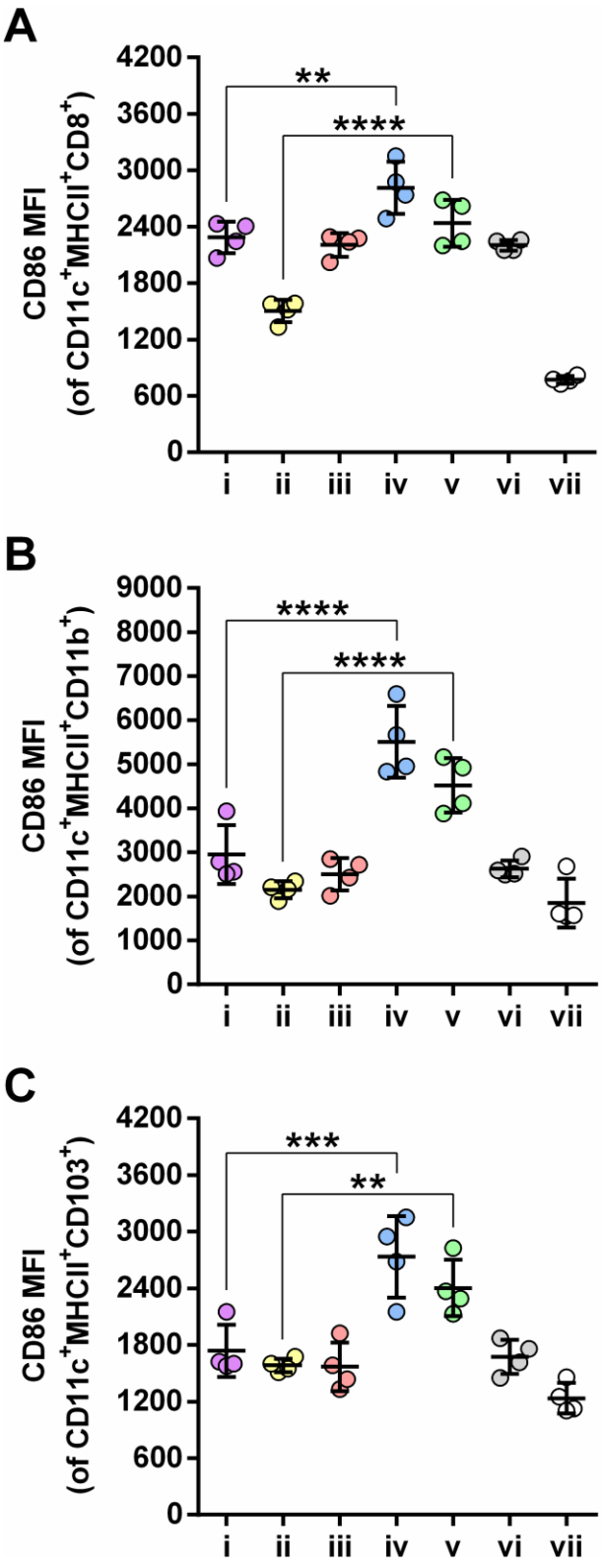

i. MMA-VIPER-Vax + R848
ii. MMA-VIPER-Vax
iii. MMA-VIPER-Vehicle + R848
iv. MMA-Control-Vax + R848
v. MMA-Control-Vax
vi. Free OVA epitope + R848
vii. PBS

Figure 5.4 **A high dose of micellar melittin abrogates dendritic cell maturation.** Mannosylated micelles were formulated at a 1:1 molar ratio of OVA epitope to melittin with 25 μg per OVA epitope. Some formulations were admixed with 20 μg of soluble R848. Formulation

parameters corresponded to a ~32 nmol (~94.4 μg) melittin dose. Maturation of **(A)** $CD8^+$, **(B)** $CD11b^+$, and **(C)** $CD103^+$ dendritic cells (DCs) from inguinal lymph nodes of mice immunized at the tail base with (i) MMA-VIPER-Vax + R848, (ii) MMA-VIPER-Vax, (iii) MMA-VIPER-Vehicle + R848, (iv) MMA-Control-Vax + R848, (v) MMA-Control-Vax, (vi) free OVA epitope + R848, or (vii) PBS was quantified by flow cytometry analysis of CD86 median fluorescence intensity (MFI) 24 h after immunization. This high dose of micellar melittin suppressed DC maturation. Data are expressed as mean ± SD, $n = 4$. Statistical significance is derived from an one-way ANOVA with post-hoc Tukey HSD test (**p-value ≤ 0.01; ***p-value ≤ 0.001; ****p-value ≤ 0.0001).

striking results. Immunization with micellar melittin abrogated maturation in $CD8^+$, $CD11b^+$, and $CD103^+$ DC subsets (**Figure 5.4**). It was also apparent that MMA-Control-Vax (not MMA-VIPER-Vax) exhibited self-adjuvant activity, as DC maturation levels generated by MMA-Control-Vax were statistically greater than those generated by MMA-VIPER-Vax, even with R848 admixed. Loading melittin into the micellar vaccine may have actually counteracted this self-adjuvant effect. Once again, no cross-presentation was detected (**Supplemental Figure 5.3**).

In a final study of DC maturation phenotype, we formulated micelles without admixed R848 to eliminate any confounding R848 bioactivity. We subcutaneously immunized mice at the tail base with MMA-VIPER-Vax micelles containing 25 μg per OVA epitope at a 2:1, 4:1, or 8:1 molar ratio of OVA epitope to melittin. MMA-Control-Vax and free OVA epitope were included as controls. As expected, DCs from mice immunized with MMA-VIPER-Vax showed reduced CD86 expression 24 h after immunization (**Figure 5.5**). Reduced CD86 expression was also observed at a 48 h end point, suggesting persistent attenuation of DC maturation by MMA-VIPER-Vax. MMA-Control-Vax elicited statistically higher CD86 expression in ILN-resident DCs than all other vaccine formulations tested, verifying the self-adjuvant activity observed in our prior study (**Figure 5.4**).[21] No analysis of cross-presentation was conducted in this final study, as no vehicle control (MMA-VIPER-Vehicle) was included for gating of H-$2K^b$/$SIINFEKL^+$ DCs (**Supplemental Figure 5.1**).

Overall, the results from this series of experiments corroborated our findings from *Chapter 4*, where we reported diminished cytotoxic T cell priming after immunization with MMA-

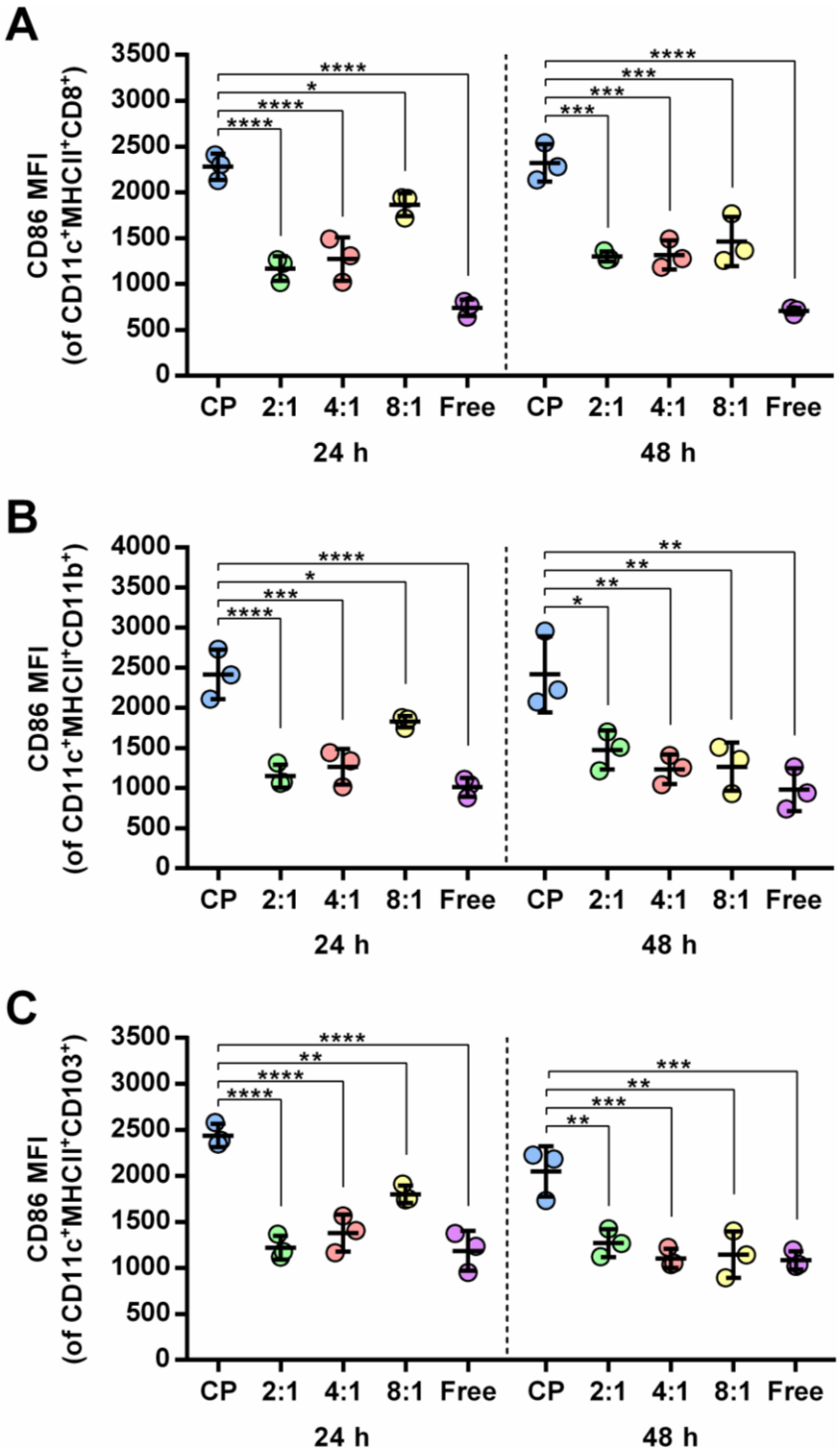

CP MMA-Control-Vax
2:1, 4:1, 8:1* MMA-VIPER-Vax
Free Free OVA epitope

*Molar ratio of epitope:melittin

Figure 5.5 **Melittin-free mannose micelles exhibit self-adjuvant activity.** MMA-VIPER-Vax micelles were formulated at the indicated molar ratios of OVA epitope to melittin (2:1,

4:1, and 8:1) with 25 μg per OVA epitope. MMA-Control-Vax (CP) and free OVA epitope (Free) were used as positive and negative controls, respectively. Maturation of **(A)** $CD8^+$, **(B)** $CD11b^+$, and **(C)** $CD103^+$ DCs from inguinal lymph nodes of mice immunized at the tail base was quantified by flow cytometry analysis of CD86 median fluorescence intensity (MFI) 24 h and 48 h after immunization. Data are expressed as mean ± SD, $n = 3$. Statistical significance is derived from an one-way ANOVA with post-hoc Tukey HSD test (*p-value ≤ 0.05; **p-value ≤ 0.01; ***p-value ≤ 0.001; ****p-value ≤ 0.0001).

VIPER-Vax. The opposite effect was observed with MMA-Control-Vax, which primed robust T cell responses. Potentiation of both DC maturation and T cell priming by MMA-Control-Vax—as reported herein and in *Chapter 4*, respectively—aligns with research demonstrating the inflammatory effects of mannose.[21] That mannose and melittin act deleteriously on maturation phenotype when co-delivered to DCs may impede further application of MMA-VIPER-Vax, especially if multiantigen cargo of high molar content is to be loaded into micelles with equimolar quantities of melittin.[25,60] In addition, the lack of detectable cross-presentation—even in DCs harvested from mice immunized with the more potent MMA-Control-Vax—indicates that intracellular unloading and processing of antigen cargo may be inefficient.[2] Cross-presentation studies focusing on DC maturation kinetics may be required to determine whether MMA-Control-Vax induces cross-presentation in situ, as cross-presentation efficiency can vary temporally, fluctuating with the maturation stage of the DC.[61]

5.4 Conclusions

Although MMA-VIPER-Vax bound soluble lectins and enhanced cross-presentation in vitro, its two primary bioactive components—a multivalent mannose corona and endosomolytic melittin—acted in concert to attenuate DC maturation. Furthermore, no DC cross-presentation was observed in situ after immunization of mice with either MMA-VIPER-Vax or its melittin-free equivalent, MMA-Control-Vax. Importantly, MMA-Control-Vax potentiated DC maturation without co-administered soluble adjuvant, suggesting that mannosylated micelle alone may serve as a potent vaccine nanocarrier for multiepitope delivery.

5.5 Acknowledgements

This work was supported by a grant from the Washington Research Foundation. We thank Prof. Kim Woodrow (University of Washington) for her kind gift of DC2.4 cells. We also thank Prof. Nilabh Shastri (formerly faculty at Johns Hopkins University, and before that, the University of California, Berkeley) for his kind gift of B3Z cells. May you rest in peace, Prof. Shastri. We are truly grateful for your contributions to the field of immunology.

5.6 Supporting Information

Dendritic Cell Subsets

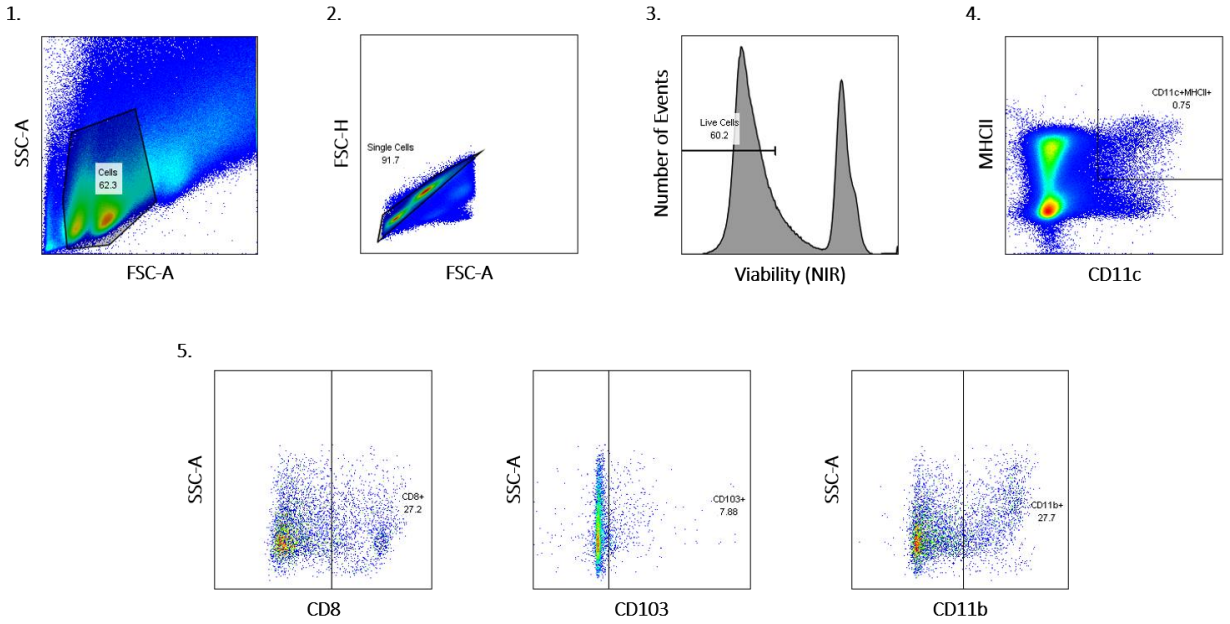

SIINFEKL Cross-Presentation

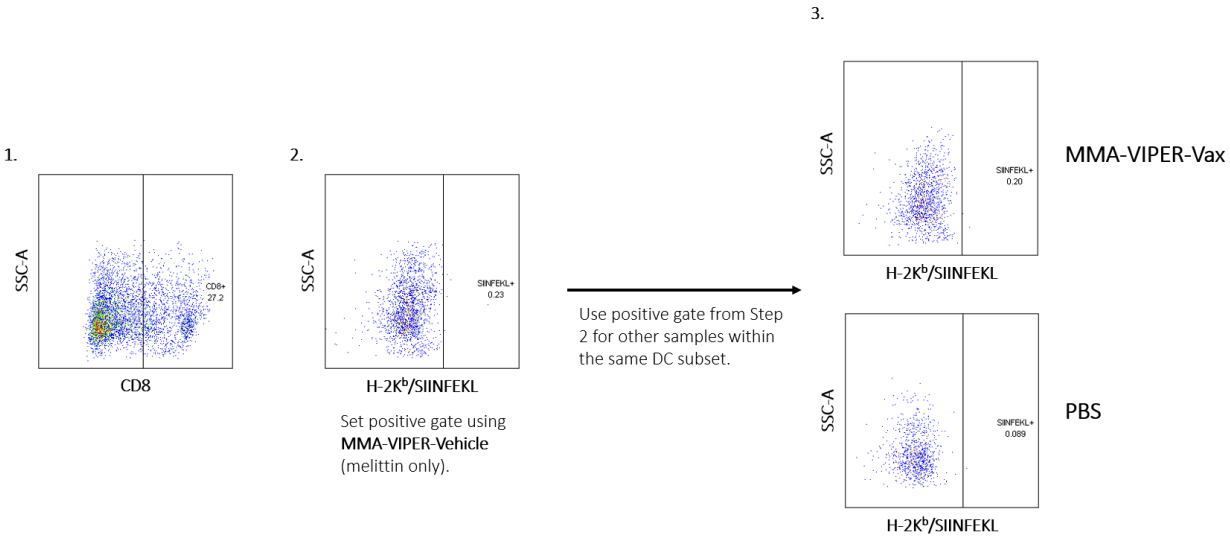

Supplemental Figure 5.1 **Flow cytometry gating strategies for analysis of dendritic cell populations.**

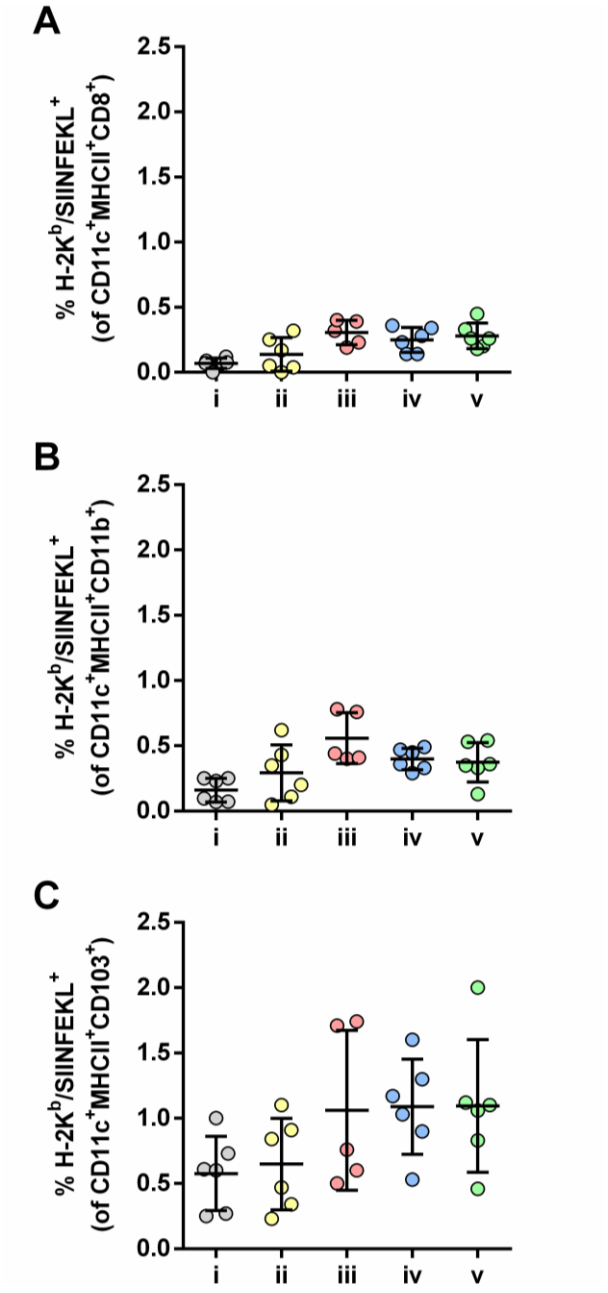

Supplemental Figure 5.2 **A low dose of micellar melittin does not induce cross-presentation in situ.** Mannosylated micelles were formulated at a 4:1 molar ratio of OVA epitope to melittin, with 10 μg per OVA epitope and 20 μg of admixed soluble R848. Formulation parameters corresponded to a ~3 nmol (~8.8 μg) melittin dose. SIINFEKL cross-presentation in **(A)** $CD8^+$, **(B)** $CD11b^+$, and **(C)** $CD103^+$ DCs from inguinal lymph nodes of mice immunized at the tail base with (i) PBS, (ii) free OVA epitope + R848, (iii) MMA-Control-Vax + R848, (iv) MMA-VIPER-Vehicle + R848, or (v) MMA-VIPER-Vax + R848 was quantified by flow cytometry analysis of cells expressing SIINFEKL-bound H-$2K^b$ (MHCI) 24 h after immunization. Data are expressed as mean ± SD, $n = 6$.

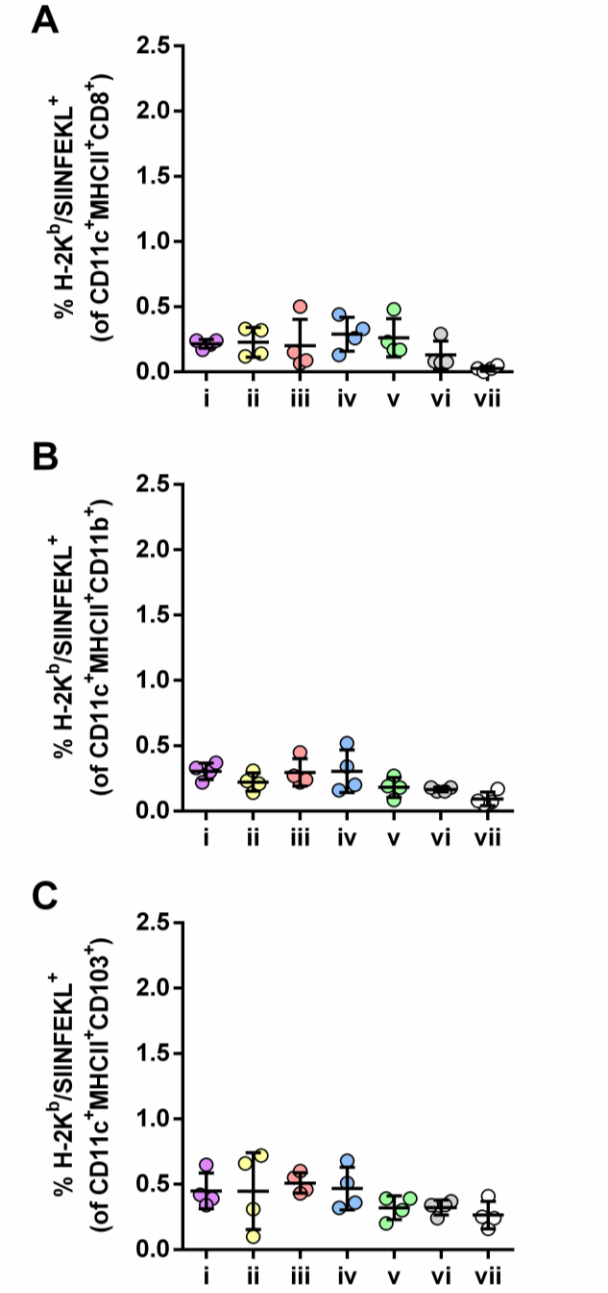

Supplemental Figure 5.3 **A high dose of micellar melittin does not induce cross-presentation in situ.** Mannosylated micelles were formulated at a 1:1 molar ratio of OVA epitope to melittin with 25 μg per OVA epitope. Some formulations were admixed with 20 μg of soluble R848. Formulation parameters corresponded to a ~32 nmol (~94.4 μg) melittin dose. SIINFEKL cross-presentation in **(A)** $CD8^+$, **(B)** $CD11b^+$, and **(C)** $CD103^+$ DCs from inguinal lymph nodes of mice immunized at the tail base with (i) MMA-VIPER-Vax + R848, (ii) MMA-VIPER-Vax, (iii) MMA-VIPER-Vehicle + R848, (iv) MMA-Control-Vax + R848, (v) MMA-Control-Vax, (vi) free OVA epitope + R848, or (vii) PBS was quantified by flow cytometry analysis of cells expressing SIINFEKL-bound H-$2K^b$ (MHCI) 24 h after immunization. Data are expressed as mean ± SD, $n = 4$.

Supplemental Table 5.1 **Dendritic cell staining panel for flow cytometry analysis.**

Marker	Vendor	Clone (If Antibody)	Fluorophore
Viability	BioLegend	N/A	Zombie NIR™
CD16/CD32	BioLegend	93	N/A
CD8	BioLegend	53-6.7	Alexa Fluor 488
CD11b	BioLegend	M1/70	Brilliant Violet 421™
CD103	Invitrogen	B-Ly7	Super Bright 600
CD11c	BioLegend	N418	APC
MHCII (I-A/I-E)	BioLegend	M5/114.15.2	PerCP-Cy5.5
CD86	BioLegend	GL-1	Brilliant Violet 510™
H-2K^{b} bound to SIINFEKL	BioLegend	25-D1.16	PE

5.7 References

(1) Peeler, D. J.; Yen, A.; Luera, N.; Stayton, P. S.; Pun, S. H. Lytic Polyplex Vaccines Enhance Antigen-Specific Cytotoxic T Cell Response through Induction of Local Cell Death. *Adv. Ther.* **2021**, 2100005.

(2) Sánchez-Paulete, A. R.; Teijeira, A.; Cueto, F. J.; Garasa, S.; Pérez-Gracia, J. L.; Sánchez-Arráez, A.; Sancho, D.; Melero, I. Antigen Cross-Presentation and T-Cell Cross-Priming in Cancer Immunology and Immunotherapy. *Ann. Oncol.* **2017**, *28* (suppl_12), xii44–xii55.

(3) Wilson, D. S.; Hirosue, S.; Raczy, M. M.; Bonilla-Ramirez, L.; Jeanbart, L.; Wang, R.; Kwissa, M.; Franetich, J.-F.; Broggi, M. A. S.; Diaceri, G.; et al. Antigens Reversibly Conjugated to a Polymeric Glyco-Adjuvant Induce Protective Humoral and Cellular Immunity. *Nat. Mater.* **2019**, *18* (2), 175–185.

(4) Keler, T.; Ramakrishna, V.; Fanger, M. W. Mannose Receptor-Targeted Vaccines. *Expert Opin. Biol. Ther.* **2004**, *4* (12), 1953–1962.

(5) Cheng, Y.; Yumul, R. C.; Pun, S. H. Virus-Inspired Polymer for Efficient In Vitro and In Vivo Gene Delivery. *Angew. Chemie Int. Ed.* **2016**, *55* (39), 12013–12017.

(6) Yen, A.; Cheng, Y.; Sylvestre, M.; Gustafson, H. H.; Puri, S.; Pun, S. H. Serum Nuclease Susceptibility of mRNA Cargo in Condensed Polyplexes. *Mol. Pharm.* **2018**, *15* (6), 2268–2276.

(7) Pack, D. W.; Hoffman, A. S.; Pun, S.; Stayton, P. S. Design and Development of Polymers for Gene Delivery. *Nat. Rev. Drug Discov.* **2005**, *4* (7), 581–593.

(8) McKinlay, C. J.; Vargas, J. R.; Blake, T. R.; Hardy, J. W.; Kanada, M.; Contag, C. H.; Wender, P. A.; Waymouth, R. M. Charge-Altering Releasable Transporters (CARTs) for the Delivery and Release of mRNA in Living Animals. *Proc. Natl. Acad. Sci.* **2017**, *114* (4), E448–E456.

(9) Rui, Y.; Wilson, D. R.; Choi, J.; Varanasi, M.; Sanders, K.; Karlsson, J.; Lim, M.; Green, J. J. Carboxylated Branched Poly(β-Amino Ester) Nanoparticles Enable Robust Cytosolic Protein Delivery and CRISPR-Cas9 Gene Editing. *Sci. Adv.* **2019**, *5* (12), eaay3255.

(10) Gong, N.; Zhang, Y.; Teng, X.; Wang, Y.; Huo, S.; Qing, G.; Ni, Q.; Li, X.; Wang, J.; Ye, X.; et al. Proton-Driven Transformable Nanovaccine for Cancer Immunotherapy. *Nat. Nanotechnol.* **2020**, *15* (12), 1053–1064.

(11) Wilson, J. T.; Keller, S.; Manganiello, M. J.; Cheng, C.; Lee, C. C.; Opara, C.; Convertine, A.; Stayton, P. S. pH-Responsive Nanoparticle Vaccines for Dual-Delivery of Antigens and Immunostimulatory Oligonucleotides. *ACS Nano* **2013**, *7* (5), 3912–3925.

(12) Peeler, D. J.; Thai, S. N.; Cheng, Y.; Horner, P. J.; Sellers, D. L.; Pun, S. H. pH-Sensitive Polymer Micelles Provide Selective and Potentiated Lytic Capacity to Venom Peptides for Effective Intracellular Delivery. *Biomaterials* **2019**, *192*, 235–244.

(13) Canton, J.; Blees, H.; Henry, C. M.; Buck, M. D.; Schulz, O.; Rogers, N. C.; Childs, E.; Zelenay, S.; Rhys, H.; Domart, M.-C.; et al. The Receptor DNGR-1 Signals for Phagosomal Rupture to Promote Cross-Presentation of Dead-Cell-Associated Antigens. *Nat. Immunol.* **2021**, *22* (2), 140–153.

(14) Nagata, S. Apoptosis and Clearance of Apoptotic Cells. *Annu. Rev. Immunol.* **2018**, *36*, 489–517.

(15) Srinivasarao, M.; Low, P. S. Ligand-Targeted Drug Delivery. *Chem. Rev.* **2017**, *117* (19), 12133–12164.

(16) Johnston, M. C.; Scott, C. J. Antibody Conjugated Nanoparticles as a Novel Form of Antibody Drug Conjugate Chemotherapy. *Drug Discov. Today Technol.* **2018**, *30*, 63–69.

(17) De Coen, R.; Vanparijs, N.; Risseeuw, M. D. P.; Lybaert, L.; Louage, B.; De Koker, S.; Kumar, V.; Grooten, J.; Taylor, L.; Ayres, N.; et al. pH-Degradable Mannosylated Nanogels for Dendritic Cell Targeting. *Biomacromolecules* **2016**, *17* (7), 2479–2488.

(18) Conniot, J.; Scomparin, A.; Peres, C.; Yeini, E.; Pozzi, S.; Matos, A. I.; Kleiner, R.; Moura, L. I. F.; Zupančič, E.; Viana, A. S.; et al. Immunization with Mannosylated Nanovaccines and Inhibition of the Immune-Suppressing Microenvironment Sensitizes Melanoma to Immune Checkpoint Modulators. *Nat. Nanotechnol.* **2019**, *14* (9), 891–901.
(19) Yang, R.; Xu, J.; Xu, L.; Sun, X.; Chen, Q.; Zhao, Y.; Peng, R.; Liu, Z. Cancer Cell Membrane-Coated Adjuvant Nanoparticles with Mannose Modification for Effective Anticancer Vaccination. *ACS Nano* **2018**, *12* (6), 5121–5129.
(20) Yu, X.; Dai, Y.; Zhao, Y.; Qi, S.; Liu, L.; Lu, L.; Luo, Q.; Zhang, Z. Melittin-Lipid Nanoparticles Target to Lymph Nodes and Elicit a Systemic Anti-Tumor Immune Response. *Nat. Commun.* **2020**, *11*, 1110.
(21) Kingeter, L. M.; Lin, X. C-Type Lectin Receptor-Induced NF-κB Activation in Innate Immune and Inflammatory Responses. *Cell. Mol. Immunol.* **2012**, *9* (2), 105–112.
(22) Sylvestre, M.; Lv, S.; Yang, L. F.; Luera, N.; Peeler, D. J.; Chen, B.-M.; Roffler, S. R.; Pun, S. H. Replacement of L-Amino Acid Peptides with D-Amino Acid Peptides Mitigates Anti-PEG Antibody Generation against Polymer-Peptide Conjugates in Mice. *J. Control. Release* **2021**, *331*, 142–153.
(23) Taniguchi, K.; Karin, M. NF-κB, Inflammation, Immunity and Cancer: Coming of Age. *Nat. Rev. Immunol.* **2018**, *18* (5), 309–324.
(24) Kasozi, K. I.; Niedbała, G.; Alqarni, M.; Zirintunda, G.; Ssempijja, F.; Musinguzi, S. P.; Usman, I. M.; Matama, K.; Hetta, H. F.; Mbiydzenyuy, N. E.; et al. Bee Venom—A Potential Complementary Medicine Candidate for SARS-CoV-2 Infections. *Front. Public Heal.* **2020**, *8*.
(25) Lee, G.; Bae, H. Anti-Inflammatory Applications of Melittin, a Major Component of Bee Venom: Detailed Mechanism of Action and Adverse Effects. *Molecules* **2016**, *21* (5), 616.
(26) Hayden, M. S.; West, A. P.; Ghosh, S. NF-κB and the Immune Response. *Oncogene* **2006**, *25* (51), 6758–6780.
(27) Chen, J.; Son, H.-N.; Hill, J. J.; Srinivasan, S.; Su, F.-Y.; Stayton, P. S.; Convertine, A. J.; Ratner, D. M. Nanostructured Glycopolymer Augmented Liposomes to Elucidate Carbohydrate-Mediated Targeting. *Nanomedicine* **2016**, *12* (7), 2031–2041.
(28) Kuai, R.; Ochyl, L. J.; Bahjat, K. S.; Schwendeman, A.; Moon, J. J. Designer Vaccine Nanodiscs for Personalized Cancer Immunotherapy. *Nat. Mater.* **2017**, *16* (4), 489–496.
(29) Cheng, C. Development of Multifunctional Block Copolymers for the Delivery of Nucleic Acid Vaccines, University of Washington, 2013.
(30) Mac-Daniel, L.; Buckwalter, M. R.; Gueirard, P.; Ménard, R. Myeloid Cell Isolation from Mouse Skin and Draining Lymph Node Following Intradermal Immunization with Live Attenuated Plasmodium Sporozoites. *J. Vis. Exp.* **2016**, No. 111, 53796.
(31) Srinivasan, S.; Roy, D.; Chavas, T. E. J.; Vlaskin, V.; Ho, D.-K.; Pottenger, A.; LeGuyader, C. L. M.; Maktabi, M.; Strauch, P.; Jackson, C.; et al. Liver-Targeted Polymeric Prodrugs of 8-Aminoquinolines for Malaria Radical Cure. *J. Control. Release* **2021**, *331*, 213–227.
(32) Saenz, R.; Souza, C. da S.; Huang, C.-T.; Larsson, M.; Esener, S.; Messmer, D. HMGB1-Derived Peptide Acts as Adjuvant Inducing Immune Responses to Peptide and Protein Antigen. *Vaccine* **2010**, *28* (47), 7556–7562.
(33) Press, A. T.; Ramoji, A.; vd Lühe, M.; Rinkenauer, A. C.; Hoff, J.; Butans, M.; Rössel, C.; Pietsch, C.; Neugebauer, U.; Schacher, F. H.; et al. Cargo–Carrier Interactions Significantly Contribute to Micellar Conformation and Biodistribution. *NPG Asia Mater.* **2017**, *9*, e444.
(34) Keller, S.; Wilson, J. T.; Patilea, G. I.; Kern, H. B.; Convertine, A. J.; Stayton, P. S. Neutral Polymer Micelle Carriers with pH-Responsive, Endosome-Releasing Activity Modulate Antigen Trafficking to Enhance CD8$^+$ T Cell Responses. *J. Control. Release* **2014**, *191*, 24–33.
(35) Irvine, D. J.; Hanson, M. C.; Rakhra, K.; Tokatlian, T. Synthetic Nanoparticles for Vaccines and Immunotherapy. *Chem. Rev.* **2015**, *115* (19), 11109–11146.

(36) Edelman, G. M.; Wang, J. L. Binding and Functional Properties of Concanavalin A and Its Derivatives. III. Interactions with Indoleacetic Acid and Other Hydrophobic Ligands. *J. Biol. Chem.* **1978**, *253* (9), 3016–3022.
(37) Nauta, A. J.; Castellano, G.; Xu, W.; Woltman, A. M.; Borrias, M. C.; Daha, M. R.; van Kooten, C.; Roos, A. Opsonization with C1q and Mannose-Binding Lectin Targets Apoptotic Cells to Dendritic Cells. *J. Immunol.* **2004**, *173* (5), 3044–3050.
(38) Kerrigan, A. M.; Brown, G. D. C-Type Lectins and Phagocytosis. *Immunobiology* **2009**, *214* (7), 562–575.
(39) Mildner, A.; Jung, S. Development and Function of Dendritic Cell Subsets. *Immunity* **2014**, *40* (5), 642–656.
(40) Merad, M.; Sathe, P.; Helft, J.; Miller, J.; Mortha, A. The Dendritic Cell Lineage: Ontogeny and Function of Dendritic Cells and Their Subsets in the Steady State and the Inflamed Setting. *Annu. Rev. Immunol.* **2013**, *31* (1), 563–604.
(41) Nierkens, S.; Tel, J.; Janssen, E.; Adema, G. J. Antigen Cross-Presentation by Dendritic Cell Subsets: One General or All Sergeants? *Trends Immunol.* **2013**, *34* (8), 361–370.
(42) Baravalle, G.; Park, H.; McSweeney, M.; Ohmura-Hoshino, M.; Matsuki, Y.; Ishido, S.; Shin, J.-S. Ubiquitination of CD86 Is a Key Mechanism in Regulating Antigen Presentation by Dendritic Cells. *J. Immunol.* **2011**, *187* (6), 2966–2973.
(43) Shae, D.; Baljon, J. J.; Wehbe, M.; Christov, P. P.; Becker, K. W.; Kumar, A.; Suryadevara, N.; Carson, C. S.; Palmer, C. R.; Knight, F. C.; et al. Co-Delivery of Peptide Neoantigens and Stimulator of Interferon Genes Agonists Enhances Response to Cancer Vaccines. *ACS Nano* **2020**, *14* (8), 9904–9916.
(44) Porgador, A.; Yewdell, J. W.; Deng, Y.; Bennink, J. R.; Germain, R. N. Localization, Quantitation, and In Situ Detection of Specific Peptide–MHC Class I Complexes Using a Monoclonal Antibody. *Immunity* **1997**, *6* (6), 715–726.
(45) van de Wetering, P.; Cherng, J.-Y.; Talsma, H.; Hennink, W. E. Relation between Transfection Efficiency and Cytotoxicity of Poly(2-(Dimethylamino)Ethyl Methacrylate)/Plasmid Complexes. *J. Control. Release* **1997**, *49* (1), 59–69.
(46) Richards, S.-J.; Jones, A.; Tomás, R. M. F.; Gibson, M. I. Photochemical "In-Air" Combinatorial Discovery of Antimicrobial Co-Polymers. *Chem. - A Eur. J.* **2018**, *24* (52), 13758–13761.
(47) Huang, C.; Jin, H.; Qian, Y.; Qi, S.; Luo, H.; Luo, Q.; Zhang, Z. Hybrid Melittin Cytolytic Peptide-Driven Ultrasmall Lipid Nanoparticles Block Melanoma Growth In Vivo. *ACS Nano* **2013**, *7* (7), 5791–5800.
(48) Karttunen, J.; Sanderson, S.; Shastri, N. Detection of Rare Antigen-Presenting Cells by the LacZ T-Cell Activation Assay Suggests an Expression Cloning Strategy for T-Cell Antigens. *Proc. Natl. Acad. Sci. U. S. A.* **1992**, *89* (13), 6020–6024.
(49) Qiu, F.; Becker, K. W.; Knight, F. C.; Baljon, J. J.; Sevimli, S.; Shae, D.; Gilchuk, P.; Joyce, S.; Wilson, J. T. Poly(Propylacrylic Acid)-Peptide Nanoplexes as a Platform for Enhancing the Immunogenicity of Neoantigen Cancer Vaccines. *Biomaterials* **2018**, *182*, 82–91.
(50) Nagl, M.; Kacani, L.; Müllauer, B.; Lemberger, E.-M.; Stoiber, H.; Sprinzl, G. M.; Schennach, H.; Dierich, M. P. Phagocytosis and Killing of Bacteria by Professional Phagocytes and Dendritic Cells. *Clin. Vaccine Immunol.* **2002**, *9* (6), 1165–1168.
(51) Jia, J.; Zhang, Y.; Xin, Y.; Jiang, C.; Yan, B.; Zhai, S. Interactions Between Nanoparticles and Dendritic Cells: From the Perspective of Cancer Immunotherapy. *Front. Oncol.* **2018**, *8*.
(52) Luo, M.; Wang, H.; Wang, Z.; Cai, H.; Lu, Z.; Li, Y.; Du, M.; Huang, G.; Wang, C.; Chen, X.; et al. A STING-Activating Nanovaccine for Cancer Immunotherapy. *Nat. Nanotechnol.* **2017**, *12* (7), 648–654.
(53) Foroozandeh, P.; Aziz, A. A. Insight into Cellular Uptake and Intracellular Trafficking of Nanoparticles. *Nanoscale Res. Lett.* **2018**, *13* (1), 339.

(54) Butora, G.; Qi, N.; Fu, W.; Nguyen, T.; Huang, H.-C.; Davies, I. W. Cyclic-Disulfide-Based Prodrugs for Cytosol-Specific Drug Delivery. *Angew. Chemie Int. Ed.* **2014**, *53* (51), 14046–14050.
(55) Moynihan, K. D.; Holden, R. L.; Mehta, N. K.; Wang, C.; Karver, M. R.; Dinter, J.; Liang, S.; Abraham, W.; Melo, M. B.; Zhang, A. Q.; et al. Enhancement of Peptide Vaccine Immunogenicity by Increasing Lymphatic Drainage and Boosting Serum Stability. *Cancer Immunol. Res.* **2018**, *6* (9), 1025–1038.
(56) Nuhn, L.; Vanparijs, N.; De Beuckelaer, A.; Lybaert, L.; Verstraete, G.; Deswarte, K.; Lienenklaus, S.; Shukla, N. M.; Salyer, A. C. D.; Lambrecht, B. N.; et al. pH-Degradable Imidazoquinoline-Ligated Nanogels for Lymph Node-Focused Immune Activation. *Proc. Natl. Acad. Sci.* **2016**, *113* (29), 8098–8103.
(57) Scott, E. A.; Stano, A.; Gillard, M.; Maio-Liu, A. C.; Swartz, M. A.; Hubbell, J. A. Dendritic Cell Activation and T Cell Priming with Adjuvant- and Antigen-Loaded Oxidation-Sensitive Polymersomes. *Biomaterials* **2012**, *33* (26), 6211–6219.
(58) Pockros, P. J.; Guyader, D.; Patton, H.; Tong, M. J.; Wright, T.; McHutchison, J. G.; Meng, T.-C. Oral Resiquimod in Chronic HCV Infection: Safety and Efficacy in 2 Placebo-Controlled, Double-Blind Phase IIa Studies. *J. Hepatol.* **2007**, *47* (2), 174–182.
(59) Gunzer, M.; Riemann, H.; Basoglu, Y.; Hillmer, A.; Weishaupt, C.; Balkow, S.; Benninghoff, B.; Ernst, B.; Steinert, M.; Scholzen, T.; et al. Systemic Administration of a TLR7 Ligand Leads to Transient Immune Incompetence Due to Peripheral-Blood Leukocyte Depletion. *Blood* **2005**, *106* (7), 2424–2432.
(60) Disis, M. L.; Gad, E.; Herendeen, D. R.; Lai, V. P.-; Park, K. H.; Cecil, D. L.; O'Meara, M. M.; Treuting, P. M.; Lubet, R. A. A Multiantigen Vaccine Targeting Neu, IGFBP-2, and IGF-IR Prevents Tumor Progression in Mice with Preinvasive Breast Disease. *Cancer Prev. Res.* **2013**, *6* (12), 1273–1282.
(61) Alloatti, A.; Kotsias, F.; Magalhaes, J. G.; Amigorena, S. Dendritic Cell Maturation and Cross-Presentation: Timing Matters! *Immunol. Rev.* **2016**, *272* (1), 97–108.

CHAPTER 6

Future Directions

Synopsis. Here, we briefly propose future work on vaccines derived from the "Virus-Inspired Polymer for Endosomal Release," or VIPER.

6.1 Proposed Work

6.1.1 Alternative routes of administration

To date, we have administered anticancer VIPER vaccines intradermally or subcutaneously at the tail base of mice, which targets the vaccine to inguinal lymph nodes.[1–3] Recent work in the nanovaccine field has shown that splenic dendritic cells—targeted via intravenous vaccine administration—are potent mediators of adaptive immune responses against cancer.[4] VIPER vaccines may have greater anticancer efficacy when administered intravenously.

6.1.2 In situ VIPER vaccines

As a corollary to the proposed approach above, VIPER vaccines may also be administered intratumorally as an "in situ" vaccine.[5–7] No antigen cargo is needed, for the cytolytic bioactivity of VIPER after intratumoral injection should release tumor-associated antigen for processing by immune cells.[8,9] Since VIPER (in its original form) is a transfection reagent, genes encoding for therapeutically useful biomolecules (e.g., inflammatory cytokines) may be also delivered into the tumor.[10,11]

6.1.3 VIPER endosomolysis and its effect on cross-presentation in situ

In *Chapter 5* of this dissertation, we reported preliminary data suggesting that VIPER endosomolysis can enhance cross-presentation efficiency.[12] Does enhanced cross-presentation induced by VIPER in vitro correlate with increased cross-presentation in situ? To date, we have no data to confirm this is true, and further in situ study of cross-presentation phenomena is necessary. Doing so may require a shift away from melittin as an endosomal escape mechanism, as mannosylated polymer-melittin conjugates (the mannosylated VIPER-Vax reported in *Chapter 4* and *Chapter 5*) appear to attenuate, not augment, dendritic cell activation.[13,14]

6.1.4 Alternative adjuvants

In *Chapter 4* of this dissertation, we described early-stage experiments with copolymers consisting of adjuvant prodrug monomers, or "drugamers." Our adjuvant of choice for drugamer synthesis was resiquimod, which has been incorporated into other nanovaccine systems in both prodrug and non-prodrug (non-degradable) form.[15–18] Are there other adjuvants compatible with drugamer synthesis schemes?[19]

6.1.5 Tolerogenic therapy

This line of research will likely involve synthesis of an entirely new biomaterial (and devising of a catchy new acronym for it—"VIPER" does not sound like a drug for autoimmune diseases). However, the same biomaterial-based strategies used for delivery of tumor antigens to dendritic cells may also be used for autoantigen delivery.[20–22]

Finis.

6.2 References

(1) Aldrich, M. B.; Sevick-Muraca, E. M.; Hall, M. A.; Robinson, H. A.; Rasmussen, J. C.; Kwon, S. Non-Invasive Optical Imaging of the Lymphatic Vasculature of a Mouse. *J. Vis. Exp.* **2013**, No. 73, e4326.

(2) Mohanan, D.; Slütter, B.; Henriksen-Lacey, M.; Jiskoot, W.; Bouwstra, J. A.; Perrie, Y.; Kündig, T. M.; Gander, B.; Johansen, P. Administration Routes Affect the Quality of Immune Responses: A Cross-Sectional Evaluation of Particulate Antigen-Delivery Systems. *J. Control. Release* **2010**, *147* (3), 342–349.

(3) Luo, M.; Wang, H.; Wang, Z.; Cai, H.; Lu, Z.; Li, Y.; Du, M.; Huang, G.; Wang, C.; Chen, X.; et al. A STING-Activating Nanovaccine for Cancer Immunotherapy. *Nat. Nanotechnol.* **2017**, *12* (7), 648–654.

(4) Baharom, F.; Ramirez-Valdez, R. A.; Tobin, K. K. S.; Yamane, H.; Dutertre, C. A.; Khalilnezhad, A.; Reynoso, G. V.; Coble, V. L.; Lynn, G. M.; Mulè, M. P.; et al. Intravenous Nanoparticle Vaccination Generates Stem-like TCF1+ Neoantigen-Specific $CD8^+$ T Cells. *Nat. Immunol.* **2021**, *22* (1), 41–52.

(5) Shae, D.; Becker, K. W.; Christov, P.; Yun, D. S.; Lytton-Jean, A. K. R.; Sevimli, S.; Ascano, M.; Kelley, M.; Johnson, D. B.; Balko, J. M.; et al. Endosomolytic Polymersomes Increase the Activity of Cyclic Dinucleotide STING Agonists to Enhance Cancer Immunotherapy. *Nat. Nanotechnol.* **2019**, *14* (3), 269–278.

(6) Mukhopadhyay, A.; Wright, J.; Shirley, S.; Canton, D. A.; Burkart, C.; Connolly, R. J.; Campbell, J. S.; Pierce, R. H. Characterization of Abscopal Effects of Intratumoral Electroporation-Mediated IL-12 Gene Therapy. *Gene Ther.* **2019**, *26* (1–2), 1–15.

(7) Min, Y.; Roche, K. C.; Tian, S.; Eblan, M. J.; McKinnon, K. P.; Caster, J. M.; Chai, S.; Herring, L. E.; Zhang, L.; Zhang, T.; et al. Antigen-Capturing Nanoparticles Improve the Abscopal Effect and Cancer Immunotherapy. *Nat. Nanotechnol.* **2017**, *12* (9), 877–882.

(8) Chen, D. S.; Mellman, I. Oncology Meets Immunology: The Cancer-Immunity Cycle. *Immunity* **2013**, *39* (1), 1–10.

(9) Huang, C.; Jin, H.; Qian, Y.; Qi, S.; Luo, H.; Luo, Q.; Zhang, Z. Hybrid Melittin Cytolytic Peptide-Driven Ultrasmall Lipid Nanoparticles Block Melanoma Growth In Vivo. *ACS Nano* **2013**, *7* (7), 5791–5800.

(10) Cheng, Y.; Yumul, R. C.; Pun, S. H. Virus-Inspired Polymer for Efficient In Vitro and In Vivo Gene Delivery. *Angew. Chemie Int. Ed.* **2016**, *55* (39), 12013–12017.

(11) Tzeng, S. Y.; Patel, K. K.; Wilson, D. R.; Meyer, R. A.; Rhodes, K. R.; Green, J. J. In Situ Genetic Engineering of Tumors for Long-Lasting and Systemic Immunotherapy. *Proc. Natl. Acad. Sci.* **2020**, *117* (8), 4043–4052.

(12) Sánchez-Paulete, A. R.; Teijeira, A.; Cueto, F. J.; Garasa, S.; Pérez-Gracia, J. L.; Sánchez-Arráez, A.; Sancho, D.; Melero, I. Antigen Cross-Presentation and T-Cell Cross-Priming in Cancer Immunology and Immunotherapy. *Ann. Oncol.* **2017**, *28* (suppl_12), xii44–xii55.

(13) Lee, G.; Bae, H. Anti-Inflammatory Applications of Melittin, a Major Component of Bee Venom: Detailed Mechanism of Action and Adverse Effects. *Molecules* **2016**, *21* (5), 616.

(14) Kingeter, L. M.; Lin, X. C-Type Lectin Receptor-Induced NF-κB Activation in Innate Immune and Inflammatory Responses. *Cell. Mol. Immunol.* **2012**, *9* (2), 105–112.

(15) Lynn, G. M.; Sedlik, C.; Baharom, F.; Zhu, Y.; Ramirez-Valdez, R. A.; Coble, V. L.; Tobin, K.; Nichols, S. R.; Itzkowitz, Y.; Zaidi, N.; et al. Peptide–TLR-7/8a Conjugate Vaccines Chemically Programmed for Nanoparticle Self-Assembly Enhance CD8 T-Cell Immunity to Tumor Antigens. *Nat. Biotechnol.* **2020**, *38* (3), 320–332.

(16) Wilson, D. S.; Hirosue, S.; Raczy, M. M.; Bonilla-Ramirez, L.; Jeanbart, L.; Wang, R.; Kwissa, M.; Franetich, J.-F.; Broggi, M. A. S.; Diaceri, G.; et al. Antigens Reversibly Conjugated to a Polymeric Glyco-Adjuvant Induce Protective Humoral and Cellular

Immunity. *Nat. Mater.* **2019**, *18* (2), 175–185.
(17) Lynn, G. M.; Laga, R.; Darrah, P. A.; Ishizuka, A. S.; Balaci, A. J.; Dulcey, A. E.; Pechar, M.; Pola, R.; Gerner, M. Y.; Yamamoto, A.; et al. In Vivo Characterization of the Physicochemical Properties of Polymer-Linked TLR Agonists That Enhance Vaccine Immunogenicity. *Nat. Biotechnol.* **2015**, *33* (11), 1201–1210.
(18) Wang, B.; Van Herck, S.; Chen, Y.; Bai, X.; Zhong, Z.; Deswarte, K.; Lambrecht, B. N.; Sanders, N. N.; Lienenklaus, S.; Scheeren, H. W.; et al. Potent and Prolonged Innate Immune Activation by Enzyme-Responsive Imidazoquinoline TLR7/8 Agonist Prodrug Vesicles. *J. Am. Chem. Soc.* **2020**, *142* (28), 12133–12139.
(19) Srinivasan, S.; Roy, D.; Chavas, T. E. J.; Vlaskin, V.; Ho, D.-K.; Pottenger, A.; LeGuyader, C. L. M.; Maktabi, M.; Strauch, P.; Jackson, C.; et al. Liver-Targeted Polymeric Prodrugs of 8-Aminoquinolines for Malaria Radical Cure. *J. Control. Release* **2021**, *331*, 213–227.
(20) Krienke, C.; Kolb, L.; Diken, E.; Streuber, M.; Kirchhoff, S.; Bukur, T.; Akilli-Öztürk, Ö.; Kranz, L. M.; Berger, H.; Petschenka, J.; et al. A Noninflammatory mRNA Vaccine for Treatment of Experimental Autoimmune Encephalomyelitis. *Science* **2021**, *371* (6525), 145–153.
(21) Carambia, A.; Gottwick, C.; Schwinge, D.; Stein, S.; Digigow, R.; Şeleci, M.; Mungalpara, D.; Heine, M.; Schuran, F. A.; Corban, C.; et al. Nanoparticle-Mediated Targeting of Autoantigen Peptide to Cross-Presenting Liver Sinusoidal Endothelial Cells Protects from CD8 T-Cell-Driven Autoimmune Cholangitis. *Immunology* **2021**, *162* (4), 452–463.
(22) Wilson, D. S.; Damo, M.; Hirosue, S.; Raczy, M. M.; Brünggel, K.; Diaceri, G.; Quaglia-Thermes, X.; Hubbell, J. A. Synthetically Glycosylated Antigens Induce Antigen-Specific Tolerance and Prevent the Onset of Diabetes. *Nat. Biomed. Eng.* **2019**, *3* (10), 817–829.